OPTICAL STUDIES OF SOME METALS AND ALLOYS

A. EXAMINATION OF HARDNESS TEST INDENTATION

B. STUDY OF CATHODE GLOW ETCHING

THESIS

SUBMITTED TO THE UNIVERSITY OF LONDON

FOR THE DEGREE OF DOCTOR OF PHILOSOPHY

BY

JOY GEORGE

OCTOBER 1955

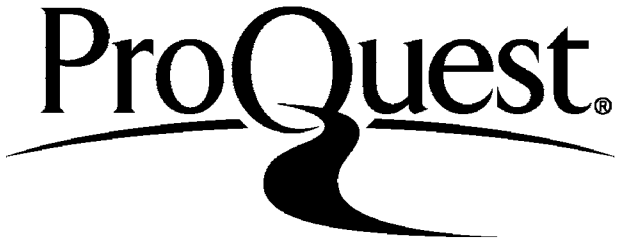

Abstract

In Part A of the thesis, the concept of hardness and its measurements are briefly reviewed at the beginning. Micro-hardness and its relation to crystal properties is also discussed. Micro-hardness test indentations with the double cone made on the (0001) plane of cleaved single crystals of zinc are measured and the variation of hardness with direction is studied. The value of hardness repeats itself for every 60 degrees due to the sixfold symmetry of the basal plane. The observations are not in conformity with theory. The distortion around the impressions is studied by multiple-beam interferometry using the microflat technique.

Kink traces on a microscopic scale are very clearly shown by phase contrast microscopy. The extent of the region of kink traces belonging to different kink systems, with the different positions of the inderter is revealed and discussed. Micro-twins are observed at the tips of the impression for certain positions only.

An X-ray study of the disordered region around the impression was also made and is discussed. Clear evidence for the process of polygonization is seen after annealing at 380°C for 2 hours.

In Part B, the equilibrium diagrams of binary alloys is briefly reviewed. The different theories of

cathode sputtering are discussed. This technique of etching by the bombardment of positive ions using the metal to be etched as the cathode in a glow discharge, is described. Tin and tin-indium alloys of low indium percentages are etched after different heat treatments and a metallographic study is made. The different phases observed are discussed. The results do not agree with the equilibrium diagram determined by Rhines, Urquhart and Hoge. Many interesting features are observed during the course of the microscopic examination and these are discussed.

An optical method for determining the rate of etching is given.

CONTENTS

PART A.

EXAMINATION OF HARDNESS TEST INDENTATION

PART B.

STUDY OF CATHODE GLOW ETCHING

PART A.

EXAMINATION OF HARDNESS TEST INDENTATION

CHAPTER I.

HARDNESS.

1·1 INTRODUCTION

Hardness as applied to metals has long been the subject of discussion among engineers, physicists, metallurgists and mineralogists and there are all sorts of conceptions as to what constitutes hardness. The overwhelming difficulty of defining hardness is that it is not a fundamental property of the material. There is hardness as measured by resistance to cutting, by scratching, by penetration, by electrical and magnetic properties, by resilience and by various other related physical properties. L.B.Tuckerman (1929) has rightly put "Hardness is a hazily conceived conglomeration or aggregate of properties of material more or less related to each other." However, the hardness measurements are of very great practical importance and it will be instructive to make a closer survey of the meaning and measurement of hardness.

1·2 DEFINITIONS AND MEASUREMENTS

All definitions of hardness imply a resistance to deformation. There are many ways of deforming a body and hence any resistance to deformation involves many factors.

Scratch Hardness.

The ability of one material to scratch another or be scratched by another, as a measure of hardness, was

probably the earliest type of test employed. This goes back to Reaumer (1722) who produced a metal bar whose hardness increased from one end to the other. The hardness was determined by the position on the bar which the metal being tested would scratch. Mohs (1822) introduced a scale of hardness for minerals by selecting ten minerals as standards beginning with talc (hardness 1) and ending with diamond (hardness 10). Each mineral in the scale would scratch all those below it. This hardness scale has served the mineralogists well but is not suitable for metals since the intervals are not of equal value in the higher ranges of hardness. Moreover the test depends to a very large extent on the shape of the point and its inclination to the surface under test.

A modern development of scratch hardness is the microcharacter. It consists of a sharp diamond stylus and is drawn across the surface to be tested, under a fixed pressure and the width of the scratch determines the hardness. The scratching process depends in a complicated way on the elastic, plastic and frictional properties of the surface. Hence the test has achieved no widespread use.

Abrasive Hardness.

Abrasive hardness is defined as the resistance

to mechanical wear, a measure of which is the amount of material removed from the surface under specified conditions. Abrasion between two surfaces depends on many factors such as the coefficient of friction, surface conditions, cold working, testing speed and other factors. Hence it is not possible to define a method of measuring abrasive hardness which will be suitable for all the practical applications for which such a quantity is required.

Static indentation hardness.

Reaumer in 1722 performed the first static indentation hardness test by applying pressure to two triangular prisms whose cones were at right angles to each other. From the depth of the two indentations made he judged the relative hardness of the two materials. A similar procedure was followed by Foeppl (1897) and Haigh (1920).

Since 1900, the static indentation hardness has been measured by pressing a hard indenter of known geometrical shape, under a given load, into the flat surface of the specimen and measuring the resulting impression. The stressing force producing the indentation is applied slowly and after a certain time of application, is carefully removed. The hardness of the material is then defined as the ratio

of the applied force to the surface area of the indentation. The hardness values so obtained vary with the indenter and the method of calculation. This has led to the compilation of many hardness conversion tables connecting one scale with another. They are not satisfactory for all materials and are all based on empirical results.

Dynamic hardness.

In the most direct case a hard indenter is dropped onto the surface of the specimen and the hardness is expressed in terms of the energy of impact and the size of the resulting indentation produced on the surface. Also the hardness may be expressed in terms of the height of rebound of the indenter as in the Shore Scleroscope (Shore 1918).

The value of dynamic hardness depends on the way in which it is defined and the velocity of impact of the indenter. Under ordinary experimental conditions the dynamic yield pressure (the ratio of the energy of impact to the volume of indentation) is of the same order of magnitude as the static yield pressure (the ratio of the load to the projected area of the indentation) and the dynamic yield pressure will invariably be slightly higher than the static yield pressure. With soft metals the difference is very much

more marked and will increase with the velocity of impact.

In conclusion it is worth mentioning the opinion of two experts. Roudie (1930) has said that "elasticity and hardness are two inseparable manifestations of molecular energy which dynamic methods alone can define and measure." But Meyer whose researches on indentation hardness are universally accepted was of opinion that dynamic effects should be eliminated from the concept of indentation hardness.

Magnetic hardness.

The magnetic properties of ferro-magnetic materials have been of considerable value from the hardness measurement point of view, for it is generally found that materials with large magnetic coercive force are also mechanically hard. If they are subsequently heat treated or mechanically deformed, so that the coercive force is changed, the mechanical hardness is changed in the same sense. Magnetic methods provide hardness tests for suitable materials without causing damage to the specimens. Non-ferrous metals and alloys on cold working and alloying produce important changes in their magnetic susceptibilities which may in turn be correlated with their hardness behaviour.

Hardness may also be considered in relation to electrical properties. For example the electrical resistivity of a metal at room temperature is changed when another element is alloyed with it and it is found that the hardness varies generally in the same way as the resistivity. Again the electrical resistivity and hardness both increase in most metals when mechanically deformed. It must be remembered that the parallelism between resistivity and hardness ceases with respect to change in temperature.

The above survey of measuring hardness serves to illustrate the complexity of the concept of hardness. Further complications arise however when one considers the structure and properties of the material under which tests are made. The material under test may be crystalline or amorphous, isotropic or anisotropic, all of which raise new questions of interpretation. The nature of the plastic properties of crystalline materials, in relation to particular planes of crystal lattice leads to a directional effect on the hardness values of single crystals.

Until recently hardness tests were made only on a microscopic scale, considering the specimen to be isotropic. Very recently micro hardness tests have

been developed and directional effects are becoming more evident.

In the present work, the change in hardness, on a microscopic scale, with direction on a particular plane of a single crystal is studied.

1.3 MACROSCOPIC INDENTATION HARDNESS

In this section a review of the development of the static indentation hardness measurements and the nature of the deformations occurring around these indentations will be given. When reference is made in scientific literature to hardness, it implies static indentation hardness, unless it is otherwise stated, as this has become the most widely used type of test. Future references to hardness in the present work means hardness as measured by static indentation methods.

The Spherical Indenter

J.A.Brinell (1900) proposed the first important indentation hardness test which has served as a basis for all subsequent tests of this type. The Brinell method consists of indenting the metal with a hard spherical indenter of diameter 10 mm. under a fixed normal load. The testing load is kept at 3000 kg. though for soft metals this is reduced to 500 kg. to avoid too deep an indentation. The load is applied slowly to fulfil the conditions of a static test. When equilibrium has been

reached after 15 - 30 seconds the load and the indenter are removed and the diameter of the permanent indentation measured. The Brinell hardness number (B.H.N.) is then expressed as the ratio of the load to the surface area of the indentation.

Thus

$$B.H.N. = \frac{W}{\frac{\pi D}{2}\left(D - \sqrt{D^2 - d^2}\right)}$$

Where W is the load in kgms, D is the diameter of the indenter in mm. and d the diameter of the indentation in mm. The diameter of the impression should be the average of the two readings at right angles. The B.H.N. is not constant for a given metal, but varies with the load and the size of the indenter.

The ratio W/A where A is the surface area of the indentation in sq.millimetres, is constant for a given material only when the applied load is the same throughout and the diameter of the ball is always the same. Whatever the actual size, for geometrically similar indentations, the hardness number should be constant and this is found to be true. That is if an indenter of diameter D_1 produces an indentation of diameter d_1 and another indenter of diameter D_2 produces an indentation of diameter d_2, the hardness number will be the same if the two indentations are geometrically

similar in which case

$$\frac{d_1}{D_1} = \frac{d_2}{D_2}$$ This is illustrated diagramatically in fig (1).

Further B.H.N. is not a satisfactory physical concept, for though at first sight it would seem that the ratio of the load to the surface area of the indentation is equal to the mean pressure over the surface, in fact it is not. Tabor (1951) has shown that the mean pressure is equal to the ratio of the load to the projected area of indentation $P = \frac{W}{\pi a^2}$ where $2a = d$, the chordal diameter of the indentation. E. Meyer (1908) proposed this mean pressure as a measure of the hardness and is referred to as the Meyer hardness number (M.H.N.).

$$M.H.N = \frac{4W}{\pi d^2}$$

Meyers Law. This law states that for a ball of fixed diameter $W = \alpha d^n$

where W = load in kg.

d = diameter of indentation in mm.

and α and n are constants for material under test.

In an extensive series of investigations, Meyer (1908) found that the index n was almost independent of the diameter (D) of the indenter but α decreased with increasing D such that

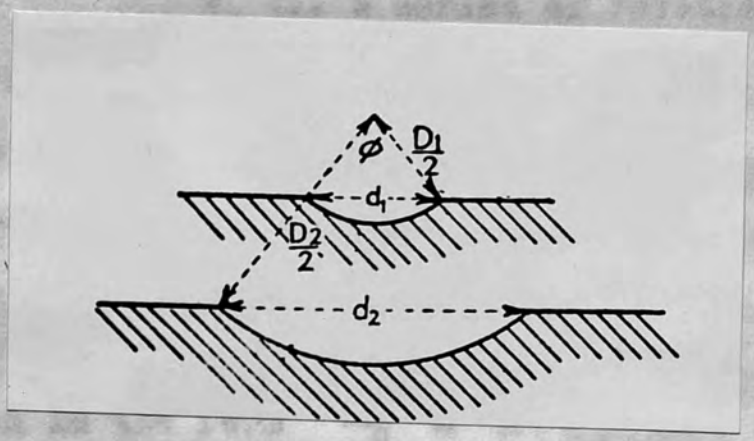

Fig. 1

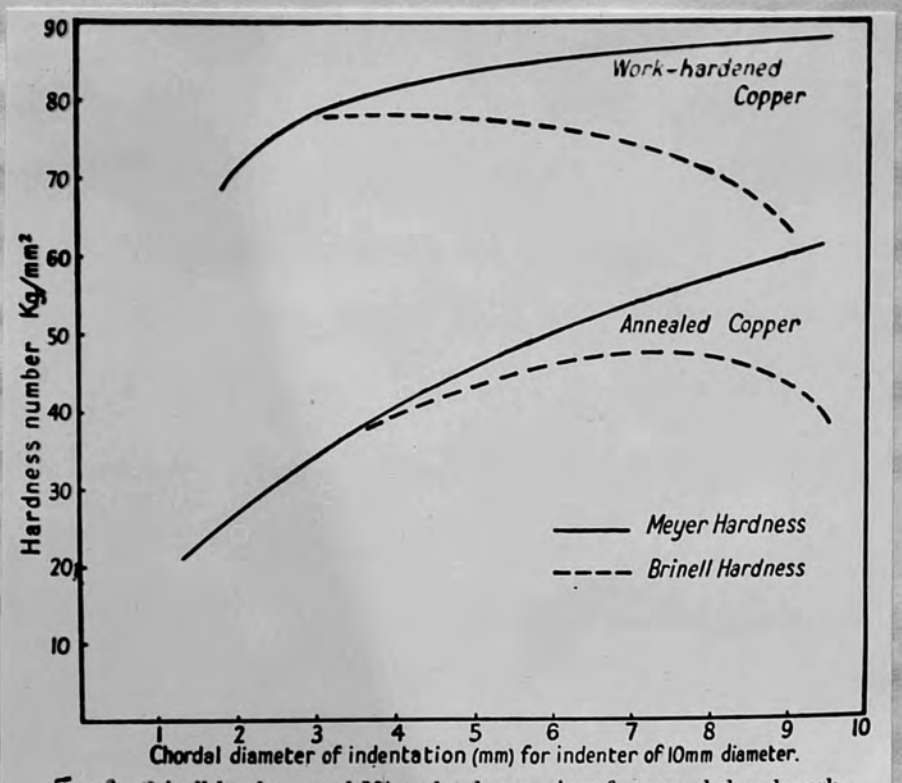

Fig. 2. Brinell hardness and Meyer hardness values for annealed and work-hardened copper as the size of the indentation is increased. The Meyer hardness values lie on a monotonic curve. The Brinell hardness values first increase and then decrease for large indentations as a result of the increasing area of the curved surface of the indentation. The Brinell values thus make it appear that for large indentations the metal is softer than for small indentations.

$$A = \alpha_1 D_1^{n-2} = \alpha_2 D_2^{n-2} = \alpha_3 D_3^{n-2}$$

For balls of diameters D_1, D_2, D_3 ... giving impressions of diameters d_1, d_2, d_3 ... a series of relations is obtained of the type

$$W = \alpha_1 d_1^{n_1} = \alpha_2 d_2^{n_2} = \cdots$$

The general equation then becomes

$$W = \frac{A d_1^n}{D_1^{n-2}} = \frac{A d_2^n}{D_2^{n-2}} = \frac{A d_3^n}{D_3^{n-2}} = \cdots$$ and may be written in the form $\frac{W}{D^2} = A\left(\frac{d}{D}\right)^n$

For geometrically similar indentations $\frac{d}{D}$ must be constant and consequently $\frac{W}{D^2}$ must be constant. Thus a ball of diameter 10 mm. and with a load of 3000 kg. will produce an indentation geometrically similar to those obtained with a 5 mm. ball and a load of 750 kg. or a 1 mm. ball and a load of 30 kg. In all these three cases the hardness values are the same and this conclusion is very useful in practical hardness measurements. Thus M.H.N. is a more satisfactory and fundamental concept. Fig.(2) gives a comparison of B.H.N. and M.H.N. for copper specimens annealed and highly deformed as quoted by Tabor (1951).

Shallowing effect.

The elastic recovery and the work hardening of the material brings in more practical difficulties in these hardness tests. When the load and indenter are removed it is found that the indentation left in

the testing surface has a larger radius of curvature than that of the indenting sphere. Foss and Brumfield (1922) have shown by careful measurements that the form of the indentation is spherical and symmetrical but that its radius of curvature for hard metals may be three times larger than that of the indenter. Shallowing behaviour of indentations were studied recently by Belk (1954) using multiple beam interferometry and showed that recovered ball indentations were only spherical if they were made with loads larger than the critical load for full plasticity.

'piling up' and 'sinking in'.

The distortions of the metal surface around the indentations are called 'piling up' and 'sinking in'. 'piling up' denotes the distortion of the metal above the original level of the surface close to the indentation (fig. 3a) while 'sinking in' denotes a distortion below the original level (fig. 3b). The 'sinking in' effect is observed close to the rim of the indentation and at distance well removed from the indentation a slight elevation of the surface is generally observed. It has long been established that these effects are due to different degrees of work hardening in the metal.

Fig. 3 - Deformation around the indentation produced by a spherical indenter: (*a*) 'piling-up' which is observed with highly worked materials, (*b*) 'sinking-in' which is observed with annealed materials. The effects have been exaggerated to show more clearly the deformation relative to the original level (dotted line).

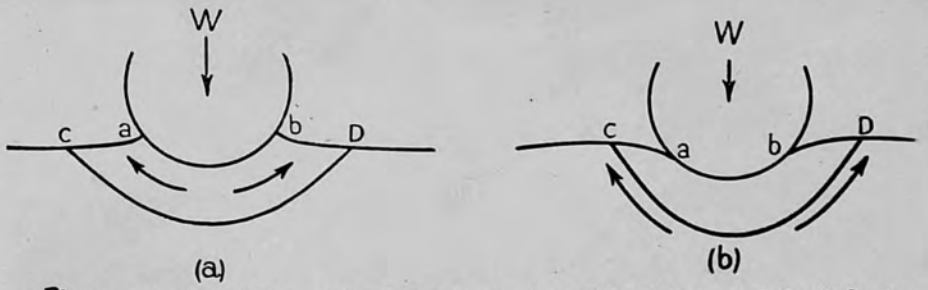

Fig. 4 - (*a*) For highly worked metals the flow of metal around the indenter produces 'piling-up', (*b*) for annealed metals the displacement of metal occurs at regions at a small distance from the indenter so that 'sinking-in' occurs.

Consideration of the plastic region gives a simple explanation for these effects. The region over which major plastic deformation occurs is shown in fig (4). For a work-hardened metal, the metal when displaced by the indenter flows out from close to the indenter (ac and bd) so that the material in this region is raised above the general level. (fig 4a). There is also a marked lateral movement near a and b because of the increasing diameter of the indenter as it descends. This is the behaviour of an ideal plastic material. If the material is in the annealed state, the early displacement of the metal in the plastic region produces work hardening and it becomes easier to displace the metal which lies deeper below the indentation, and the displaced material flows out at the region outside c and d (fig. 4b). Once this material has yielded it also work hardens and further displacement occurs at a still greater depth.

Strainless indentation.

During a hardness test the formation of the indentation itself leads to an increase in the effective hardness of the metal so that the hardness number obtained is not the actual hardness of the metal in the initial state. This is due to work hardening of the metal during the process of indentation.

Attempts have been made to determine the absolute hardness by eliminating work-hardening. This can only be done if the method does not appreciably deform the metal plastically. Two methods have been attempted first by Harris (1922) and later by Mahin and Foss (1939). They found that the 'absolute' hardness was about one third of the 'normal' hardness.

Conical indenters.

A conical indenter for hardness measurement was first used by Ludwik in 1908. He employed a sharp pointed diamond cone of included angle 90° and defined the hardness as the ratio of the load to the area of the curved surface of the indentation. Thus if for a load w the diameter of the impression is d then the Ludwik hardness number is given by $H_L = \frac{4w}{\sqrt{2}\pi d^2}$ The Ludwik hardness is independent of load, as all the indentations are geometrically similar, but varies considerably with the angle of the cone. This is probably because friction becomes increasingly important as the included angle of the cone decreases. The 'piling up' and 'sinking in' effects mentioned before occur to a much greater extent causing errors in depth and diameter measurements.

Rockwell test.

This test is based on the measurement of the depth of penetration. A minor load is first applied followed by a major load which is then removed and with the minor load still applied the additional depth of penetration is measured directly on a dial gauge. The value obtained may be correlated with Vickers or Brinell hardness values. There are two scales of Rockwell hardness utilising different major loads and indenters. For softer materials a spherical indenter is used (Rockwell 'B') and for harded metals a conical indenter with a hemispherical tip (Rockwell 'C') is used.

The pyramidal indenter.

The diamond pyramidal indenter for hardness measurements was first used by Smith and Sandland (1922) and was later developed by Messrs. Vickers-Armstrong Ltd., The indenter is in the form of a square pyramid, the opposite faces making an angle of 136° with one another. The diamond pyramid hardness method follows the Brinell principle in that an indenter of definite shape is pressed slowly into the material to be tested, the load removed, the diagonals of the indentation measured and the hardness number defined as the ratio of the load to the surface area of the indentation. It also follows

the Brinell test in the choice of the shape of the pyramid. In the Brinell test using a ball of diameter D, the range of indentation diameter is allowed to vary between 0.25 D and 0.5 D. The average of these is 0.375 D and tangents drawn to a circle at the ends of a chord of length 0.375 D, include an angle of 136°. Hence the angle between the faces of the pyramid indenter.

The diamond Pyramid hardness (D.P.H.) also known as Vicker hardness (V.H.) is defined by the formulae

$$D.P.H = \frac{2\,w \sin\frac{\theta}{2}}{d^2}$$

Where w is the load in kg, d is the diagonal of the impression in mm. and θ is the angle between the opposite faces of the indenter (= 136°)

$$D.P.H = \frac{1.854\,w}{d^2}$$

There are two advantages of this test which call for some comment. The first is that the indentations are geometrically similar for all the loads and hence the hardness is independent of the load for a homogenous material. The second is that the load can be varied from 1 to 120 kg, which means that all hardness variations met with in metals can be measured on the same hardness scale.

The main difficulty in the D.P.H. test is that the specimen requires careful preparation and must be set horizontally to the axis of the pyramid, otherwise the impression obtained will not be symmetrical.

The effect of "piling up" and "sinking in" is evident in pyramid indentation as well. If the pyramid is forced into a work hardened metal, the displaced material will flow up the faces of the indenter but will be constrained at the corners thus producing the characteristic 'barrel-shaped' indentation whereas in the case of annealed metal the sinking is manimum at the centre giving rise to "pincushion-shaped" indentation. The length of the diagonal is affected by this but to a much lesser extent than if the measurements were made to the centre of the sides. The deformation will be small along the edges of the pyramid compared with the deformation at the centre of the faces. This principle is more fully used in knoop and double cone indentations.

1.4 PHYSICAL SIGNIFICANCE

Following the review of the development of static indentation hardness measurements, a brief survey of the physical process involved by considering the elastic and plastic properties of an ideal metal

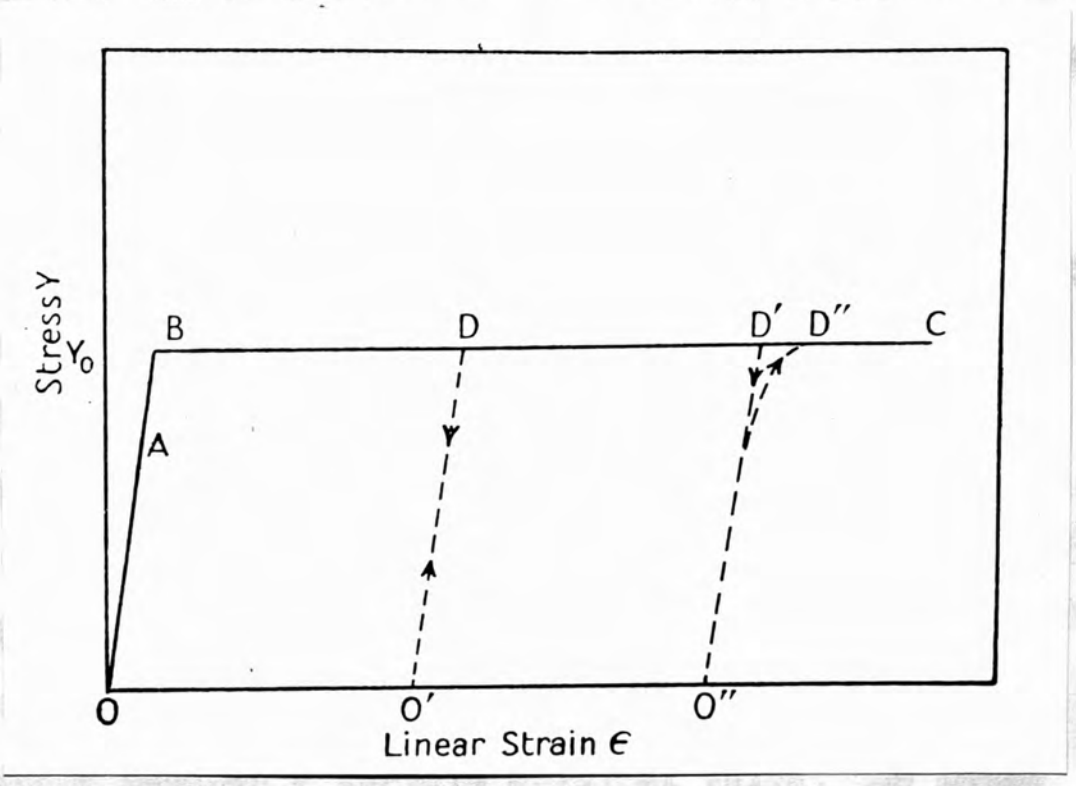
Stress Y
Y_0
B
D
D′
D″
C
A
O
O′
O″
Linear Strain ϵ

Fig. 5

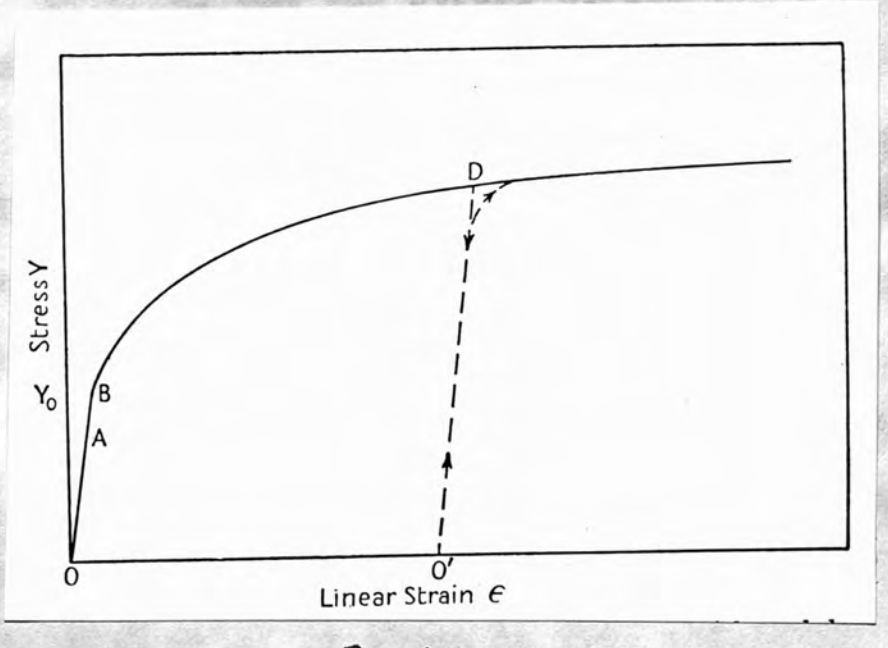
D
Stress Y
Y_0
B
A
O
O′
Linear Strain ϵ

Fig. 6

and how the properties of real metals differ from these is given. A theoretical analysis of hardness tests is also reviewed.

Ideal plastic metals.

The stress-strain curve for a cylinder of 'ideal' plastic metal under tension is shown in fig (5). The linear strain E is plotted against the true stress Y. Over the region A the material increases in length proportional to the applied stress and if the stress is removed the cylinder assumes its original length, i.e. the path OA is reversible. When the stress reaches a certain critical value, the metal deforms in a non-reversible way and the stress at which this occurs is called the elastic limit or the yield stress Y_o. The yield stress is constant for an 'ideal' material and the stress-strain curve BC is parallel to the strain axis. If at some point D the stress is released, the cylinder contracts along the line DO^1 having suffered a permanent plastic deformation of amount OO^1. If the stress is now applied again, the deformation will proceed along O^1DC.

The stress-strain curve for real metals differ widely from these 'ideal' plastic (strictly-elastic plastic) materials. The stress-strain curve for a typical metal is shown in fig. (6).

At any point D the stress required to produce further deformation is no longer the initial yield stress Y_o, and beyond this point, the yield stress increases only slightly with increase in strain and in this region the metal specimen has approached the 'ideal' plastic form. Thus if the stress-strain curve of a specimen that has already undergone considerable plastic deformation is plotted, it takes the form shown in fig.(7). A heavily work-hardened metal then has the plastic properties similar to those of an 'ideal' metal.

When an indenter is pressed on to the surface of a metal, the stresses are not simply tensile or compressive in nature. Instead stresses in various directions are set up and one should treat the resultant plastic flow as a result of these combined stresses.

Experimentally it is shown that hydrostatic pressure does not affect the yield stress of metals. Hence if a metal is subjected to combined stresses, the reduced stress after the hydrostatic components have been subtracted, must only be taken into account. If P_1, P_2, P_3, are the principal (orthogonal) stresses,

then for plastic flow

$$(P_1 - P_2)^2 + (P_2 - P_3)^2 + (P_3 - P_1)^2 = 2Y^2 \quad \ldots\ (1)$$

where Y is the yield stress. This relation is known as Huber-Mises criterion of plasticity (Huber, 1904; Von Mises, 1913) and is supported by a large body of experimental data.

An alternative criterion for plastic flow proposed by Tresca (1864) assumes that plastic deformation occurs when the manimum shear stress reaches a certain critical value. The Tresca or Mohr criterion is $P_1 - P_3 = Y$ when $P_1 > P_2 > P_3$ .... (2) With materials such as annealed mild steel there is evidence that the condition for plastic yield at the upper yield point is nearer the Tresca criterion than the Huber-Mises criterion. However there are two conditions under which these criteria become essentially the same. If $P_2 = P_3$ is substituted in equation (1) the two equations are identical and for plain strain (two diamensional deformation) the condition for plastic deformation in the direction P_2 is $P_2 = {}^1/_2 (P_1 + P_3)$. Substituting this value in equation (1), the Huber-Mises criterion becomes $P_1 - P_3 = 2Y/\sqrt{3}$. In both criteria the condition for plasticity for a two diamensional plastic flow is a manimum shear stress condition there being merely a

change in the value of the manimum shear stress when it reaches a critical value k where $2k = 1.15\ Y$ for the Huber-Mises criterion, or $2k = Y$ for the Tresca criterion.

When plastic deformation occurs, the stresses at any point may be expressed in terms of a shear stress k which is constant for an ideal metal and a hydrostatic pressure p, which vary from point to point. The lines of manimum shear stress k are called sliplines, but they should not be confused with slip lines, or slip bands observed under the microscope. The whole domain of plastic flow may be covered by two families of slip lines, the and the curves, each of which cuts the other orthogonally . The two principal stresses of the two diamensional flow P and Q are then given by $P = p + k$ and $Q = p - k$. Detailed mathematical treatment shows that if the slip lines are straight, p is constant throughout the plastic region.

The only indentation problems for which rigorous solutions have been found are two diamensional in character. Hill, Lee and Tupper (1947) has obtained a solution for a two diamensional wedge. The shape of the indentation is geometrically similar whatever its size and consequently the flow pattern is

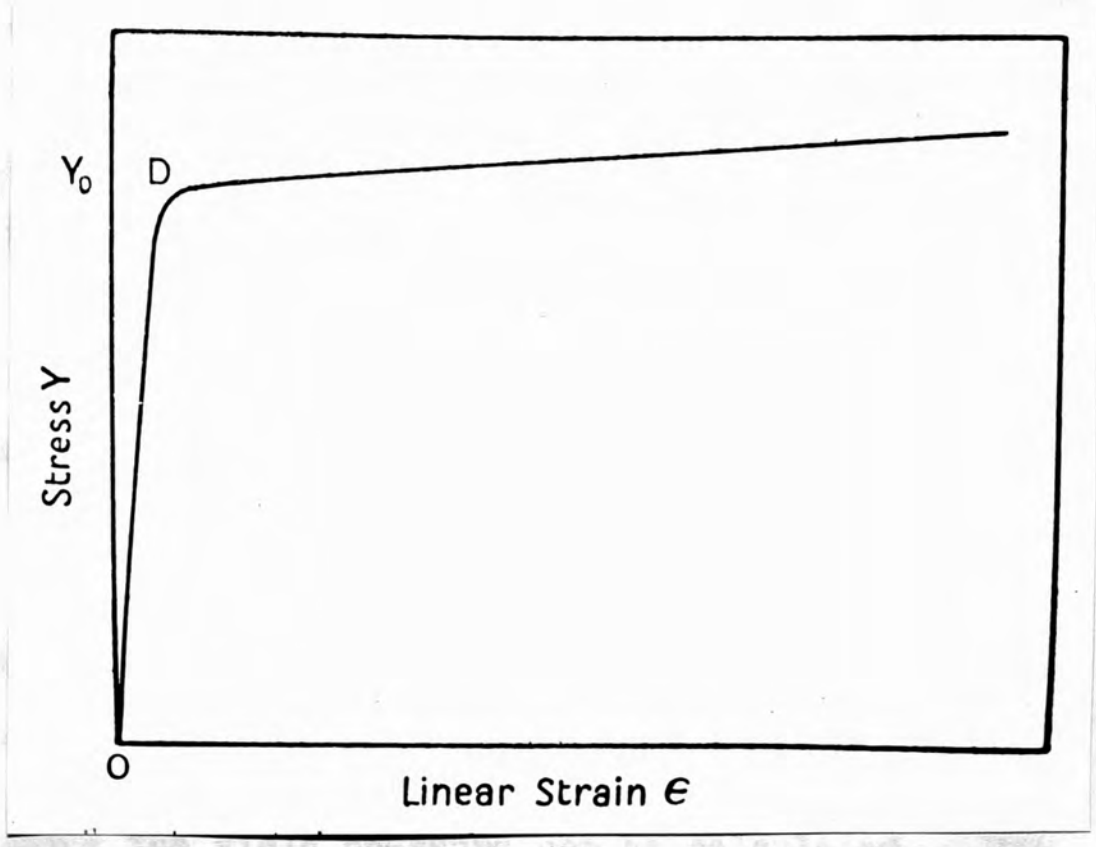

Fig. 7.

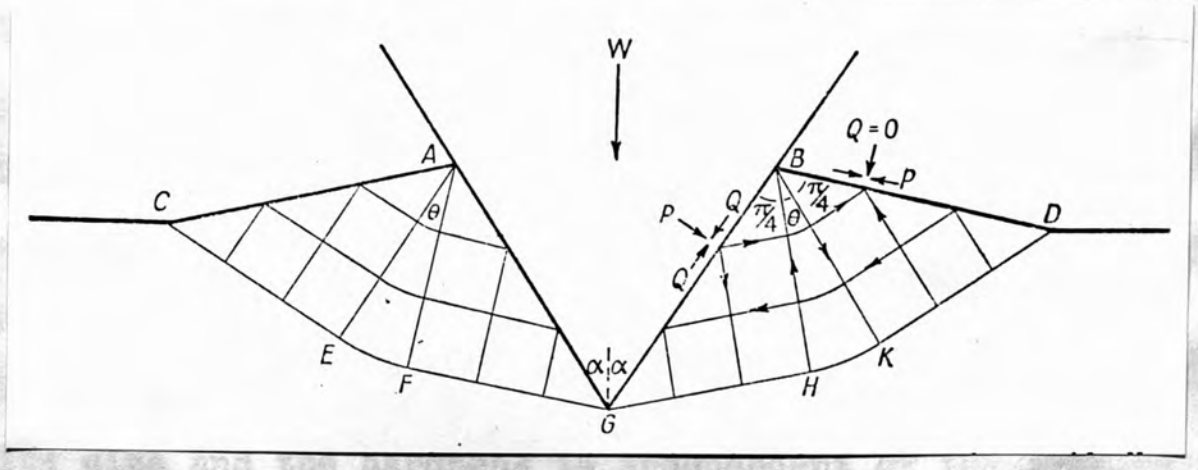

Fig. 8

always the same. The slip line pattern is shown in fig.(8). Experiments show that there is good agreement between the theoretical flow pattern and that observed in practice. This analysis takes into account the deformed surface.

The pressure normal to the surface of the indenter is given by $P = P + K$. It can be shown that for the Huber-Mises criterion

$P = 1.15\ Y\ (1 + \theta)$ where θ is $\angle$HBK in radians.

The angle θ is related to the semi-angle α of the wedge by the relation $\cos(2\alpha - \theta) = \frac{\cos\theta}{(1 + \sin\theta)}$ and thus for a particular wedge angle the yield pressure can be calculated. The solution for the two diamensional wedge is roughly valid for the three diamensional indenter if the semi-angle is not too small.

In the above analysis it is assumed that the material does not work harden whereas in practice all metals do work harden to some extent. For any sharp pointed indenter there is no elastic deformation of the surface as the region of full plasticity is reached for the smallest loads. The indentations are all geometrically similar whatever its size and the hardness is independent of the load. With spherical indenters, however, the shape of the

indentation varies with size, the work hardening increases with the size of the indentation. The yield pressure as a result increases with load. The pressure over the surface of the indenter is not uniform being higher at the centre than at the edges as shown by Ishlinsky (1944).

However, as the present investigation consists mainly in the study of micro-hardness indentations on single crystals, a close examination of the crystal properties is necessary to understand more fully the physical significance of micro-indentations and will be briefly reviewed in the next Chapter.

CHAPTER II

MICRO-HARDNESS AND CRYSTAL PROPERTIES

The term 'micro-hardness' means "micro-indentation hardness" as it actually refers to small indentations. This type of testing is used for thin materials; small precision parts; exploring hardness variations over small areas; and has been of great use in measuring the hardness of different electroplates.

2·1 EQUIPMENT

Micro-hardness testers fall into two groups - the scratch method and the indentation method. Most scratch hardness testers are of historical interest only and because of the limitations of the scratch test metallurgists prefer indentation methods, although mineralogists have used the scratch method.

The Knoop Indenter

The first indenter for the micro-hardness testing of metals was developed by Knoop (1939). The Knoop indenter is a sensitive diamond indenting tool of pyramidal form that produces a "diamond"-shaped indentation having long and short diagonals of the ratio 7 to 1. The pyramid form has included longitudinal angles of 172°30' and included transverse angle of 130°0'. (Fig.9.) The depth of the indentation is about 1/30th of its length. The method of carrying out the hardness tests is similar to that used in the Double cone hardness tests which will

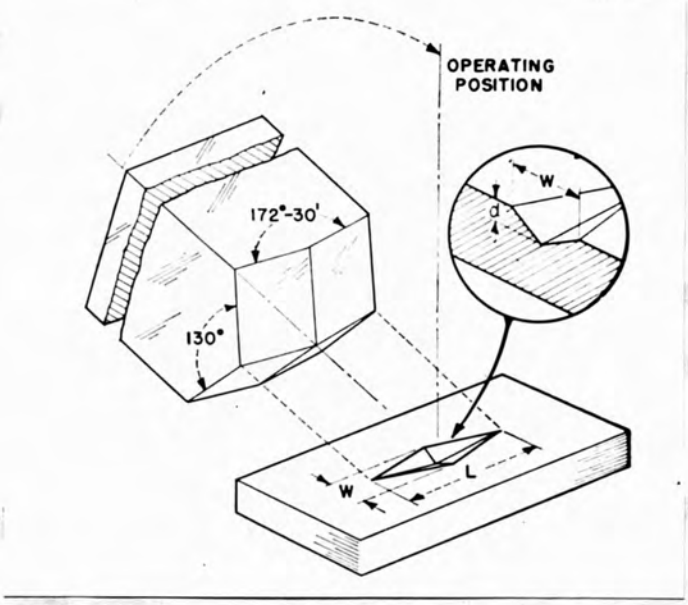
OPERATING
POSITION
172°-30'
130°
W
d
W
L

Fig. 9

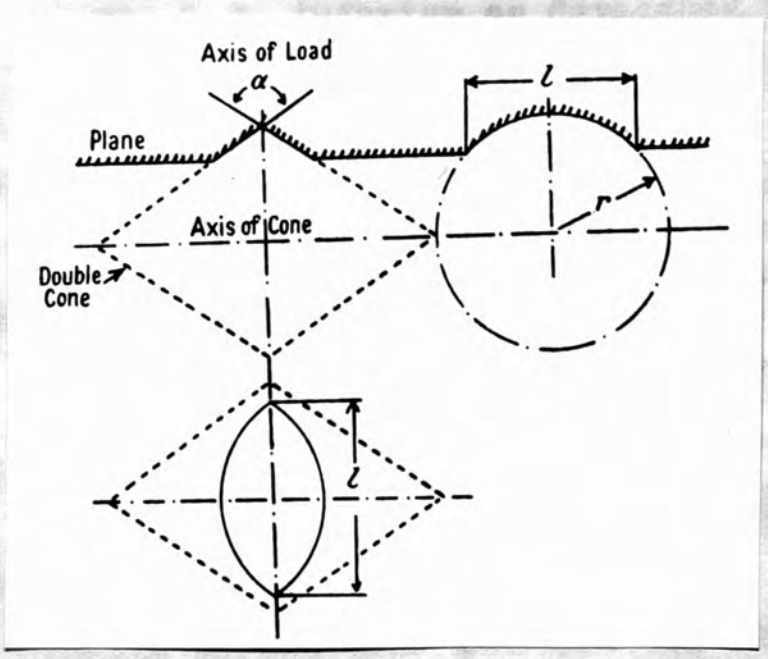
Axis of Load
α
Plane
Axis of Cone
Double
Cone
l
r
l

Fig 10

be described in detail later.

The Knoop hardness number is defined as the ratio of the applied load to the unrecovered projected area

i.e. $$I \ (K.H.N) = \frac{W}{l^2 c}$$

Where W = load in kg.

l = length of long diagonal in mm

and c = constant relating to projected area.

The length of the long diagonal is little affected by elastic recovery when the load is removed and is used as the basis for the hardness measurement. In actual practice the Knoop number is read from a table constructed for the purpose.

The Double cone Indenter

The D.C. indenter as developed by Grodzinski (1952) and used in the present work consists of two cone faces joined on equal bases, the axis being in a line. The indenter has a V-shaped section in one plane and a circular cross-section in the perpendicular plane (as shown in Fig.10)

The hardness number is given by

$$H_{D.C} = \frac{W}{A}$$ where W = load in kg

A = area of unrecovered impression in sq.mm.

The Double cone indenter has all the advantages of Knoop Indenter, apart from the fact that the indentations are not geometrically similar for different loads. But in practice this is not a great disadvantage with the diamensions

chosen for the indenter as the effect of non-similarity of indentations is very slight. The main disadvantage with the pyramid indenters is the production of a sharp point especially when micro-hardness indenters are made. This difficulty has been overcome in the double cone by the sharp edge obtained by the intersection of the two curved faces. The greater ratio of length to width of the indentation has the same advantage as the Knoop indenter. This greater length than width property of these indentations in effect gives the hardness a directional property; the meaning of this will be fully considered later.

2·2 SINGLE CRYSTALS. PLASTIC PROPERTIES AND HARDNESS.

Before discussing the relation of hardness to the plastic properties of single crystals, a survey of the fundamental mechanisms of plastic flow in crystals is of interest.

Slip.

The most common mode of plastic deformation is the slip which is characterised by the displacement of one part of the crystal relative to another along certain crystallographic planes. The movement is concentrated in a succession of planes leaving the intervening layers undeformed, like the movement of cards in a pile when the pile is distorted. Fig.(11) shows how the deformation takes place. The crystallographic plane along which the

displacement takes place is called the slip plane or glide plane and the direction of displacement is called the slip direction. These elements are joined by the lattice structure of the crystal and usually the slip planes are those of low indices and the directions those of closest packing of atoms.

A plane of slip and a direction of slip lying in that plane constitute a slip system. According to the symmetry of the crystal there can be more than one slip system. There are three slip systems in a hexagonal crystal and face-centred cubic metals have twelve slip systems. Slip is commonly recognised by the presence of slip lines which are formed by the intersection of slip planes with the surface of the crystal. When the slip plane has the same indices as the indices of the surface plane of the crystal, there will be no slip traces on the surface, as for example, on the cleaved surface of zinc crystals, on which the present investigation is being carried out. Slip lines which appear single at low magnification will resolve into groups of closely spaced lines at high magnification. They are usually spaced about a micron apart with considerable regularity, a fact that has led to much speculation as to their formation. The difference in the spacing of slip bands with increasing deformation has led to the conclusion that where little

strain hardening has occurred, deformation takes place on the previously existing bands, whereas in cases where marked strain hardening results, subsequent regions that are soft, slip.

Slip, for any specimen, occurs on a crystallographic plane, when the component of shearing stress in that plane along the slip direction reaches a critical value. This stress is called the critical resolved shear stress. It should be noted that the normal stress has no influence on the resolved shear stress. The slip direction is not the direction of greatest stress (shown by the long arrow in fig.11). There is a critical shear stress for each plane in the crystal and slip occurs in practice only in the observed slip planes since the shearing stress reaches the critical value in the latter first and relieves the applied stress before the critical value is reached on any other plane.

The shear stress necessary to cause slip is always increased with the degree of cold working. The presence of impurity or alloys elements raises the critical stress especially when such elements are dissolved in the lattice. The critical shear stress for a metal decreases with increasing temperature and drops to zero at the melting point. Hexagonal crystals show only a small dependence on temperature particularly in the neighbourhood of the melting point.

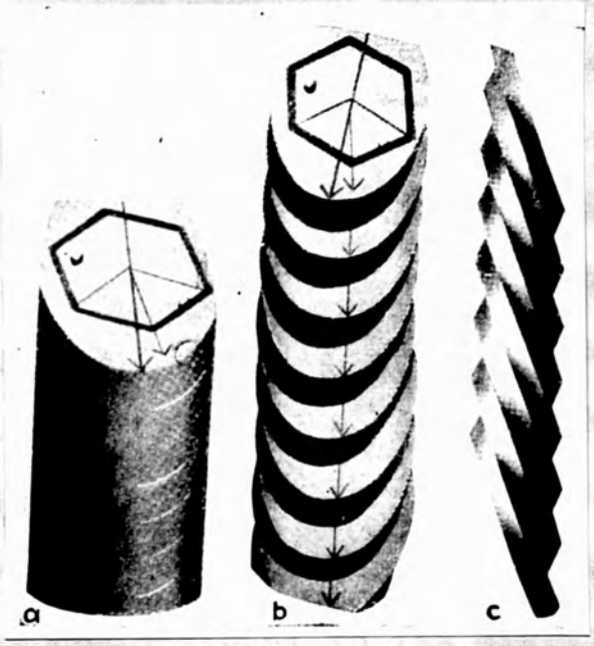

Fig. 11

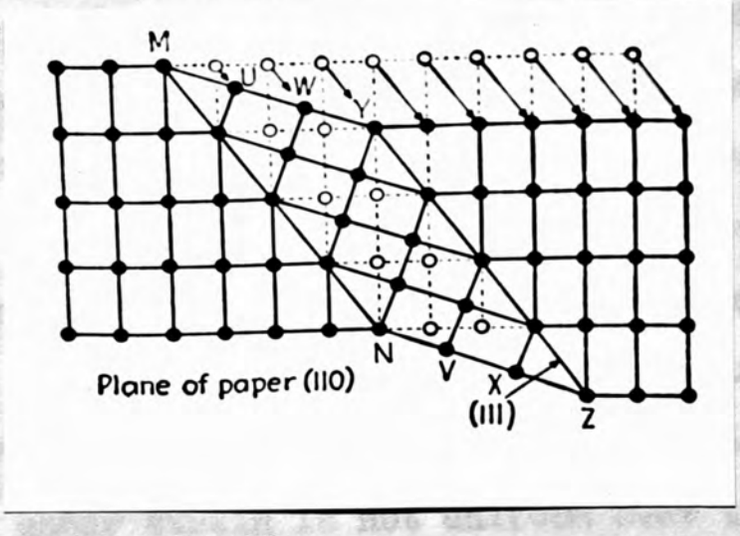

Fig. 12

Twinning.

Certain crystals may also deform by twinning, a mechanism by means of which a portion of a crystal may change lattice orientation with respect to the other in a definite symmetrical fashion. The lattice within the twinned portion is a mirror image of the rest and the plane of symmetry relating the deformed to undeformed part is called the twinning plane. Schmid and Boas (1955) describes twinning as the simple sliding of one plane of atoms over the next, the extent of the movement of each plane being proportional to its distance from the twinning plane. Fig. (2) illustrates the twinning mechanism in the face centred cubic system.

During deformation, the formation of twins takes place with a click and a rapid succession of clicks is responsible for the 'cry' of tin heard when a tin bar is bent. Twins also appear in some metals during annealing.

Whereas in slip, shear cannot amount to less than an interatomic distance in the direction of slip the magnitude of displacement in the case of twinning is usually not more than a small fraction of the lattice spacing. Again the shear strain is not uniform over the whole length of the crystal in the slip process whereas all planes in the deformed part lying parallel to the shear plane are identically displaced with reference to the neighbouring plane. Deformation twins are distinguishable from slip

lines on the surface in that the tilt of the twinned region gives a definite reflection at a different angle to the main surface. Also when seen under high magnification, two boundaries to the twin band can be seen whereas slip occurs as a narrow line.

Quantitative values like critical shear stress and the yield-stress curve characterising glide are not yet available in the case of mechanical twinning. The reasons for this are to be sought on the one hand in the very pronounced sensitivity of twinning to inhomogenetics within the crystal, thus causing the twins to develop in a more or less extended range. On the other hand crystals invariably slip before twinning, as a result of which twinning cannot be studied in the initial state but only in an already hardened state.

Cleavage.

It is well known that some crystals split along a certain crystallographic plane, with ease, and a crystal is then said to be cleaved along this plane. Just as a resolved shear stress is required for slip, a certain stress resolved normal to the cleavage plane is required for cleavage. If ϕ is the angle between the normal to the cleavage plane and the axis of tension, and A the area of cross-section, then the resolved normal stress is given by

$$N = \frac{F}{A} \cos^2\phi$$

The load required to break a crystal varies with orientation, but the resolved stress normal to the cleavage plane (N) is found to be constant. As such there is probably a critical cleavage stress for any plane in the crystal but only the value for the one or two planes of lowest cleavage strength can be measured for critical values are never reached on the others. In hexagonal close packed crystals if tensile stress is applied almost perpendicularly to the basal plane, cleavage takes place before slip as the component of the stress available for slip is less than the critical stress required for slip. Cooling to liquid air temperature facilitates cleavage for at this temperature, the increase in critical stress for slip is more than the critical stress for cleavage.

How single crystals of zinc are cleaved and liquid air temperatures for the present study, will be described later.

Shear strength of crystals.

It has already been pointed out that there is a critical shearing stress for slip and it seems that a critical shearing stress exists for twinning as well as a definite normal stress which is required for cleavage. When a stress is applied to a crystal it should cause slip, twinning or cleavage according as the resolved stress on the slip plane in the slip direction or on the twinning plane in the twinning direction or normal to the cleavage

plane exceeds the critical value for the process concerned.

Calculations of the theoretical values of shear stress required to cause slip in single crystals is 1,000 or 10,000 times the observed value. This discrepancy between calculated and observed yield strength of crystals has led to the development of many theories on the plastic properties of crystalline materials. The most successful theory is the dislocation theory and the concept was applied to slip by Orowan (1934), Polanyi (1934) and Taylor (1934) and later developed by many others. Though the dislocation theory explains the process of slip, work hardening, the temperature effects and the plastic properties, no satisfactory explanation has been given to the mechanism of twinning (Clark and Craig. 1952) in terms of the theory of dislocations.

Directional properties.

It is seen that in the deformation of single crystals certain crystallographic planes and directions play a very important part. The crystal lattice in itself leads to anisotrophy in crystal properties. R.Houwink (1938) in a report on 'viscosity and plasticity' refers to these properties thus: "Even in a crystal of the regular (cubic) class there is a large difference between a lattice plane and a plane making an arbitrary angle with it. There is also to be considered differences in intensity between bonds in various directions. In crystalline substances with large

molecules, such features can become more and more prominent. They will lead to characteristic anistropies in the deformation behaviour of a crystal....."

Even as early as 1690, variation in hardness values for different directions on a crystal face was detected by Huygens during scratch hardness tests on Iceland spar. Though tests of this type are difficult to apply and analyse, it has given sufficient evidence for the anisotropy existing in metal crystals. O'Neill (1934) showed that the scratch hardness of a crystal is least in the direction parallel to the cleavage plane.

Though during static indentation tests with the ball and pyramid indenters, irregular impressions are produced, which is in fact a directional variation of the hardness, a quantitative investigation of the directional hardness has not been made until Daniels and Dunn (1949) used Knoop indenter on crystals of zinc and silicon ferrite. Later A.P.Williams (1953) studied the directional hardness variation on single crystals of tin and bismuth, with particular reference to the deformation around the indenter, using a double cone. The results of their work will be discussed later in connection with the present work.

The present investigation consists in studying this directional variation giving special attention to the deformation around it, using multiple beam interferometric and phase contrast techniques. An Xray study of the surface

after indentation is also made. A heat treatment of the crystal has confirmed certain interesting phenomena. The results are striking and will be discussed. The procedure and techniques used will be reviewed in the next Chapter.

CHAPTER III

OPTICAL TECHNIQUES.

3.1 MULTIPLE BEAM INTERFEROMETRY.

In the preceding Chapter mention has been made of the interferometric technique. This is a well established optical technique developed by Tolansky (1944, 1945, 1946, 1947) for the study of surface features and has been fully discussed by Tolansky (1948). A review of the subject is given by Kuhn (1951) in his article on "New techniques in optical interferometry". This method was first applied to the study of deformation features on metal surfaces by Tolansky and Nickols (1949 a and b, 1952) and later by Williams (1953). More recently Belk (1954) has used the method to examine the surface distortions by spherical indenters.

As the present investigation is confined to the study of metal surfaces, most of the observations were carried out using the reflection system and both techniques of Fizeau fringes and fringes of equal chromatic order have been used. The main advantages of these techniques are that the whole of the surface deformation is revealed, the accuracy of the measurement is inherently high and it is very simple in operation.

Theory.

For an interferometer with two component surfaces parallel to each other, separated by a dielectric of thickness t and refractive index μ, have reflection and

and transmission coefficients of R and T respectively, the intensity distribution in the transmitted system is given by the formulae

$$I = \frac{T^2}{(1-R)^2} \cdot \frac{1}{1+\frac{4R}{(1-R)^2}} \cdot \sin^2\frac{\delta}{2}$$

where $\delta = \frac{2\pi}{\lambda} \cdot 2\mu t \cos\theta$ is the constant phase lag between successive beams, θ the angle of incidence. This is referred to as the Airy formulae for intensity distribution and represents sharp maxima on a dark background.

For two surfaces inclined to each other to make a small wedge angle, the Airy summation should apply with the difference that there will be a progressively varying phase lag between the successive reflected beams, and when this becomes π (i.e. the corresponding path difference is $\lambda/2$) there will be a tendency to destroy the condition for the formation of sharp fringes. Tolansky (1946) and Brossel (1947) have shown that the path difference, in this case, between the first and the n^{th} beam is $(2n t - \frac{4}{3} n^3 \phi^2 t)$ where ϕ is the wedge angle. The value $\frac{4}{3} n^3 \phi^2 t$ must therefore be less than $\lambda/2$. i.e. t should be made as small as possible and must in any case be less than the cricical value. In practice it is found that this must be of the order of a few wavelengths, otherwise the fringe definition will suffer considerably.

The corresponding treatment for the reflection system is much more complicated. The theory of reflection

system is discussed by Hamy (1906) and Holden (1949). The complications arise from the fact that the first reflected beam suffers a phase change with respect to the second beam which is quite different from that between any other two successive beams. For silver films of high reflectivity ($R > 80\%$) the intensity distribution in the reflected and the transmitted systems are very nearly complimentary although the experimental conditions for good reflection fringes are far more critical than in transmission.

Thus when two highly reflecting surfaces are brought close together and illuminated with parallel monochromatic light at normal incidence interference fringes are observed which are localized in the wedge formed by the two surfaces. These localized multiple beam fringes obey the formulae

$$n\lambda = 2\mu t \cos\theta$$

Where n is the order of interference (and is an integer), λ is the wavelength of light, μ is the refractive index of the material between the plates, t is the thickness of the gap and θ is the angle of incidence. With θ and λ constant, Fizeau fringes of equal thickness are formed. If θ is kept constant and λ allowed to vary, the value of λ/t which represents the order of interference becomes constant for each fringe and have been termed fringes of equal chromatic order by Tolansky (1945).

Fizean fringes.

The optical set up for the observation of these fringes is shown in fig.(13) A metallurgical microscope is adapted so that the image of the light source is formed in the back focal plane of the objective O, the light emerging from the objective thus being made parallel and fall normally on the interferometer x. The objective lens forms an image of the interferometer and so the fringes can be observed through the microscope.

The experimental conditions for the production of fine multiple beam Fizeau fringes in the present study have been obtained by

(1) coating the reference flat with silver films of high reflectivity by thermal evaporation (this is a well established technique) thus ensuring the minimum absorption. The surface under study like the cleaved crystals of zinc had a natural reflectivity of more than 85% while for other specimens the polishing gave a high reflectivity.

(2) using a mercury source with Wratten 77A filter to produce a monochromatic source.

(3) applying the microflat technique described in Section 5 of Chapter 4 in the case of zinc to ensure a small wedge angle.

(4) setting the optical arrangement as shown in fig.(13) to make a parallel beam fall normally on the interferometer.

It has already been seen that the Fizeau fringes are fringes of equal thickness of the wedge. When the incidence

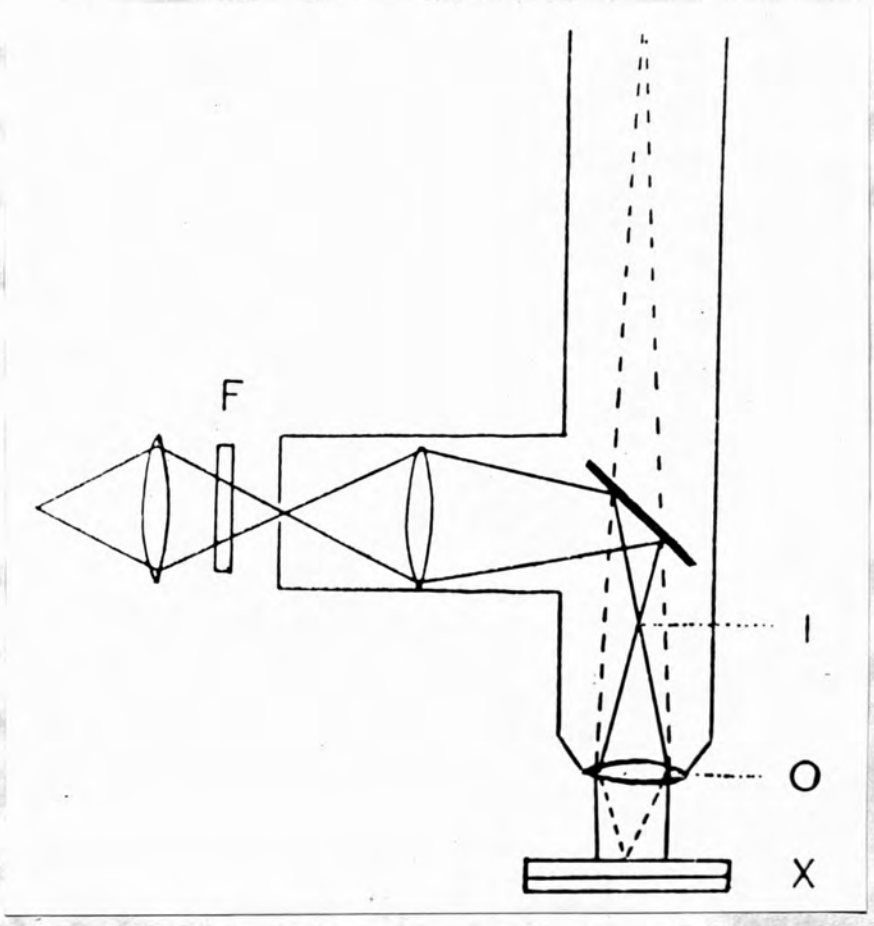

Fig. 13

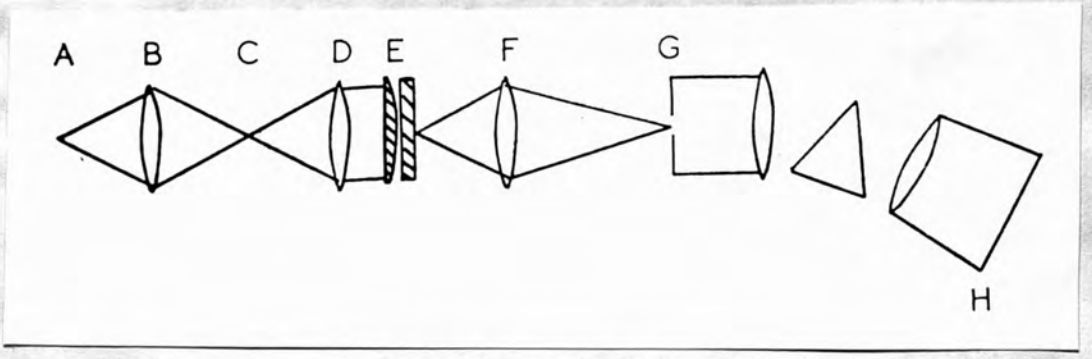

Fig. 14

is normal and the gap is an air gap as is invariably the case, then the height displacement of successive fringes is which means any displacement can be measured as a fraction of the distance between adjacent fringes and thus the change in height can be measured as a fraction of

$\frac{\lambda}{2}$ = 2730 A units.

Fringes of equal chromatic order.

The identical system as with Fizeau fringes (but with white source and no filter) is used, the image of the interference system being projected on to the slit of the spectrograph. The experimental set up for the fringes of equal chromatic order in transmission is shown in fig.(14). A is a white source the image of which is projected on to the circular aperture C by means of the condenser lens B. The lens D sends a parallel beam of light (since C is at the focus of the lens D) on to the interferometer E, the incidence being normal. With the microscope objective the image of the film E is projected on to the slit G of the spectrograph. The fringes appear at H.

The formulae governing the formation of these fringes is $n\lambda = 2\mu t \cos\theta$,

if $\mu = 1$ and $\theta = 90^{\circ}$.

then $n\lambda = 2t$ or $t = \frac{n}{2}\lambda$

For any fringe $\frac{t}{\lambda}$ is a constant. If t is increased by an amount δt, λ increases by an amount

given by $\delta t = \frac{n}{2} \delta\lambda$. Hence if any one fringe in the spectrum deviates towards the violet (which means λ is decreasing) that shows that the interferometric gap is decreasing and that there is a "hill" or "elevation" in the surface under examination with reference to the optically flat second surface. This is shown diagramatically in fig.(15). Each fringe is thus a section of the surface under examination along the line the image of which is projected on the slit of the spectrograph.

In order to measure the change in height on the surface, i.e. δt in the equation above, the quantity n the order of a particular fringe and $\delta\lambda$ the wavelength change corresponding to δt should be known. The latter can be obtained from the dispersion curve of the spectrograph by measuring the variations in the distance of the fringe from a standard spectral line superimposed on the fringe system by a mercury source. The quantity n is obtainable since $n\lambda_1 = (n+1)\lambda_2$ for two adjacent orders i.e. $n = \frac{\lambda_2}{\lambda_1 - \lambda_2}$ the order for blue end of the spectrum being higher. The value of λ_1 and λ_2 can be again obtained from the dispersion curve of the spectrograph.

Thus it is possible to convert fringe displacements into surface measurements and hence a line section of the surface may be studied.

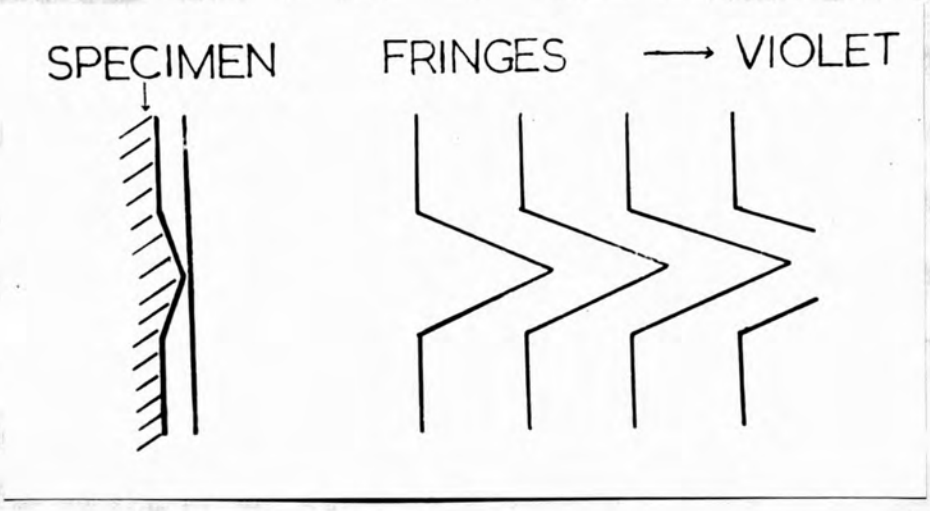

Fig · 15

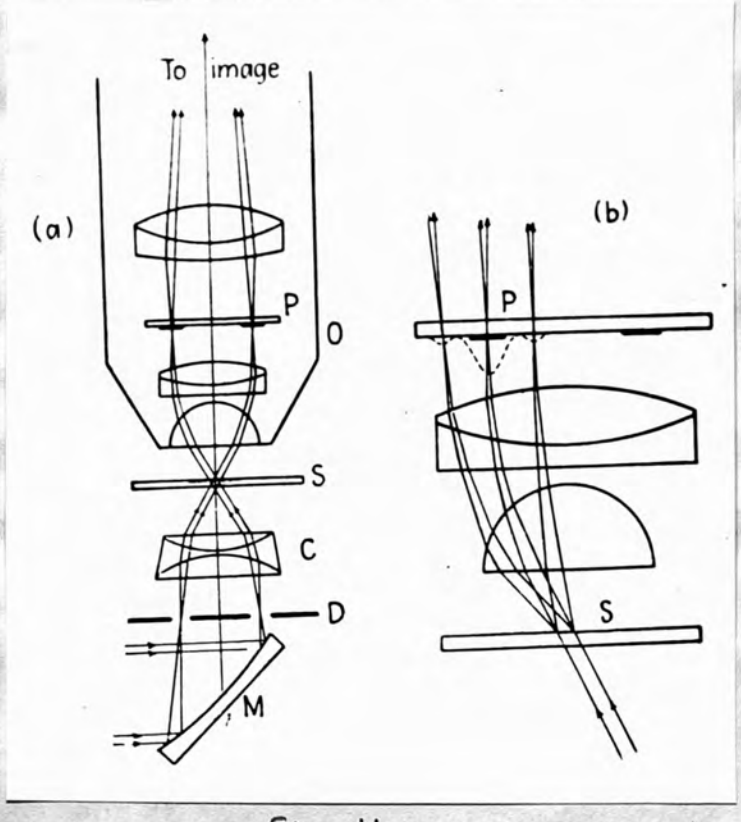

Fig · 16

In the present study a Vickers projection microscope was used to get the Fizeau fringes and along with it Hilger's constant deviation spectrograph was used to obtain the fringes of equal chromatic order. In practice, with the slit of the spectrograph wide open, and setting the spectrograph for the green region, Fizeau fringes were viewed through the eyepiece and thus it was possible to locate the particular region where the line section was to be studied using the fringes of equal chromatic order.

3·2 PHASE CONTRAST MICROSCOPY

The principles of phase contrast microscopy were first given by Zernicke (1934). In this method slight variation in a wave-front produced say by slight non-homogenities of refractive index in the medium traversed could be transformed into corresponding variation of amplitude and thus rendered visible as corresponding variations of (apparent) transparency. A good account of this technique is given by Bennett, Jupnik, Osterburg and Richards (1951).

Fig.(16) shows how the variation of phase is converted into variations of intensity in the plane of the image. In part (a) the annular diaphragm D is placed in the front focal plane of the substage condenser C of an ordinary microscope and an image of the light source is focussed upon D by the concave mirror M, and the hollow cone of light falling on the object is focussed by the

objective lens system to form an image of D on the phase plate P (which ordinarily consists of a dielectric layer of optical thickness $\lambda/4$), assuming that there is no diffraction by the object. The size of this ring is to match the image of D. A thin metallic film is deposited is to reduce its transmission.

Let some structure on the object cause diffraction of the light passing through it. The central portion of the diffracted wave continues undeviated and the remaining portion is deviated. The undeviated wave will undergo a phase change of $\pi/2$ on passing through the phase plate. But the diffracted wave-front is already one quarter vibration behind the central undeviated wave. (For simplicity suppose the object produces a diffraction pattern like the Fraunhofer pattern of a single aperture as indicated by the dotted curve below p in part (b).) Therefore the phase plate brings the two waves into phase resulting in a large increase in the intensity at the final image. Retarding the direct light by $\lambda/4$ to bring the direct and diffracted waves into phase is called a negative phase contrast. Here the portions of the object giving greater retardation are rendered brighter than the background. Advancing the direct waves by one quarter wave length gives rise to what is known as positive phase contrast where regions of greater retardation are imaged darker than the background. Generally the diffracted wave is much weaker than the undeviated wave and

to obtain best results the annular portion of the phase plate is made absorbing to decrease the intensity of the central light. Thus by introducing phase changes in the plane of diffraction images inhomogenities of the object producing change in optical path is made visible provided such an object produces a diffraction pattern. Although diffraction is not pronounced as that produced by amplitude changes, such a pattern always exists.

The apparatus used in the present work was the Cooke Troughton and Simms phase contrast equipment for reflection fitted on to a Vickers projection microscope. The arrangement is shown diagramatically in fig.(17). The annular diaphragm serves as an entrance pupil of the optical system. The light source is focussed on this by the condenser lens C. The field lens and the objective form a real image D_2 of the diaphragm after the light has been reflected from the specimen surface and passed through the objective again. Image D_2 becomes the exit pupil and it is here that the phase plate is located.

In this equipment, the objective lenses, the beam splitter and the phase plate are mounted on the objective. The principle of positive phase contrast is used with a single phase plate of 80 per cent absorption and giving a phase retardation of $\pi/2$. Adjustments can be made to get the surface of the specimen perpendicular to the optic axis of the microscope and to superimpose the

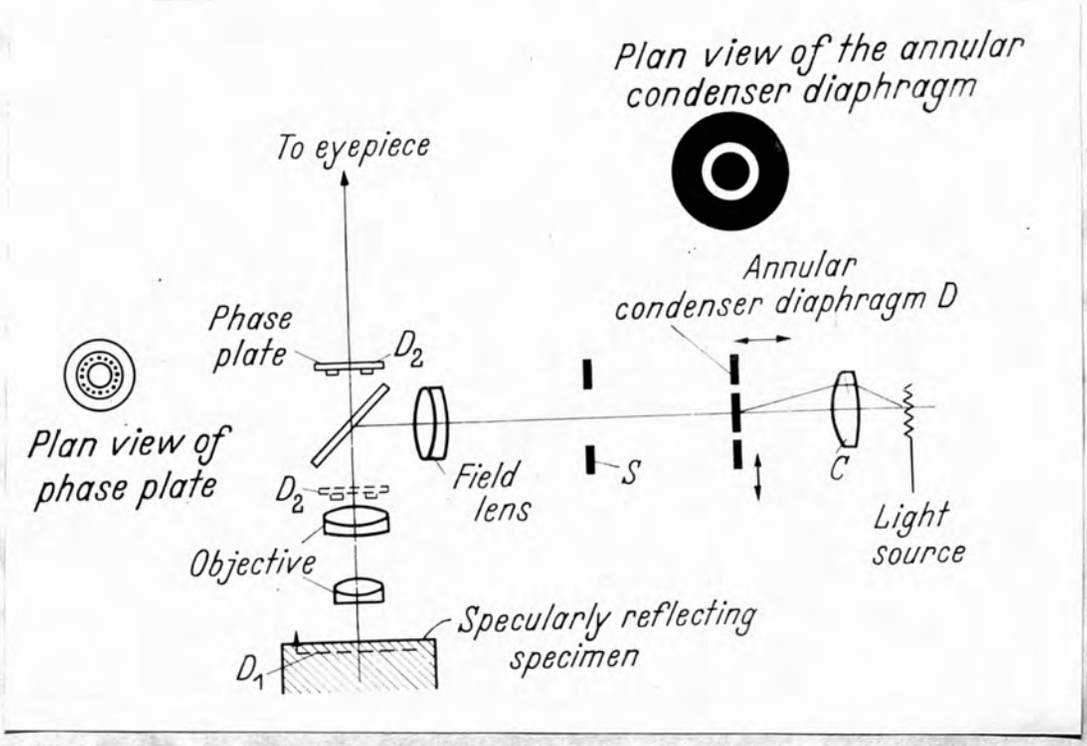
Plan view of the annular condenser diaphragm
To eyepiece
Annular condenser diaphragm D
Phase plate
D_2
Plan view of phase plate
D_2
Field lens
S
C
Light source
Objective
Specularly reflecting specimen
D_1

Fig. 17

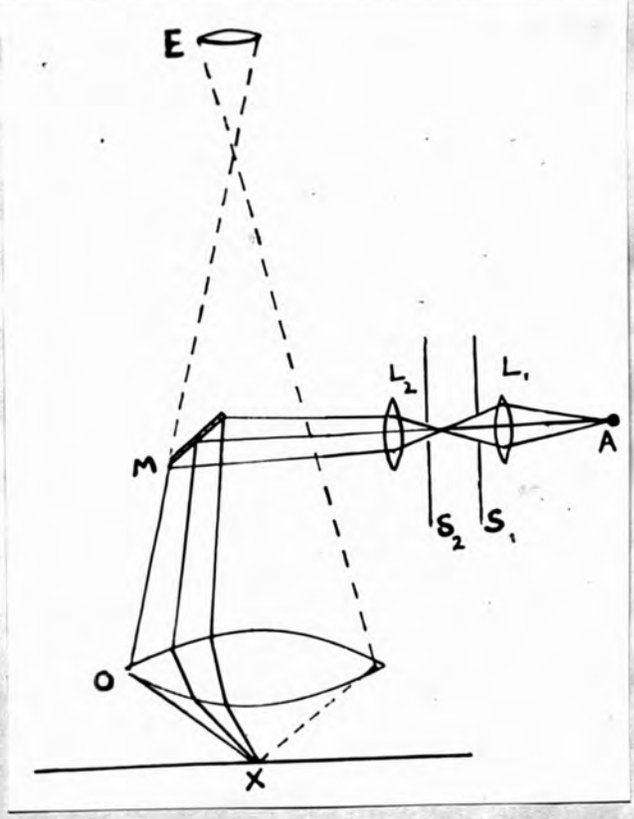
E
L_2
L_1
M
A
S_2
S_1
O
X

Fig. 18

image of the annular diaphragm exactly on the annulus of the phase plate by viewing the back focal plane of the objective with the auxiliary microscope provided.

Unlike bright field microscope where slight shift in focus is used to observe specimens of low contrast, phase contrast microscope gives the best contrast when the specimen is exactly in focus and this gives a true representation of the surface under examination. Moreover the phase contrast microscope is operated at full aperture and there is practically no decrease in resolution. A limitation of this method is that the surface should be specularly reflecting in order to form a sharp image of the annular condenser diaphragm in the back focal plane to be able to make exact superimposition on the phase plate annulus. Very contrasty B20 Kodak plates were used together with a contrasty developer Kodak D8 to get maximum contrast.

3·3 LIGHT PROFILE MICROSCOPY.

This technique developed by Tolansky (1951) was used in the present work when multiple beam interferometry could not be applied due to the coarseness of some of the surfaces under study. This is a considerable development of the light cut procedure by Schmaltz (1936). The light cut method had several disadvantages which were overcome with the development of the light profile where any microscope can be used as a profile microscope by making a minor adaptation and having a universal illuminator.

Fig.(18) shows the schematic arrangement. A is a monochromatic source which is very necessary as off-centre illumination brings in severe chromatism. L_1 is the condensing lens. S_1 is a diaphragm and S_2 is the field iris. The profile is kept as near as possible to the field iris in the universal illuminator. The profile consists of a mounted thin wire or a scratch on a glass or the edge of a coverstrip. The metal tongue reflector M gives the off-centre illumination. Objective O up to 2 mm. (oil immersion) can be used to obtain high magnification. E is the eyepiece where the image is seen. In actual practice, the surface X to be studied is first focussed and then the profile is adjusted until its image is in the plane of the surface of the specimen. The profile magnification is shown to be $M^1 = \frac{M \tan i}{\mu}$ where i is the angle of incidence of the illuminating pencil of light, μ is the refractive index of the medium surrounding the surface and M is the microscope magnification. For practical purposes the profile constant $\frac{M^1}{M}$ is obtained by interferometric calibration. In the case of the 2 mm. oil immersion objective this constant is 1 so that the linear magnification is equal to profile magnification.

An additional advantage is that the depression or elevation on a surface feature can be detected at once from the direction of displacement of the profile image. Magnification up to ×2000 can be used and the accuracy of measurements is of the order of 1000°A when this objective is used.

CHAPTER IV.

PREPARATION OF THE SPECIMEN AND METHOD OF TESTING

4·1 PREPARATION OF SINGLE CRYSTALS

Single crystals of zinc were prepared from 99·99 per cent pure zinc by the same method as given by Bridgman (1925). A pyrex tube containing the metal was lowered slowly through a vertical silica tube furnace maintained at a temperature of about 450°C emerging into cool air.

The pyrex tube was drawn initially into the shape shown in fig.(19). The lower chamber A was about 4 mm. wide separated from the chamber B of diameter about 1·5 cm. by a capillary of very small diameter. After introducing zinc metal in granulated form into the chamber C the wide open end of the tube was narrowly drawn off to be connected to a rotary pump. The system was evacuated for a few minutes and the metal inside heated by a bunsen burner with the tube in a nearly horizontal position, agitating the molten metal to drive off occluded gas and the tube was given sudden jerks so that it flowed slowly into the A-B system leaving the impurities and oxide if any in the Chamber C. The quantity was adjusted to fill B almost completely. It is always better to leave a small quantity of the metal inside C with the oxide and solid impurities at the top, at the same time leaving the constriction free of any solid metal. The tube was sealed off at the narrow constriction between B and C.

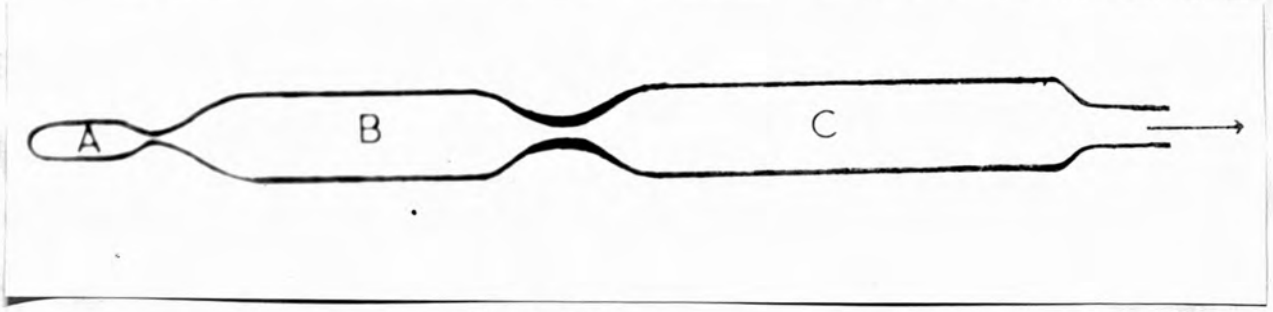

Fig: 19

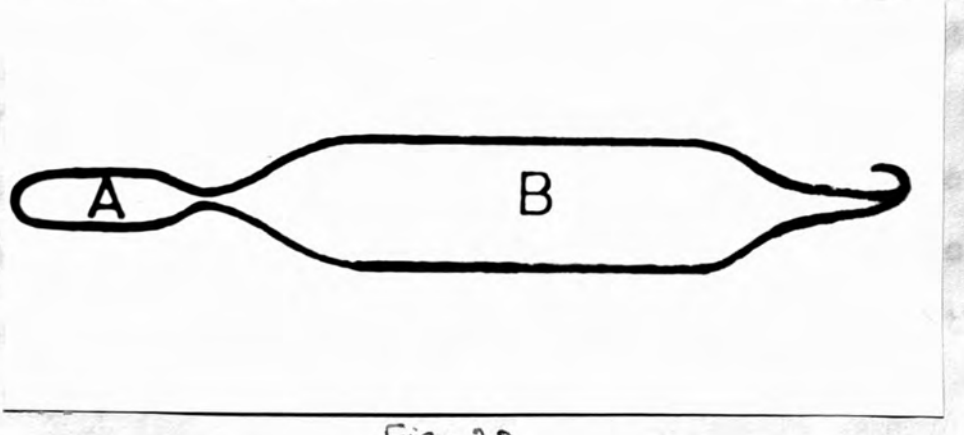

Fig. 20

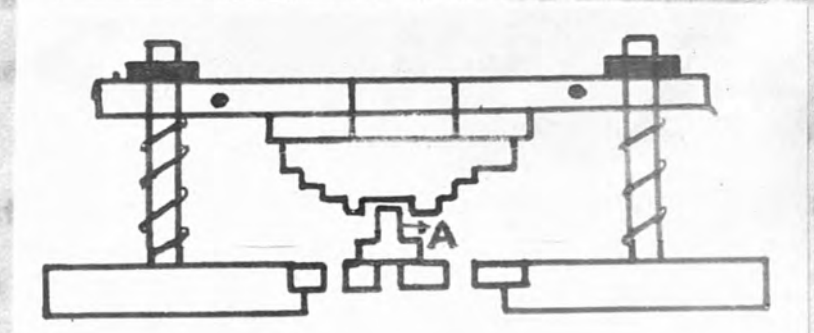

Fig. 21.

This constriction should be thick in order to avoid the glass being drawn in, due to the evacuation of the system, during sealing. The capillary between A and B acts as a filter allowing only one of the several grains which may have formed initially in the lower part of A and this Chamber was made fairly long so that the most favourably situated grain might have as much chance as possible to form below the filter instead of above. The final form of the tube is shown in fig.(20).

To the hook of this mould was tied a very thin metal wire, the other end of the wire was passed over a tiny pulley and then wound over the spindle of a reduction gear driven by a motor. After lowering the tube into the vertical furnace, it was adjusted to hang vertical without touching the sides of the silica tube and left at the position of maximum temperature, covering almost the whole length of the mould, to get the metal in the molten state.

The motor was then started and the tube was allowed to fall down gradually through a falling temperature gradient, the rate of lowering of the specimen was less than 1 cm/hour. Crystallisation started at the bottom and the selective action of the capillary caused the crystallisation of one large crystal in the main part of the tube, with its cylindrical shape.

Most of the specimens prepared in this way were single crystals and the cleavage plane in most cases was not

far from being perpendicular to the length of the crystal. To determine the cleavage plane, the crystal having been removed carefully from the mould was dipped in liquid air and after the crystal had attained the temperature of liquid air, was taken out and a light blow was given at the narrow portion of the crystal. If it is a single crystal the tip splits along the cleavage plane exposing the cleaved surface. This served a method of determining whether the crystal was single or not. Only single crystals of zinc split along the cleavage plane. Thus single crystallites of about a cm. thick were cleaved along the length of the cylinder for the purpose of present study and were dried by a warm blast of air from a hair drier.

4·2 THE DOUBLE CONE INDENTER.

The form of the double cone indenter has already been described in Chapter 2 Section 1.

The hardness value is given by the relation

$H_{D.C.} = \frac{W}{A}$ where W is the load in kg and A the area of unrecovered impression in sq.mm. An approximate value for A as given by Grodzinski (1952) is as follows

$$A = \frac{\tan(\frac{\alpha}{2}).d^3}{6\gamma}$$

Where α = included angle between the two conical faces

γ = radius in mm. of interseating circular arc.

d = measured length in mm. of indentation.

$\frac{\tan \frac{\alpha}{2}}{6\gamma}$ = C is a constant for the given indenter

$$H_{DC} = \frac{W}{C d^3}$$

As γ = 2 mm. and α = 154° in the case of the indenter used, C works out to be equal to 0·361

$$H_{DC} = \frac{W}{0{\cdot}361\ d^3}$$

The hardness value for a constant load varies with the cube of the length of the indentation (d) which means that any small variation in d leads to a large variation in the value of hardness. This may be considered an advantage as it gives a hardness scale of great spread. One should not forget the fact that the factor C having a length diamension reduces d to a square function the same as in the Vickers and Knoop hardness formulae.

The value of the width of the indentation does not enter in the formulae for the hardness number. It is assumed that very little recovery takes place in the length and that all recovery due to deformation occurs along the width. The indenter gives a shallower depth compared with length than in the case of the pyramid and the Knoop types.

The numerical comparisons as applied to a hard specimen are given in the table below. (Grodzinski)

	H.N.	Length mm	Width mm	Depth mm	Width/Length	Depth/Length
D C	2013	0.155	0.005	0.0015	$1/31$	$1/103$
V P	1678	0.33	0.33	0.00475	1	$1/7$
K	1663	0.0925	0.13	0.0042	$1/7$	$1/22$

For zinc used in the present test, the ratio of width/length for the D C was of the order $\frac{1}{8}$ and depth/length $1/60$.

4·3 METHOD OF MEASURING HARDNESS.

For making indentations, the standard micro-hardness tester (Cooke Troughton and Simms) set up on a projection microscope was used with the double cone replacing the pyramid indenter objective.

To start with, the first indentation made should be along a certain known direction on the crystal face so that this could be made as a reference for all subsequent indentations on the same surface as well as on the cleavage planes of other single crystals of zinc. In the present study of hardness, the direction of twin trace seen on the cleavage face of the crystal was taken as the reference which meant that the length of the first indentation should be parallel to the twin trace. An indentation was made on the crystal as described earlier in the chapter. The eyepiece was rotated such that the length of the indentation was parallel to the eyepiece graticule scale. The stage of the microscope was then rotated and the twin trace was brought

parallel to the same scale. Then any other indentation made on the crystal surface should be parallel to the twin trace. Indentations were made at 10° intervals by rotating the stage (the specimen rotated with the stage) the angle of rotation being given by a scale and vernier. The stage could also be moved across or longitudinally.

The length of the indentation was measured accurately by photographing it and measuring the length of the image using a travelling microscope reading to 0·001 cm. The tapering out of the end of the indentations is of great importance in measuring their length. The angle formed by the Knoop indentation with the centre line is $\gamma = 8°8'$ for all lengths of the indentation whereas the corresponding angle in the double cone varies with the length of the indentation and is in general given by the formulae $\tan \gamma = 3 c d$. During the present study a comparative value was the main aim and hence this error could not affect the results very much.

4·4 MICROFLAT TECHNIQUE

In order to apply the interferometric technique described in Chapter III Section 1 for studying the deformation around the indentation, ordinary optical flat could not be used as the flat when matched against the cleaved surface did not make the necessary wedge angle due to the roughness of the surface when a large area was

considered. So the microflat technique suggested by Tolansky and Omar (1953) was followed. Microflats of the form shown A in fig.(21) with flat tops of very small diameter up to 1.0 mm, were made by the author in the laboratory following the same method of Pandya (1954) with slight improvements. An optical glass flat (true to $\lambda/40$ over quite a large area) was covered on both sides with galva cement to protect the surface from being scratched. A cylindrical piece of about 0.5 cm. in diameter was cut out using a cylindrical hollow drill, the pressure being applied slowly and intermittently. To facilitate cutting, a liquid paste of carborundum in water was often applied to the surface. This small glass piece was then fixed to a metal rod with galva. The rod was fixed in a lathe and the glass piece was reduced to the required shape and size by grinding against carborundum powder spread over a copper strip wetted with water. The shape of the microflat shown in the figure was found to be more convenient as the area of the top surface could be reduced without reducing the area of the base and is found easier to manipulate when cleaning, mounting and silvering.

A special type of jig (Pandya 1954) to hold the crystal and the microflat with the convenience of moving the crystal surface was used. Though this was an improvement on the type described by Tolansky and Omar (1953) so that high power objectives up to 8 mm. could be used with

the flat cut from a photographic plate, the author had to make further improvements for an easier approach to this technique. The indentations were scattered over the surface of the crystal and with the objective focussed through the one hole at the base of the jig it was found very difficult to locate a particular indentation even with the movement of the crystal surface in two perpendicular directions - so a disc of diameter 2•5 cm. was cut out from the base of the jig and another disc with 4 or 5 holes to hold the microflat was made just to fit in a groove cut in the base (cross-sectional view is shown in fig.(21). Then keeping the jig on the stage of the microscope, after removing the disc, the exact position was located by moving the stage or moving the crystal if necessary. The disc was then replaced in position and rotated slightly so that light could be seen through any of the holes, which confirmed that the surface required could be seen through that hole. Then the microflat was placed against that hole and interference fringes obtained by adjusting the top screws. Thus any particular area of the surface could be studied using the same high power objective. By taking the disc off, it was possible to take microphotographs of the desired magnification of the surface without removing the specimen.

CHAPTER V.

HARDNESS TEST INDENTATIONS

Several crystals of zinc were grown and cleaved and double cone indentations made as described in the last Chapter, the length of the indenter in the initial case being along the [1 2 $\bar{1}$ 0] direction and the stage rotated through 10 degrees after every indentation. The double cone has many advantages over the pyramid indenter for measuring hardness variations of single crystals. The impressions have a much greater diamension along their length than their width and the length is taken as a measure of the hardness and any change in length gives a variation in hardness in that direction. This means the hardness and its variation with respect to direction can be studied. Also the force exerted by the indenter is concentrated in the centre of the side faces of the indenter and falls off at the ends, Unlike the pyramid where the extent of the faces is not great enough to allow the force due to the indenter to diminish sufficiently before reaching the diagonal edges. Due to the square symmetry of the pyramid, though the anisotropic nature of the deformation is revealed, the directional effect cannot be accurately measured.

A number of crystals were tested and a whole series of indentations were made. Only one example is given here as the indentations in all cases are identical

(the load being the same) since the plane of indentation is the same. Cleaved surfaces as it were, were chosen for this study as the surface would then be free from any disturbed layer due to polishing and which might affect the hardness especially when it was done on a micro-scale. Also portions of the surface which could be taken as smooth for all optical purposes were easily available over the surface. The fringes over these portions of the surface were almost straight and parallel. Such surfaces free from twins and cleavage lines were chosen in which to make the indentations. It was found however, that the presence of the cleavage lines near the indentation did not affect the value of the hardness.

5·1 OBSERVATIONS.

Figs. 22 and 28 show the interferograms for each individual indentation and the distribution of the flow of the material around the indentation is shown very clearly in each case. By slightly pressing the specimen towards the optical flat it was found that the shift in the fringe to the top was due to the elevation of the surface. From the amount of shift as a fraction of the distance of the adjacent fringe (the distance between two successive fringes corresponds to a change in wedge thickness $\frac{\lambda}{2}$) it can be seen that the distortion is a maximum in the initial case (fig.22) and as the direction of the indenter is varied the plastic flow becomes more and

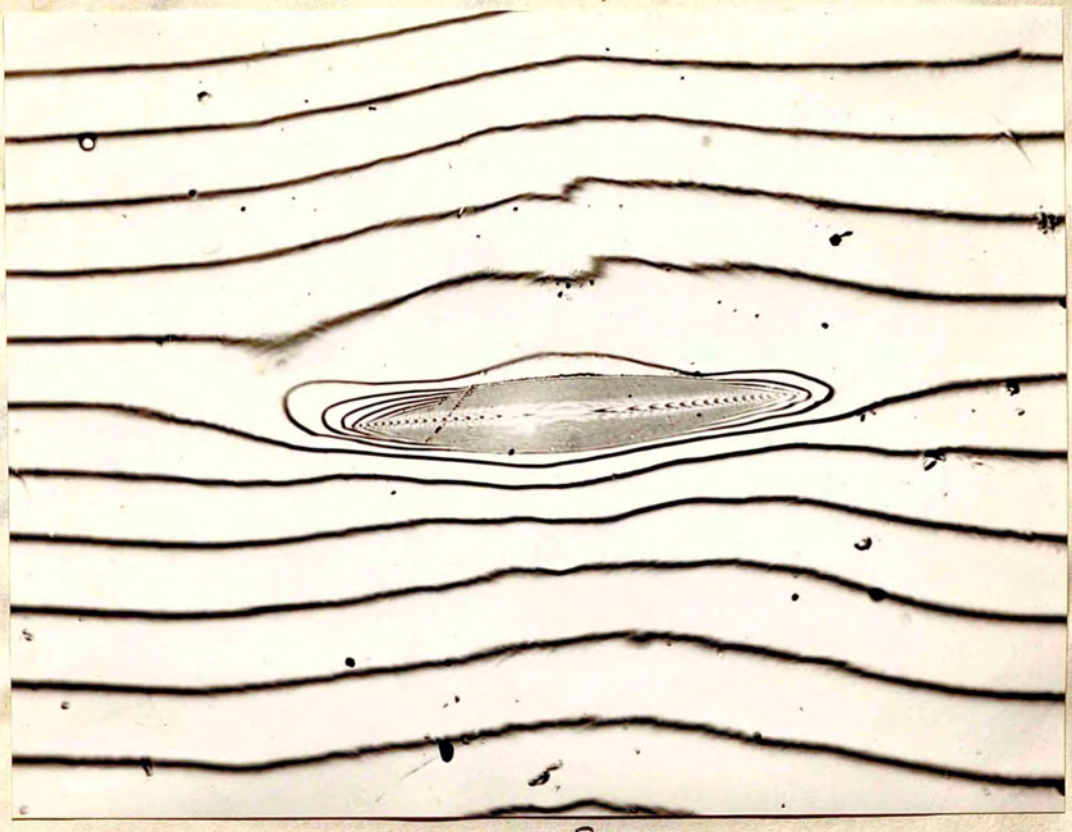

x150

Fig. 22

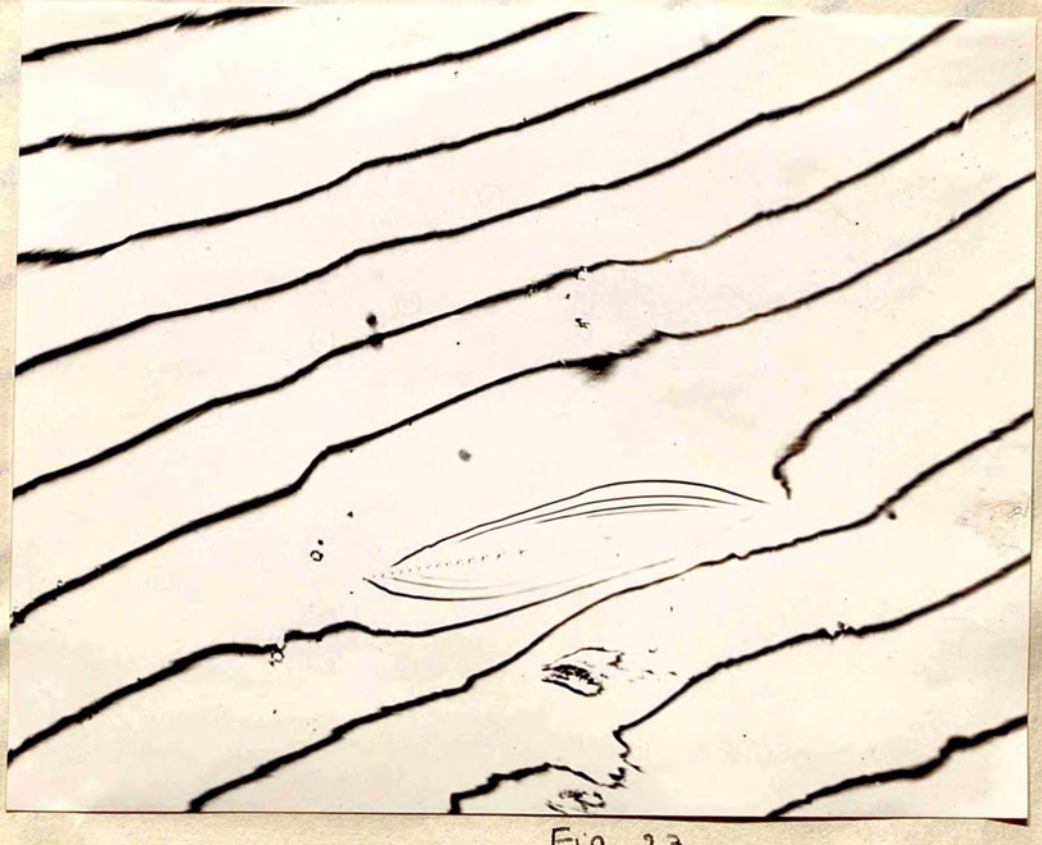

x150

Fig 23

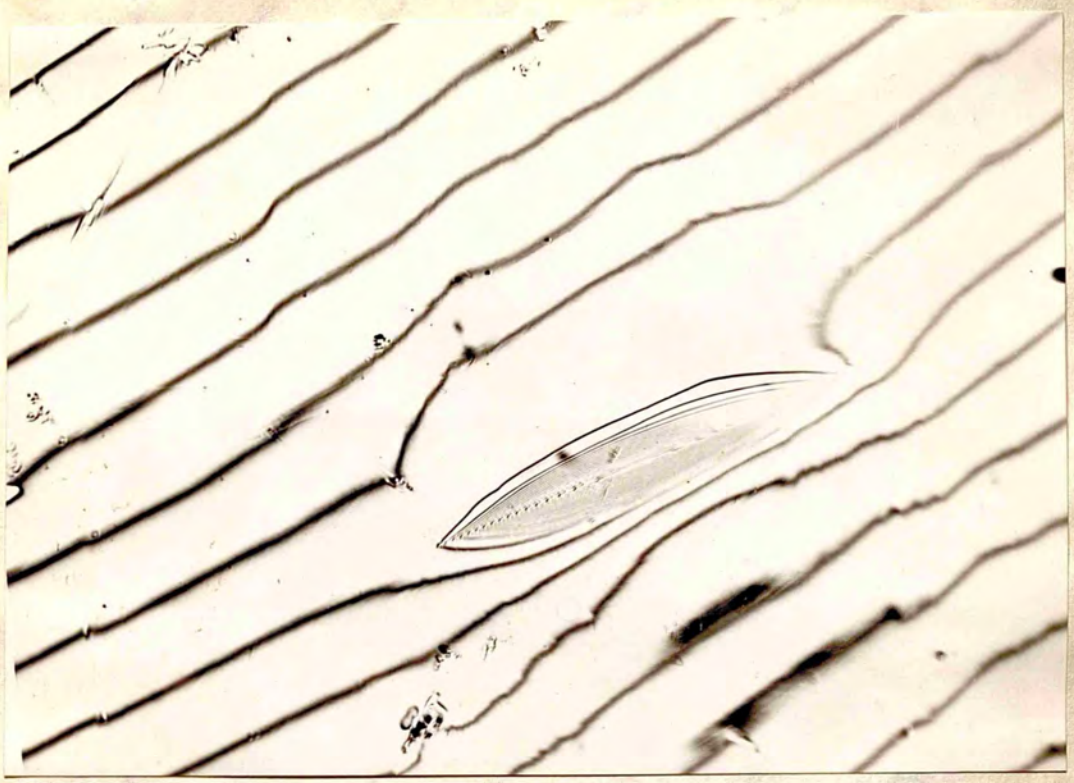

×150

Fig. 24

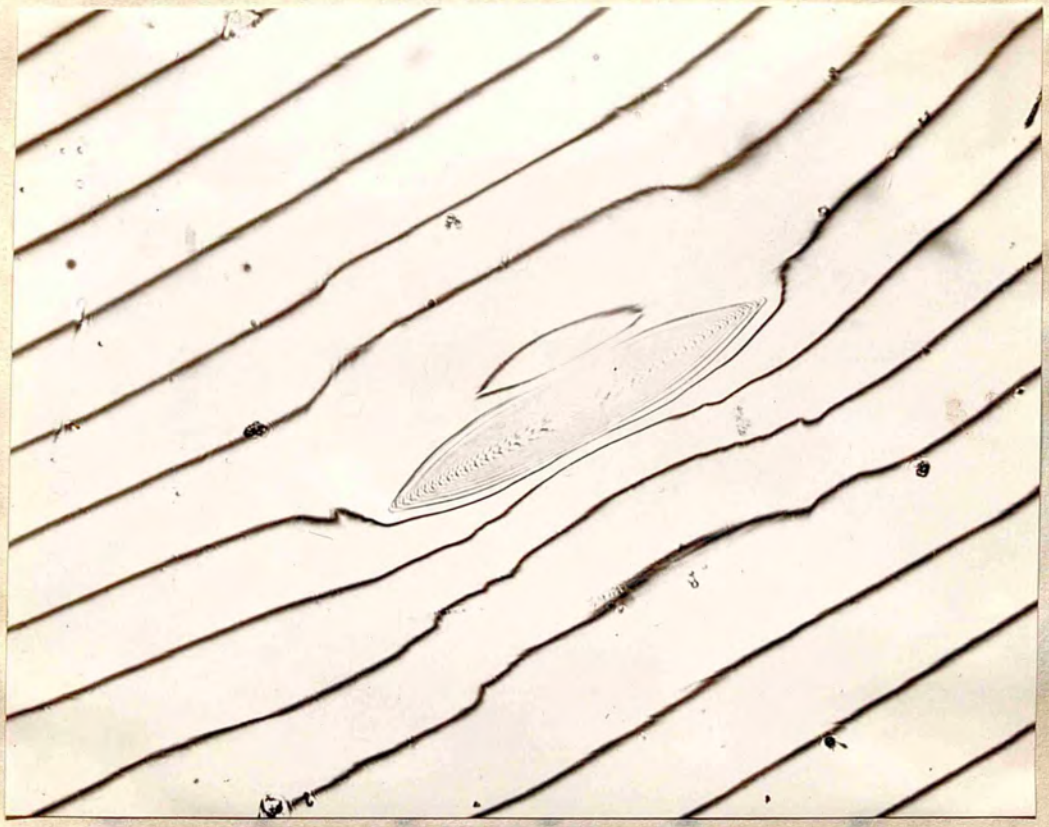

×150

Fig. 25

×150

Fig. 26

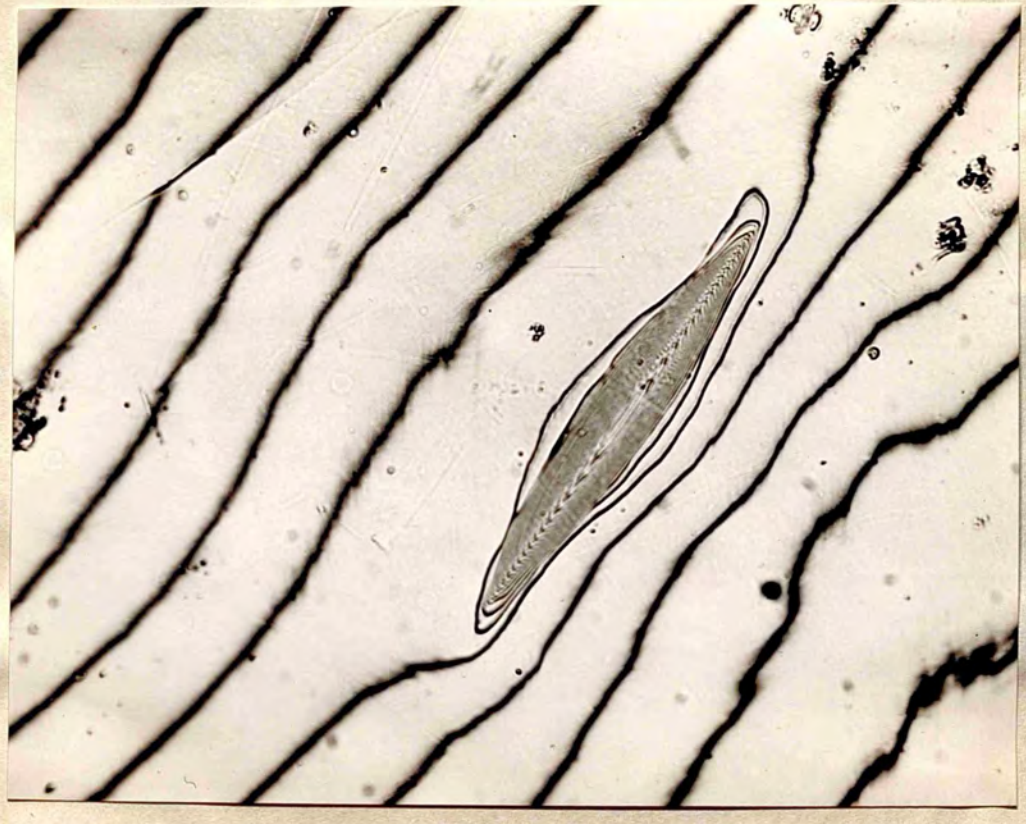

×150

Fig. 27

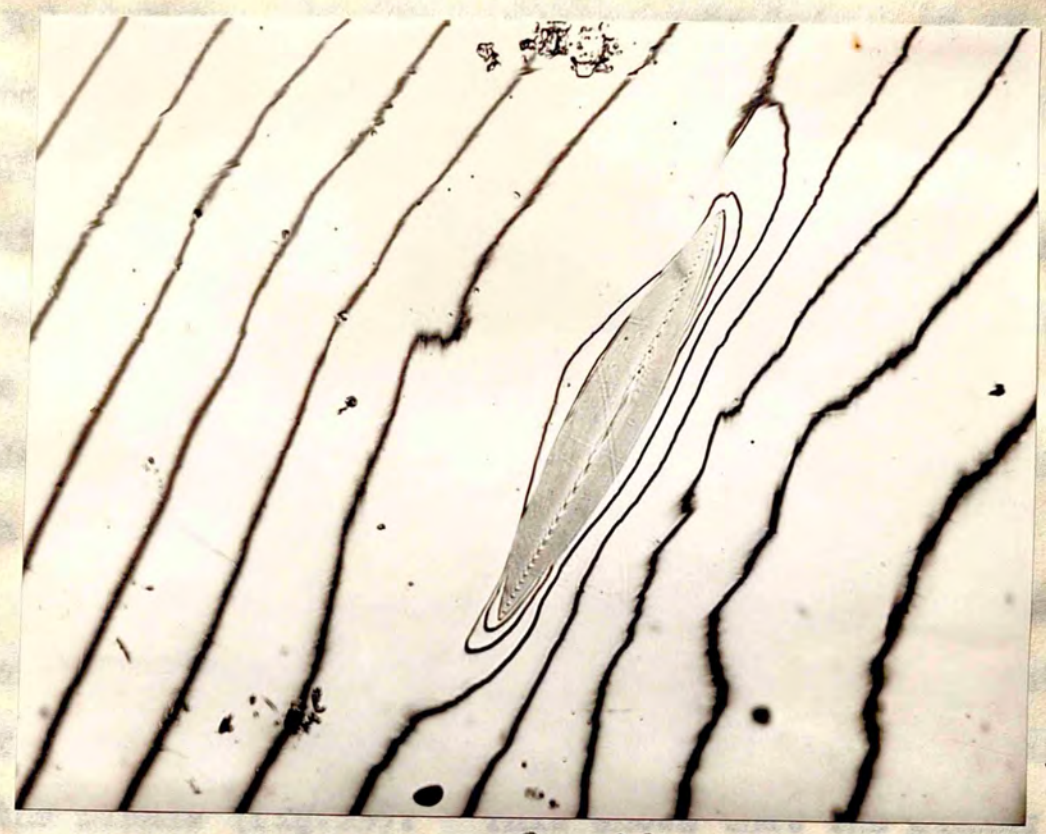

×150

Fig. 28

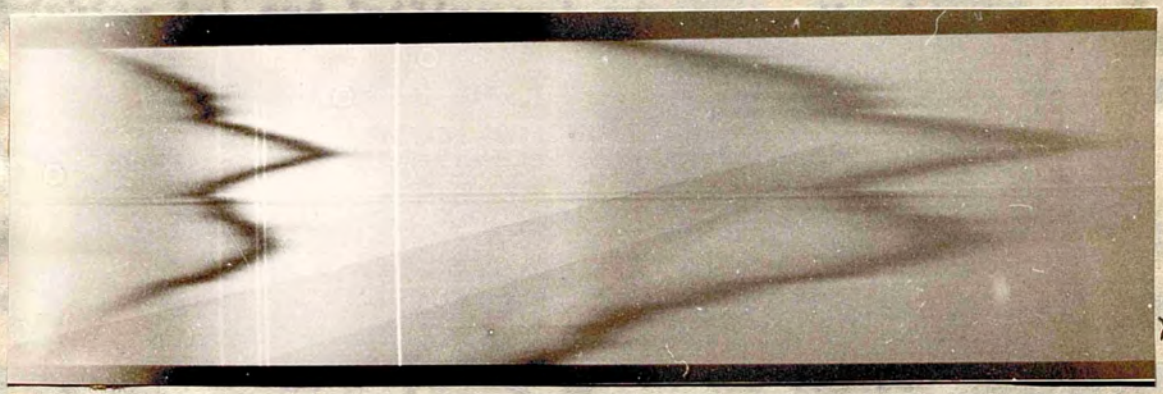

×105

Fig 29

more evenly distributed till the indenter makes an angle of 30° with the original position (fig.25). At 60° the fringe pattern is almost identical with that at 0° as one could anticipate from the sixfold symmetry of (0001) plane of zinc crystal and the fringe pattern repeats itself for further change in direction of the indentation. (In this chapter, the position of the indenter given in terms of degrees means that the indenter makes that much angle with the initial position of the indenter).

The fringes of equal chromatic order taken across a section parallel to the length of the indenter of fig.22, show the formation of two hills with a valley at the middle (fig.29). This shows that the piling up is in two directions inclined to the length of the indenter.

Close examination of the fringes within the indenter shows that at the centre there is a 'sinking in' and on either side of the centre 'piling up' is shown where the fringes move towards the indentation. In fig.(23) the 'sinking in' and 'piling up' are seen, the 'sinking in' moving further away from the centre. On the other side of the same indentation, the 'sinking in' and 'piling up' are in the same direction respectively as before. In fig.(25) there are two 'sinking in' directions on either sides of the centre position and a 'piling up' at the centre. In fig.(28) the same features as in fig. (22) are seen.

A system of fringes can be seen inside the indentations. The depth of the indentations can be accurately determined by counting the number of fringes inside each indentation. The depth was found to vary in the same manner as the length of the indentations. The fringes are visible only along the major axis, as the sides of the indentations along the minor axis were too steep for the fringes to be resolved.

The length of the indentations in each case was found out by taking a photomicrograph of the indented surface and then measuring the length by a travelling microscope reading correct to 0.0001 mm. The readings are given below :-

TABLE I.

Direction	Length mm. X105	Hardness No. Kg/Sq. mm.	Direction	Length mm. X105	Hardness Kg/Sq. mm.
0	33.513	17.05	90	32.197	19.21
10	33.019	17.80	100	32.894	18.02
20	32.000	19.58	110	33.164	17.79
30	31.918	19.72	120	33.465	17.12
40	32.072	19.45	130	33.132	17.64
50	33.055	17.75	140	32.477	18.72
60	33.564	16.97	150	32.390	18.88
70	33.154	17.62	160	32.599	18.50
80	32.612	18.50	170	33.052	17.77

The variation in hardness with direction is best shown by the polar plot (fig.30). The radial distance from the centre represents the hardness measured in this

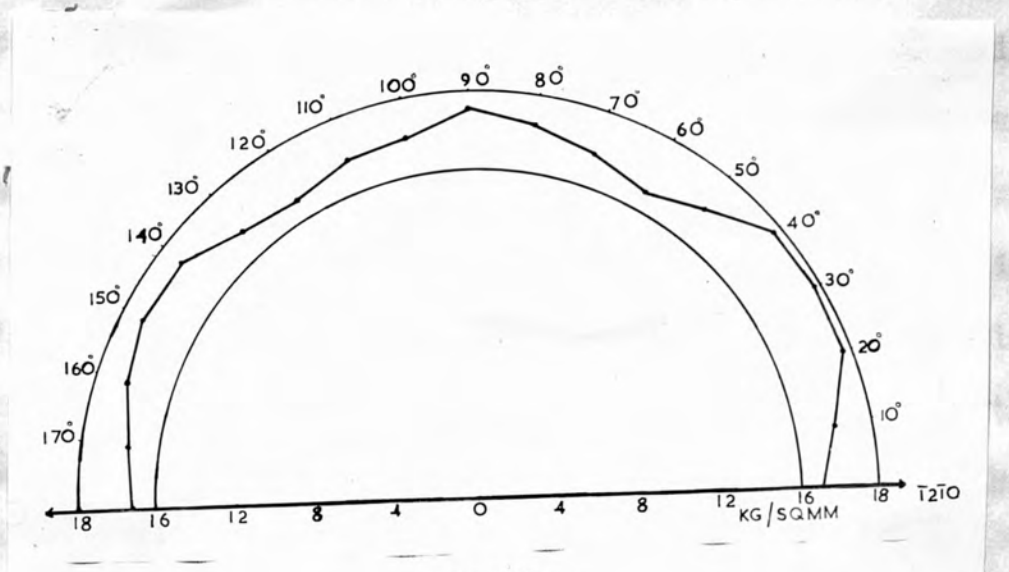
90°
100°
110°
120°
130°
140°
150°
160°
170°
80°
70°
60°
50°
40°
30°
20°
10°
18
16
12
8
4
0
4
8
12
16
18
KG/SQMM
T2T0

Fig. 30.

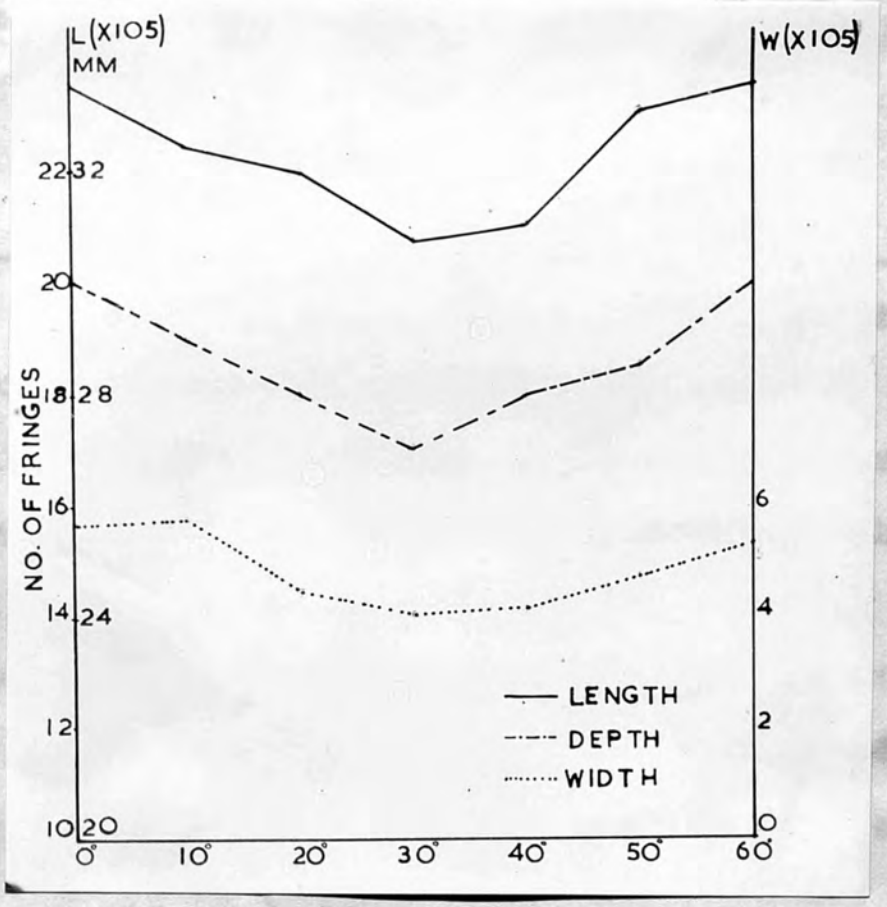
L(X105)
MM
W(X105)
NO. OF FRINGES
22.32
20
18.28
16
14.24
12
10.20
6
4
2
0
0°
10°
20°
30°
40°
50°
60°
LENGTH
DEPTH
WIDTH

Fig. 31

direction on the crystal face. The curve very nearly forms one half of a regular hexagon, with the initial direction bisecting the hexagon. The values of hardness are maximum when measured along $[\bar{1}10]$ and its family of directions. This means that the direction of minimum hardness is measured along the close packed direction. The values for the depth (as measured by counting the number of fringes inside) and the width are given below.

TABLE II.

Direction	Width in mm. X105	Depth No. of fringes
0	5.637	20
10	5.562	19
20	4.464	18
30	4.015	17
40	4.130	18
50	4.723	$18\frac{1}{2}$
60	5.283	$19\frac{1}{2}$

Fig.(31) shows the variation of depth and width, following similar variations to those occurring in the length. The fringes inside the indentations are of the 'Newton's rings' type along the major axis of the impression as can be seen from the graph (fig.32), showing a linear relation between the squares of the measured diameters D of the fringes and the number of fringes counted from the centre of the indentation. The radius of curvature was

found to be of the order of 3 mm. But the radius of curvature of the indenter as measured by Grodzinski is 2 mm. which means that considerable elastic recovery has taken place in the depth of the indentation after removal of the indenter.

5•2 Analysis of the deformation.

Daniels and Dunn (1949) made a study of the variation of Knoop hardness on single crystals of silicon ferrite and zinc. Assuming that the force exerted by the indenter was acting parallel to the line of greatest slope of the facet of the indenter, they calculated the resolved shear stress on the slip plane along the slip direction and found apparent agreement between the reciprocal of the hardness value and the value of the shear stress for different orientations of the indenter, in all cases except for the basal plane of zinc. Miebs in a note following the paper pointed out that the force direction normal to the face would be more reasonable. Tolansky and Williams (1955) studied the directional hardness with a double cone indenter on virgin faces of cast single crystals of tin and bismuth. Williams in the appendix following the paper has shown consistent agreement between the reciprocal of the hardness value and the value of shear stress when the force direction was taken normal to the faces. If F is this force acting and ϕ the angle between F and the normal to the plane and λ,

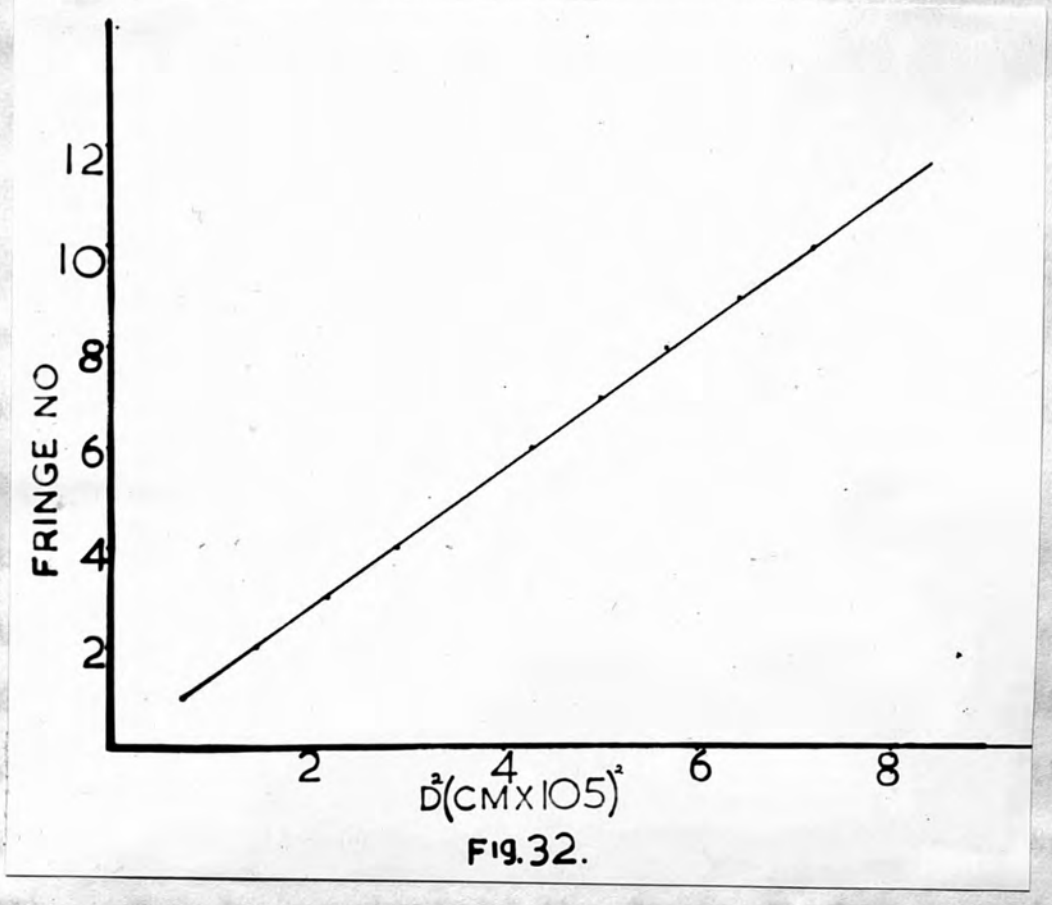

Fig. 32.

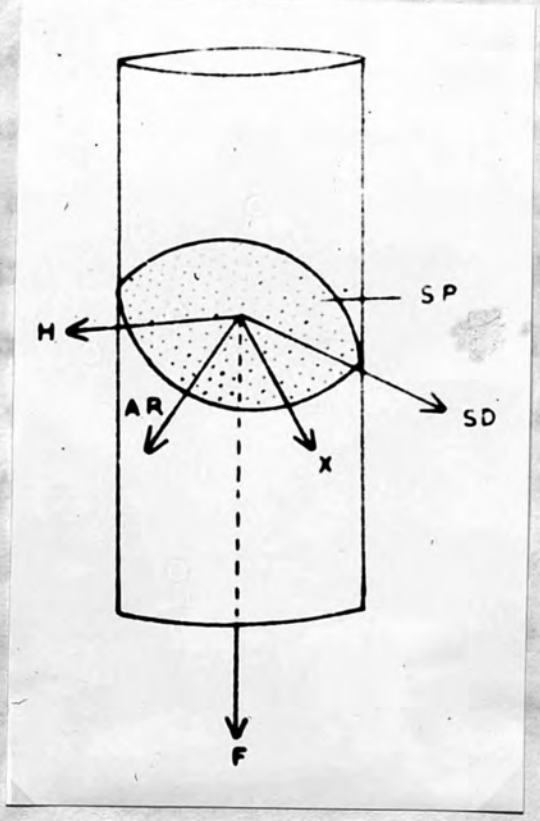

Fig. 33

the angle between F and the slip direction, then the resolved component of the force in the slip plane along the slip direction is $\frac{F}{A} \cos \phi \cos \lambda$ (Barrett 1943). A correction factor for the presence of a constraining force on the slip due to the indenter which Daniels and Dunn calculated was also added to the abovd equation. Consider the deformation of the metal to be due to the compression of long parallelepiped elements whose long axes lie parallel to and along the direction of the force F causing the deformation and as each element elongates by slip there is a constraint on the lattice. A particular slip plane will tend to rotate about an axis A R in the slip plane S P and perpendicular to the slip direction S D (fig.33). Due to constraints the force F has a maximum rotational effect about an axis H perpendicular to F and parallel to the length of the indenter. If ψ is the angle between the two axes, then the larger this angle, the less will be resolved shear stress effective in promoting deformation. So a modifying function which would decrease the resolved shear stress as ψ increases from o to 90° is $\cos \psi$ and hence the effective resolved shear stress is

$\frac{F}{A}$ cos λ cos ϕ cos

The value of cos λ cos ϕ cos λ varies as the orientation of the crystal with respect to the indenter is changed and is therefore a function of θ between the long

diagonal of the indenter and the index line on the specimen. $\frac{F}{A}$ was assumed constant as the load was the same throughout. The angles ϕ, λ and ψ for each position of the indenter were calculated with the aid of a stereographic projection of the crystal and the indenter using the crystal face as the plane of projection. The crystal face and the slip plane were the same, and from the directions of twin trace, A R, S D were found. The positions are shown in the stereographic projection (fig.34). Since the angle of the wedge of the double cone in the width direction is 154° (as given by Grodzinski 1952.), the angle between the directions of F and F' is 26° and the positions of F and F' as the indenter rotates are on a small circle with the centre of the projection as its centre and radius equivalent to 13° on the Wulff net. Hand H' were taken at the ends of the diameter of the projection in the direction of the long diagonal of the indenter (the angle of the indenter along the major axis is 177° from a measurement of the fringe inside the indentation).

The initial position of the indenter is parallel to one of the slip directions. A R is the direction perpendicular to this direction. The constraining factor which is cos ψ is zero since ψ = 90°, (ψ = the angle between the position of H and A R) and the resolved shear stress at this position is a minimum and hence the deformation

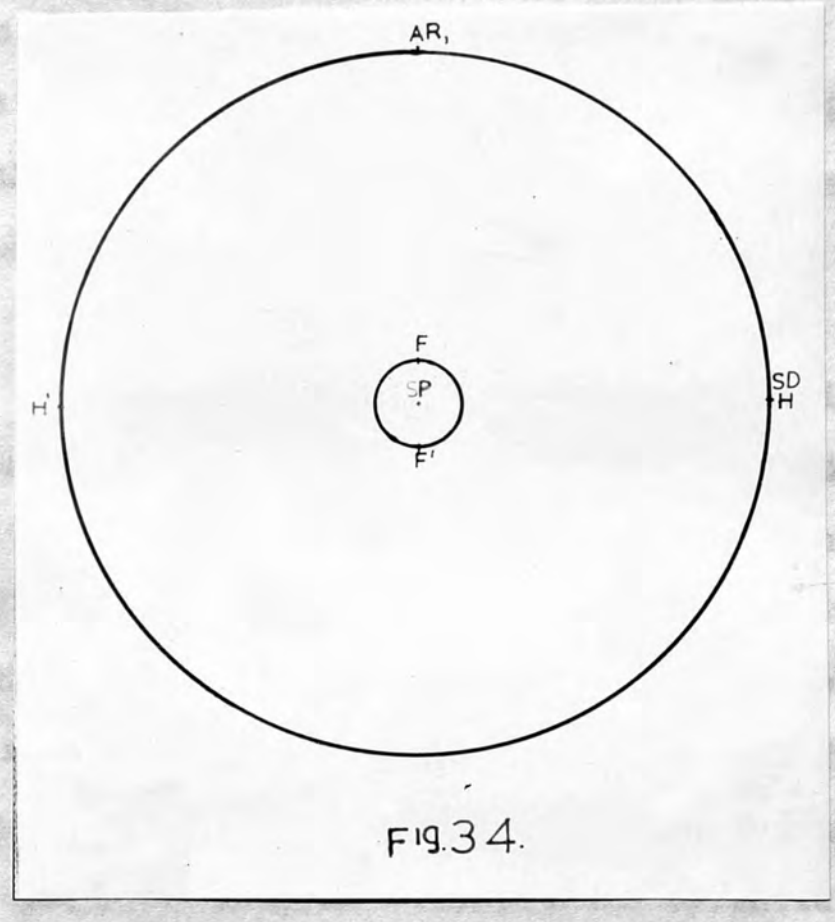

Fig. 34.

produced by the indenter as measured by the length of the indenter should be a minimum. Rotation of every 60° of the indenter is along a slip direction and hence there is a minimum value of shear stress resolved along the slip plane in the slip direction at each of these positions.

This is not in agreement with the experimental results. The polar plot of variation of hardness with direction (fig.30) shows that the hardness is a minimum along the directions of slip. Disagreement between the reciprocal of the Knoop hardness and shear stress curve is also reported by Daniel and Dunn in the case of (0001) plane of zinc.

An attempt is made to explain this discrepancy in the light of the distortions formed around the indentation. Figs.(35 to 41) show a whole series of phase contrast photographs of the indentation corresponding to the interferograms of fig.(22 to 28). These traces were not visible under ordinary microscopy; careful phase contrast adjustment was necessary to obtain these photographs. The traces show a definite chrystallographic orientations oriented along six directions. When the indenter is along $[\bar{1}2\bar{1}0]$ directions, traces along two pairs of directions $[01\bar{1}0]$ and $[\bar{1}100]$ are more prominent than the third pair $[10\bar{1}0]$ though at the tip of the indenter these traces can also be seen. When the

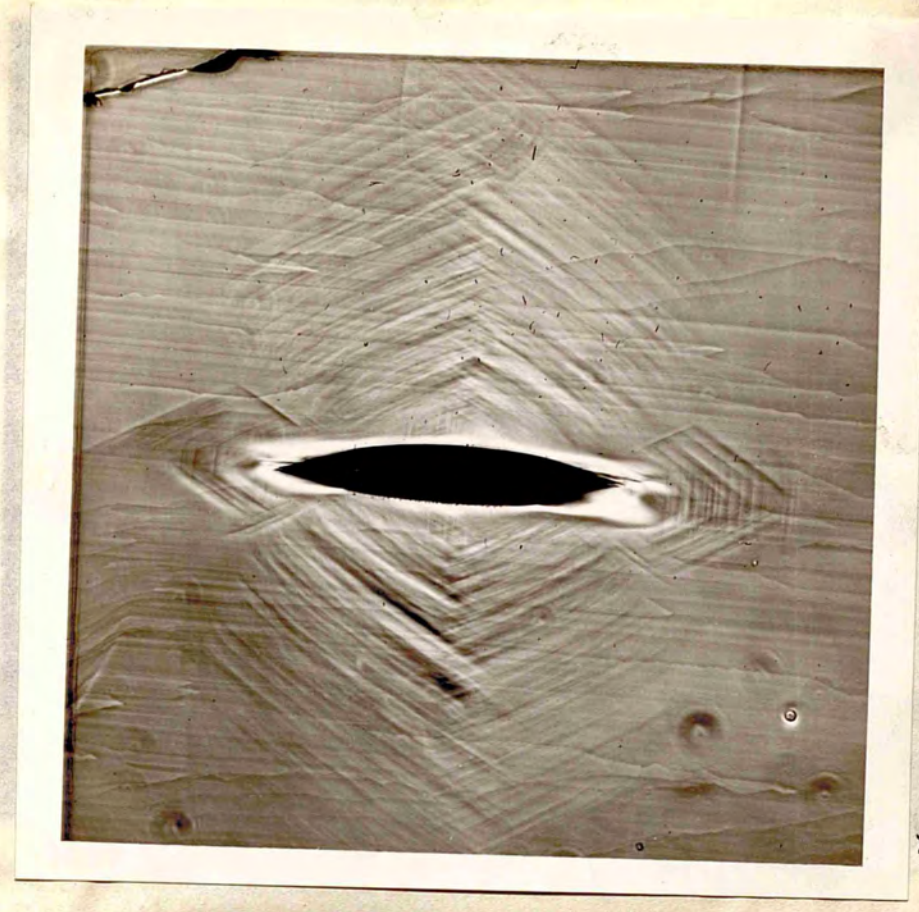

Fig. 35

×150

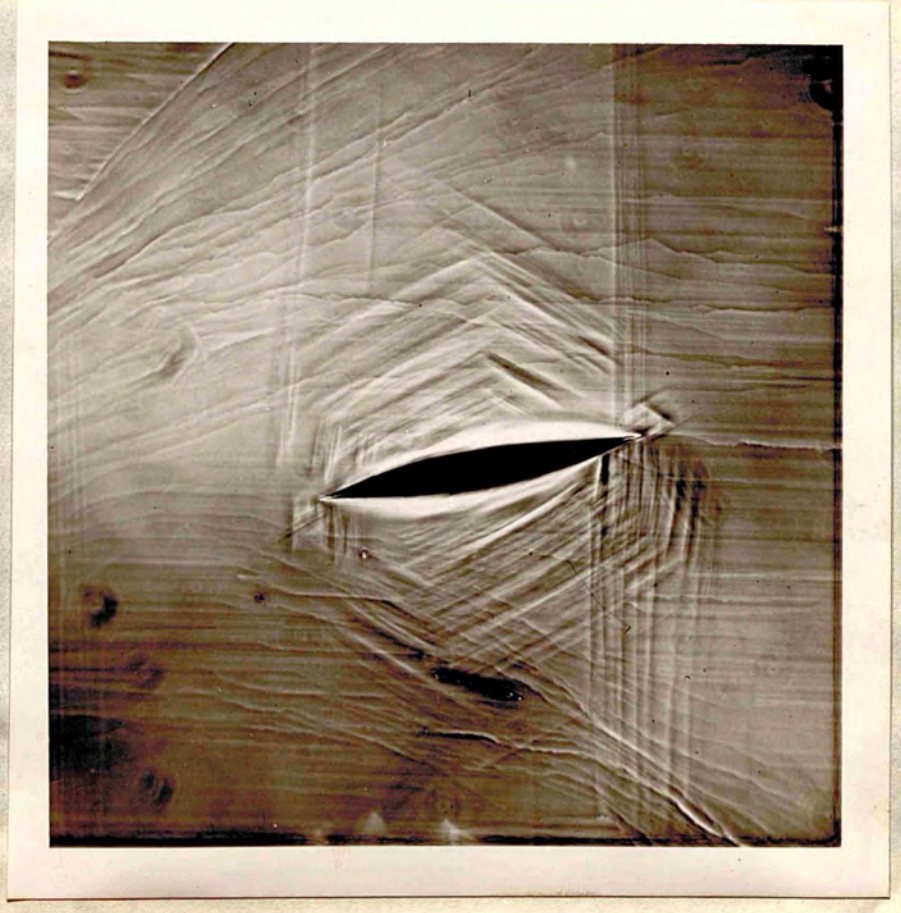

Fig. 36

×150

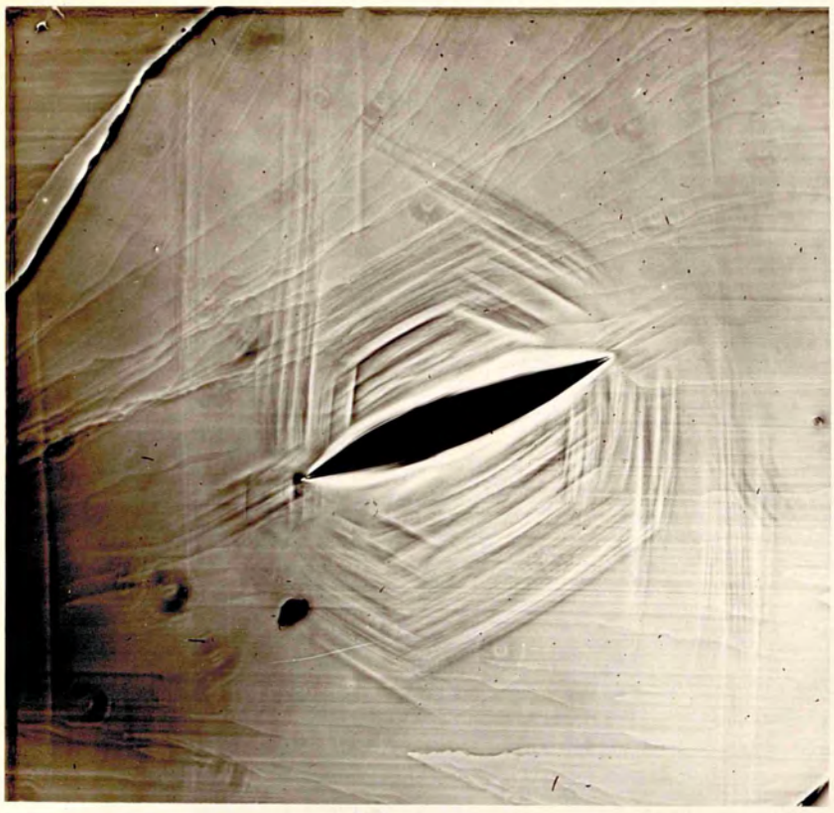

Fig. 37

×150

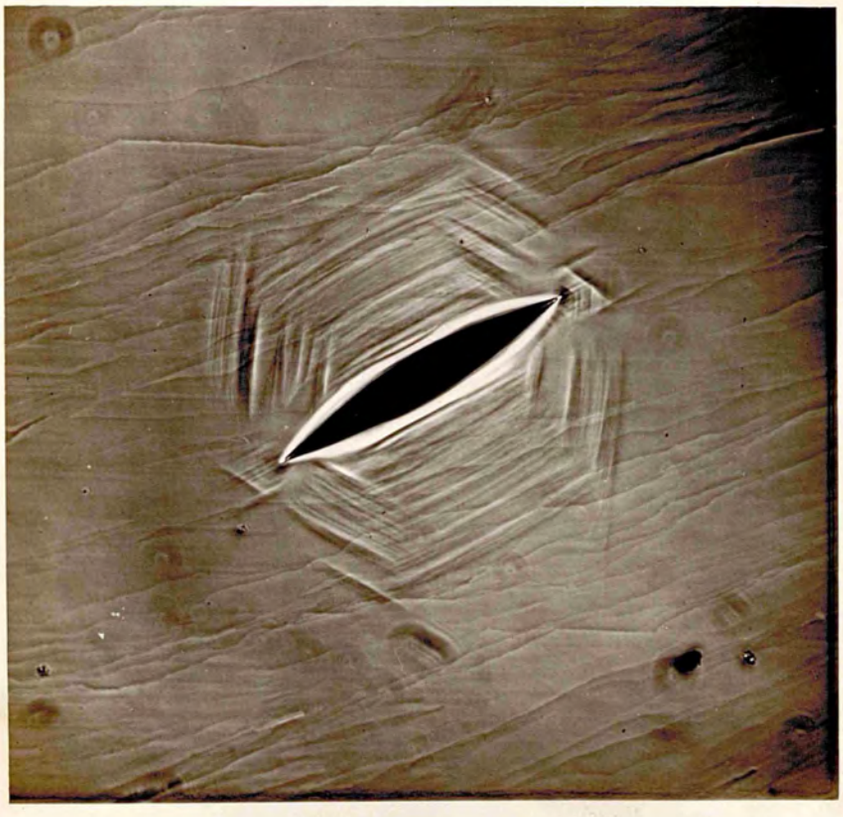

Fig. 38

×150

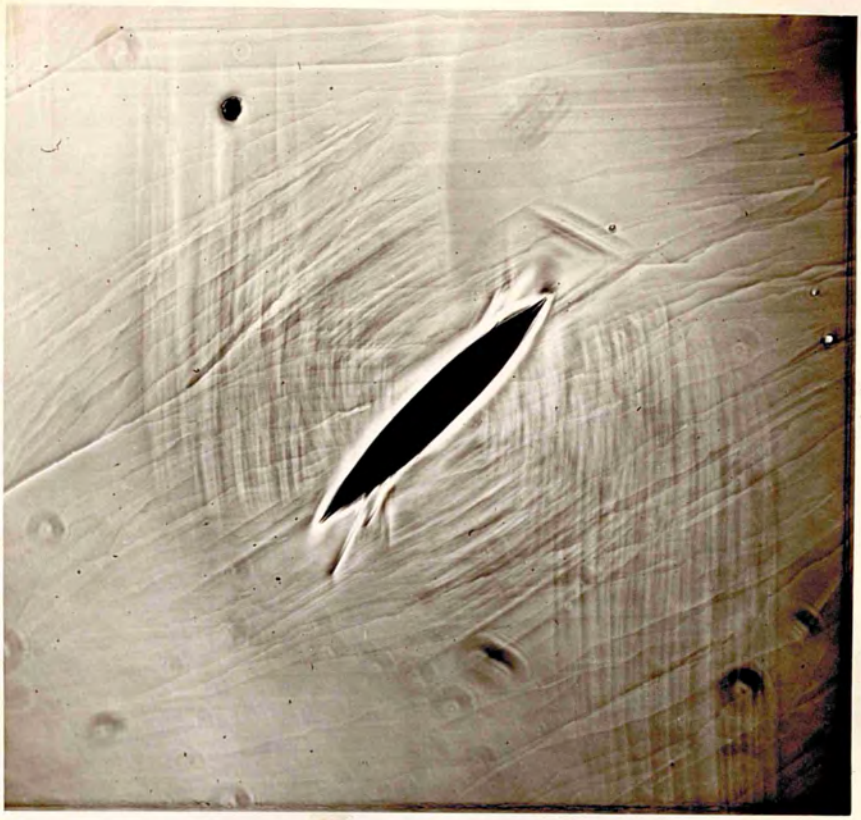

Fig. 39
×150

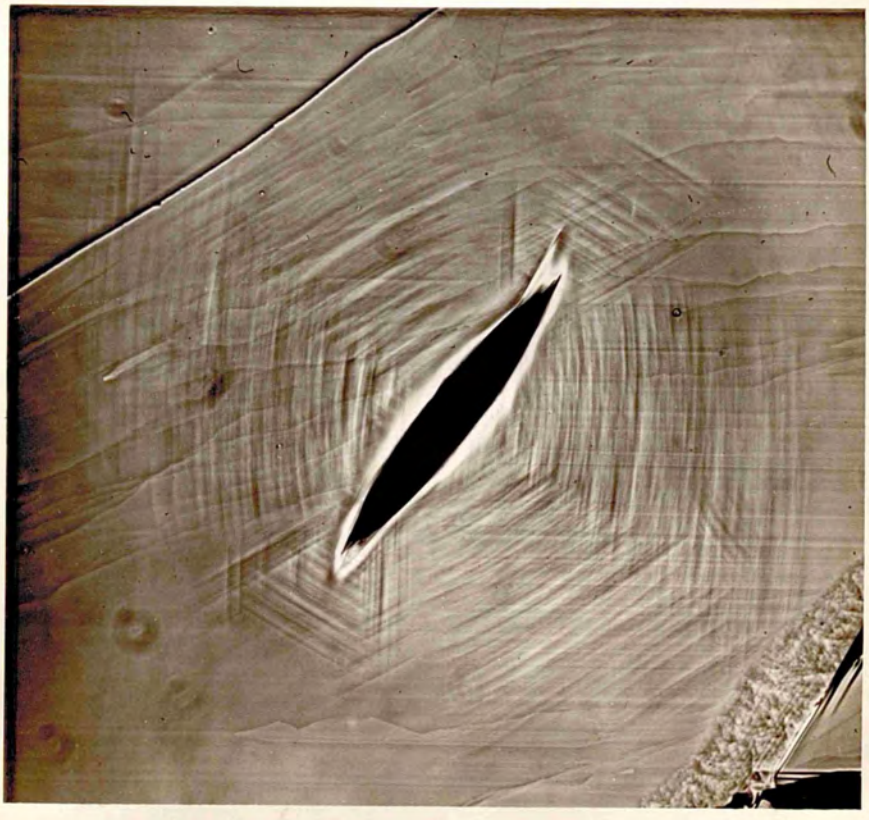

Fig. 40
×150

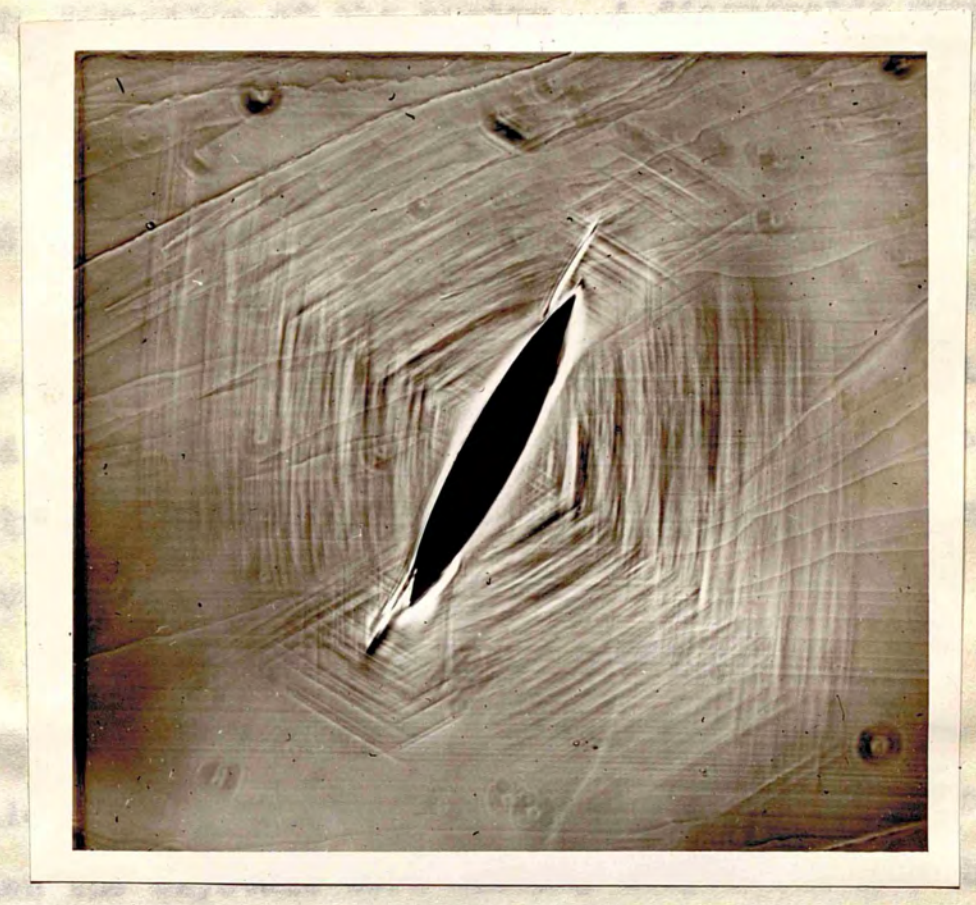

x150

Fig. 41

direction of indentation is turned, the traces which are not prominent before become more and more prominent till it reaches a position 30° to the initial position and there the six directions are equally prominent. The pattern is repeated at 60° degree to the original position, i.e. when the length of the indenter is along the next slip direction of the system. A diagramatic representation of the traces, with respect to the indenter and the hexagonal symmetry of the basal plane, at positions 0° and 30° are shown in figs. 42 and 43 respectively.

These traces are due to kinking, a mechanism first reported by Orowan (1942) and later by Jilson (1950) and some others. Single crystal wires of zinc or cadmium extremely soft in general are as hard as pollycrystalline wires when the slip plane is nearly parallel to the axis of the wire such that the slip mechanism cannot work in extension or compression. Orowan attempted to operate glide mechanism in cadmium crystals of such orientation, when the crystals were axially compressed and when the load increased, and he found that they suddenly collapsed by forming peculiar kinks with sharp edges and he classed this kinking along with slip and twinning as one of the three fundamental mechanisms of deformation in metal. Jilson suggested "that this phenomenon, manifested in bending, rumbling, buckling or kinking and probably in other forms

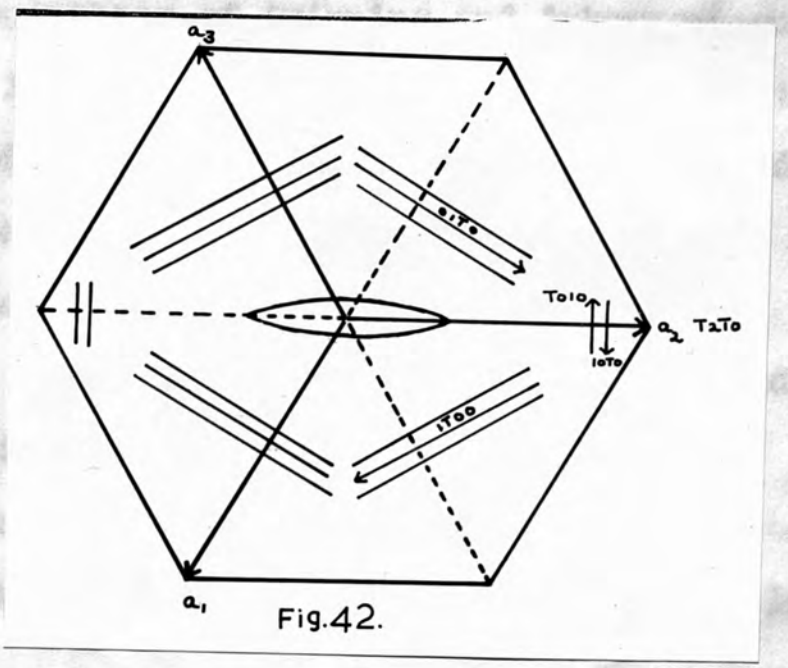
a3
0110
T0T0
a2 T2T0
10T0
1100
a1
Fig.42.

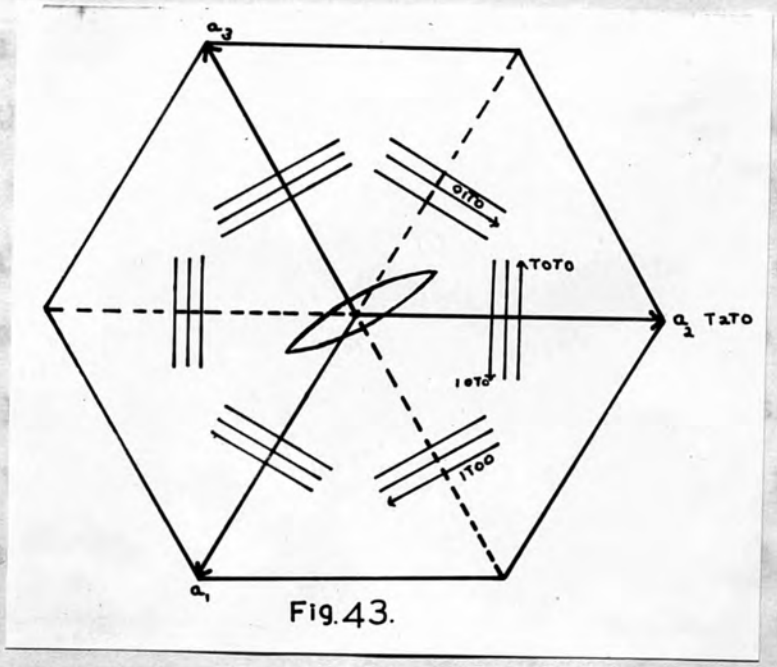
a3
0110
T0T0
a2 T2T0
10T0
1100
a1
Fig.43.

may be the essential difference between the apparently homogeneous shear of twinning and inhomogeneous shear observed in gliding or slip process.... In other words bending of the slip plane may be the more fundamental phenomenon and inhomogeneous shearing of slip may be a consequence."

Washburn and Parker (1952) produced kinking in zinc single crystals deformed in tension. They suggest that a non-uniform distribution of flow produced by or combined with constraints are the conditions leading to kinking.

Considering the deformation around the indentation, the piling up is in a direction at right angles to the kink traces. The material had been pushed up in the direction of slip and the bending had taken place about an axis in the slip plane perpendicular to the slip direction. The kink traces on a microscopic scale were formed, which were parallel to this axis. The fringes of equal chromatic order taken across a section perpendicular to these traces show the piling up. Fig.(44) shows the section when the indenter was along the initial direction and fig.(45), when the indenter was at 30°. The profile of the deformation at these two positions are shown graphically in figs.(46 & 47) respectively. The original level is shown by means of broken lines. At 30° position the material sinks in

×175

Fig. 44

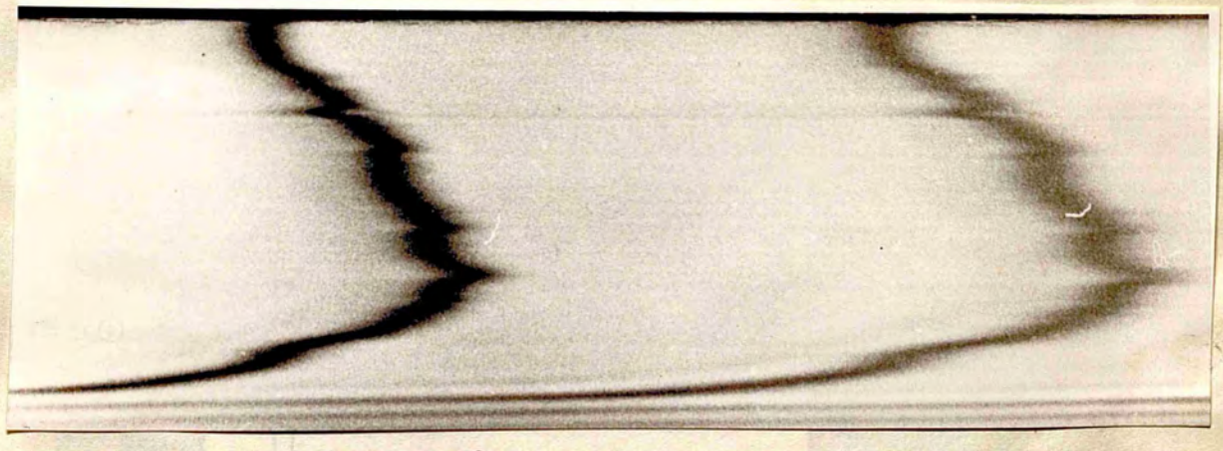

×175

Fig. 45

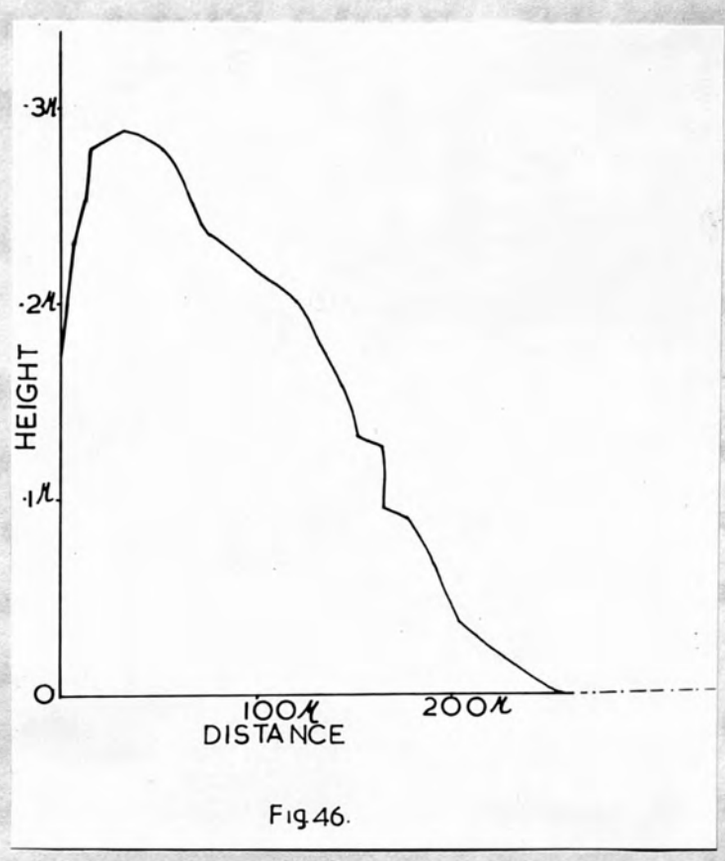
·3ft
·2ft
·1ft
O
HEIGHT
100ft
200ft
DISTANCE

Fig.46.

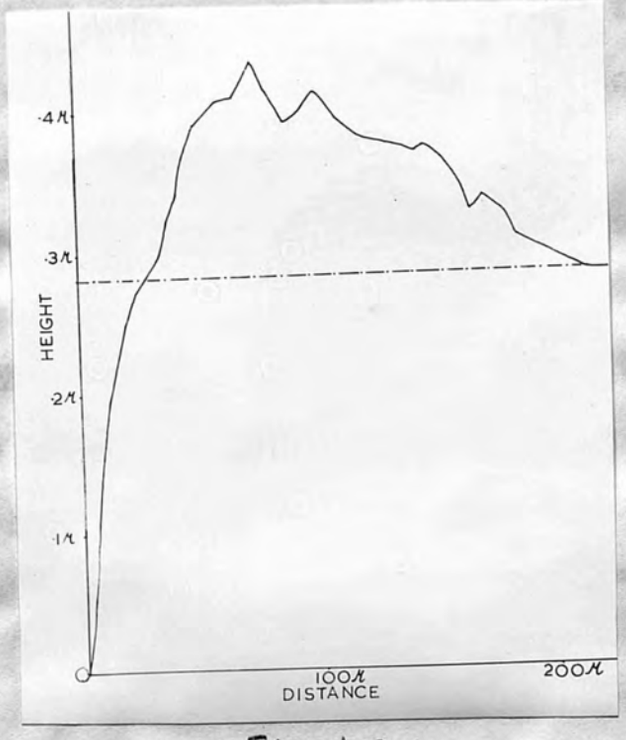
·4ft
·3ft
·2ft
·1ft
HEIGHT
100ft
200ft
DISTANCE

Fig. 47

below the original level very near the indenter and piles up away from the indenter. This sinking in can be noticed on either side of the centre of the indenter. The amount of piling up is also very much smaller than the zero position.

The kink traces extend much farther on either side of the indenter at 0° position than at 30° position. Taking the forces into consideration and assuming that the force is acting at the centre, then at 0° position, the components of this force will be acting along the two directions perpendicular to the kink traces since they are the directions of maximum piling up. When the indenter is at 30° position, the force acting at the centre is along the direction along which the deformation is taking place and hence should favour for more extensive deformation. The observations are completely contrary to expectations. Even if it is assumed that kinking is a sort of restraint to slip or any other type of deformation, then the lesser the extent of kink traces, the greater should be the deformation.

The indentations are not geometrically similar for the same load in different directions as can be seen from these photographs. Though the force is maximum at the centre and decreases towards the edges, depending on the

position of the indenter, the material may be pushed greater or less in one direction than in another. The anisotropic effect is seen in the width direction also.

There is one important observation which Daniel and Dunn had not mentioned. When the indenter was at 0°, invariably in all cases micro twins were seen on either side at the tips of the indenter whereas at 30° there was no evidence of micro twinning. This means that 0° degree position is most favourable for the formation of twins. It can be said that the stress is relieved at this position by the formation of twins and hence a maximum deformation at this position. This is a very plausible explanation for the discrepancy between the resolved shear stress curve and the reciprocal of the hardness. Tolansky and Williams (1955) found that twinning had no effect on the hardness curve of bismuth. It should be understood that unlike the present case, deformation by slip was the primary mechanism and twinning was only a secondary phenomenon.

5·3 HIGH-DISPERSION FIZEAU FRINGES.

Figs.(48, 49, 50) show the surface structures for indentations at 0°, 30° and 60° respectively. These are very high dispersion Fizeau fringes. If the wedge angle is reduced so that the two surfaces are as nearly parallel as possible with the residual angles still

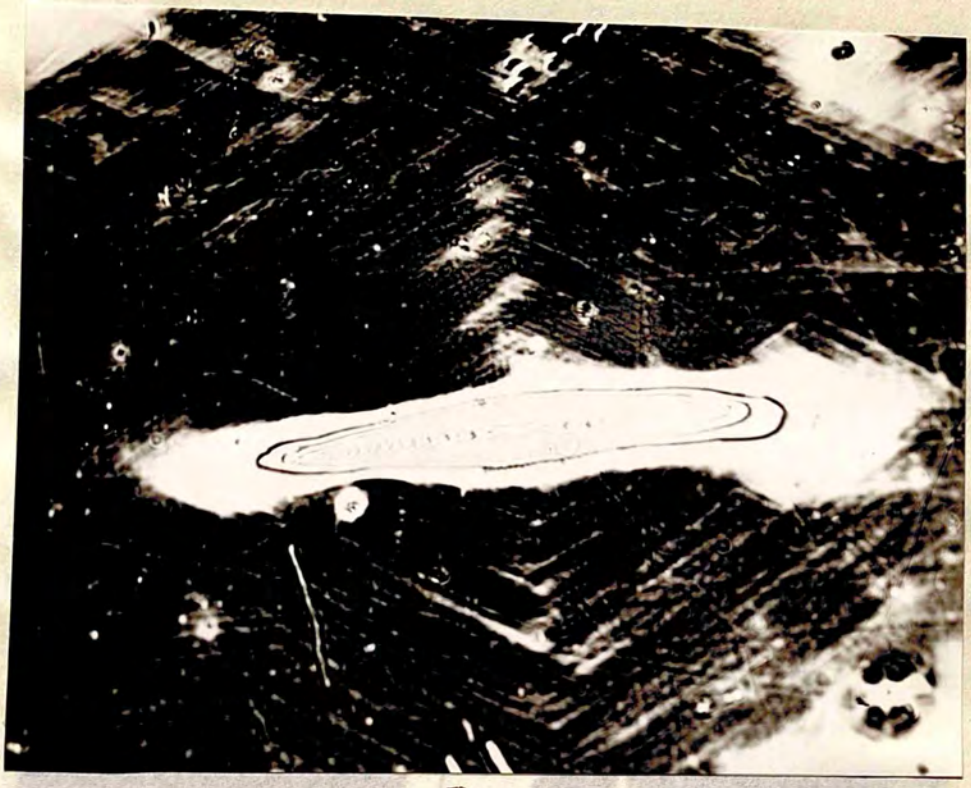

x150

Fig. 48

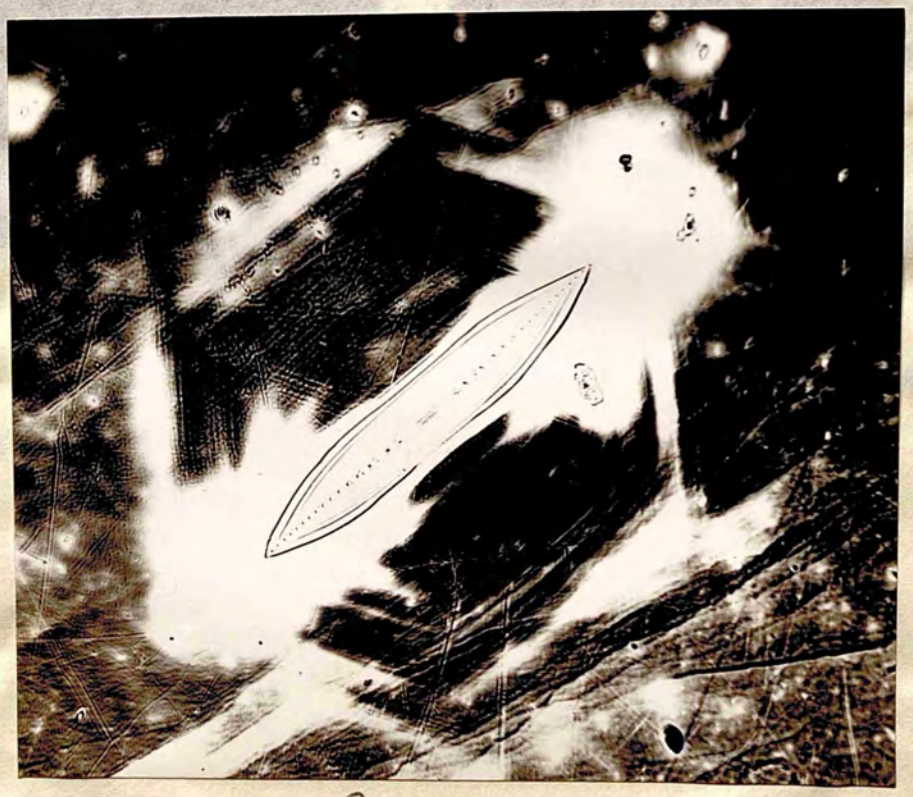

x150

Fig. 49

×150

Fig. 50

remaining due to inherent topographical features, a high dispersion pattern results showing a complete picture of the surface revealing with high contrast minute structural details. It is not always possible to obtain any quantitative information about the heights (depths) of features from such a picture. However an area of uniform tint means that such an area is of uniform height (depth) to within a very small fraction of a light wave. Tolansky and Wilcock (1946) have shown theoretically that a 10 per cent change in intensity is produced by a change in depth of 5 A Units in the case of transmission fringes of R = 0.90.

It can be shown that in the case of reflection fringes, such very high dispersion fringes is a powerful method for detection of changes in thickness of the order of 10 A units. The uniform tint of intensity is determined by the distance between the plates in accordance with the Airy formulae maxima occurring at $n\lambda = 2t$ where n is an integral. The fringe shape is such that the maximum tint-change sensitivity to a change in thickness occurs if t is selected such that approximately half the peak intensity is within the field of view.

Therefore $I_R = \frac{1}{2} I_{R\,(Max)}$

$$I_R = \frac{4R \sin^2 \frac{\delta}{2}}{(1-R)^2 + 4R \sin^2 \frac{\delta}{2}} \quad \text{(Airy's formulae)}$$

where $\delta = \frac{4\pi t}{\lambda}$

when $\sin^2 \frac{\delta}{2} = 1$, This is a maximum.[15]

$$I_{R(Max)} = \frac{4R}{(1-R)^2 + 4R}$$

Therefore $$\frac{4R \sin^2 \frac{\delta}{2}}{(1-R)^2 + 4R \sin^2 \frac{\delta}{2}} = \frac{1}{2} \left\{ \frac{4R}{(1-R)^2 + 4R} \right\}$$

Supposing a 10 per cent change in tint intensity is produced by a change of t to t' corresponding to a new value δ' (where $\delta' = \frac{4\pi t'}{\lambda}$)

Then $$\frac{4R \sin^2 \frac{\delta'}{2}}{(1-R)^2 + 4R \sin^2 \frac{\delta'}{2}} = \cdot 45 \left\{ \frac{4R}{(1-R)^2 + 4R} \right\}$$

If R = ·7 which is usually used for sharp and contrasty fringes, the value of t - t' = 14 A units. Thus by selecting the correct value of t a change of ± 14 A.U. in the topographical height can be detected.

As a 10 per cent change in intensity is readily recognizable, the method is very useful in revealing minute

structural details. The individual kink bends can be easily detected from these high dispersion fringes. Yet the interferogram as it is cannot be interpreted safely.

5·4 VICKERS PYRAMID INDENTATIONS.

Pyramid indentations were also made on these crystals to study the nature of deformations around it. In the case of the pyramid, though an absolute study of the directional variation of hardness could not be made, the anisotropic nature of the metal could be easily detected. It has long been established that in the case of the square pyramid, the maximum force acts at the centre and gradually decreases towards the edges and the "pin cushion" and "barrel shaped" indentations are formed in annealed and work hardened material respectively. Tolansky and Nickols (1952) made an extensive study of pyramid indentations on isotropic as well as single crystals. The single crystal studied was tin (99.992% purity) prepared by casting the molten metal on a polished glass plate. The impression they obtained after a pyramid indentation was of irregular shape, two opposite sides being convex and two concave. In accordance with O'Neill's principle of simple geometrical considerations assuming the metal remained in contact with the diamond, the convex sides should correspond with the piled-up regions whilst the concave sides were those which had sunk in. But in the case of sintered

Fig. 51 ×250

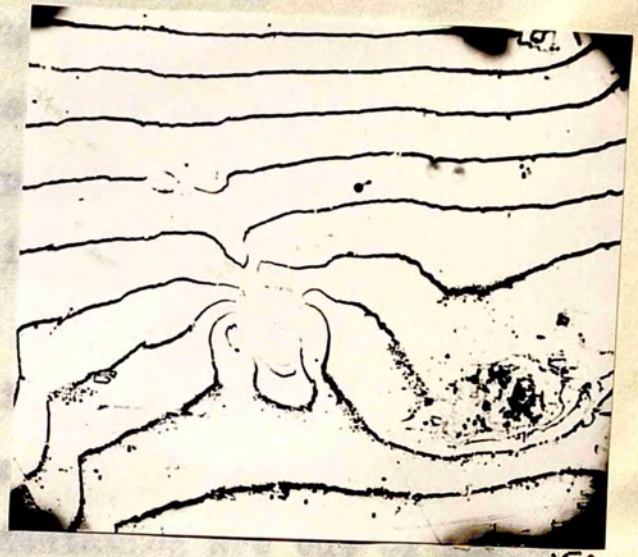

Fig. 52 ×50

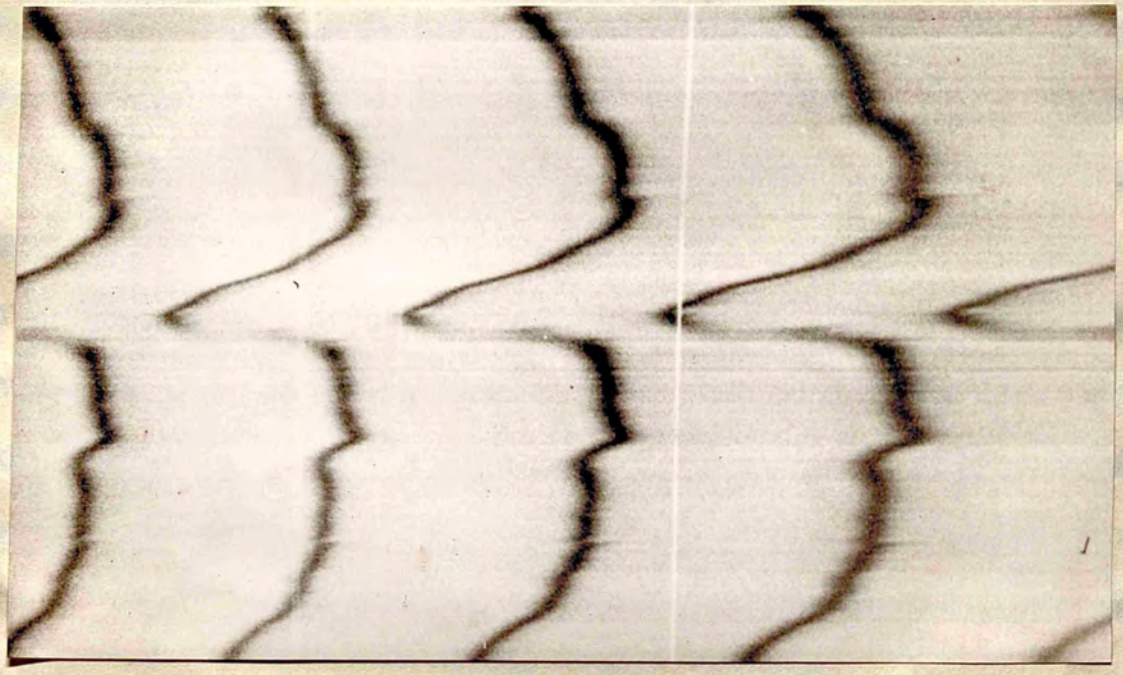

Fig. 53 ×210

tungsten carbide, a small scale piling up with concavity was observed.

Fig.(51) shows a pyramid indentation on zinc (0001) face with 100 gm. load. The indentation is not symmetrical. The concavity is clearly seen. The concavity is purely crystallographic and depends only in a secondary manner on the particular orientation of the pyramid. Fig.(52) shows the Fizeau fringes over the impression. A striking asymmetry is evident. Since the Feussner surface of fringe localization being at some distance from the metal surface the edges of the indentation are out of focus when the fringes are in focus. There is a 'sinking in' at the two diagonally opposite ends. Unlike indentations produced on isotropic media, the distortion projects beyond the diagonals. The shift of the straight fringe on the left towards the tip of the diagonal end, shows that there is a depression. It should be understood that this fringe is farther away from the actual indentation. The fringes of equal chromatic order taken across this position (Fig.53) shows this 'sinking in' effect. The fringes of equal chromatic order taken across the two concave sides is very revealing (Fig.54). Here the material rises rather abruptly from the inside of the indentation and falls off gradually, the height above the original level being of the order of 1100 A units. Hence as in the case of sintered Tungsten

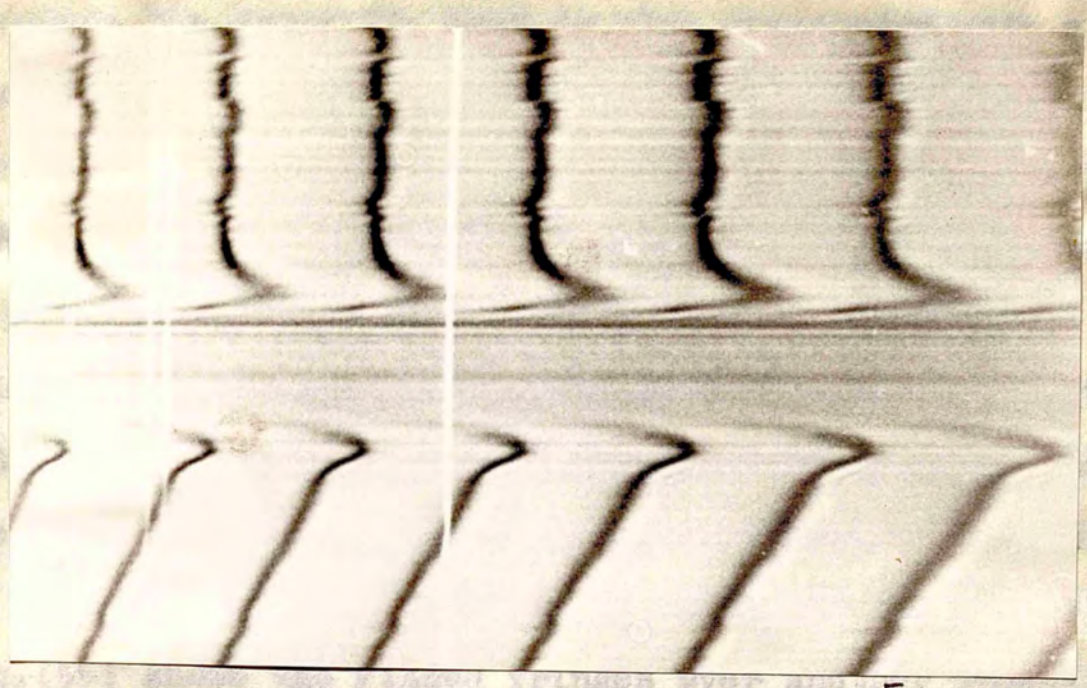

×210

Fig. 54

×150

Fig. 55

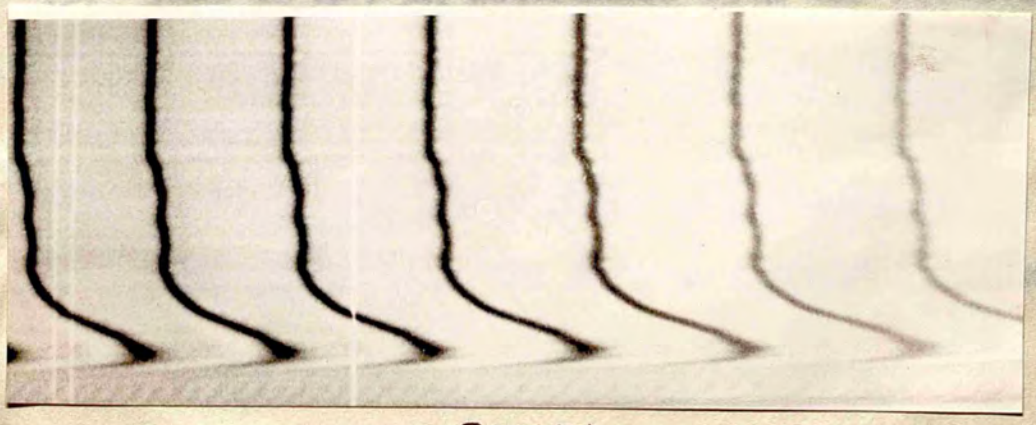

×210

Fig. 56

carbide, the concavity here is also associated with a small scale piling up. It has already been seen from the shape of the double cone indentations that there is a marked recovery after the indentation. The directions of maximum deformation recover more than the others. Hence along these directions of maximum deformation, there occur the piling up and when the indenter has been removed, the material recovers back producing concavity. Thus there is the simultaneous occurring of piling up and concavity. Fig.(55) shows the Fizeau fringes over another indentation. The fringes of equal chromatic order (Fig.56) taken across one of these concave sides shows again the short scale piling up. The position of the indenter was such as to produce a more symmetrical impression than in the former case.

5·4 SUMMARY OF RESULTS.

(1) The anisotropic nature of the crystal plane is fully revealed.

(2) The hardness as measured along the close packed direction is a minimum.

(3) This is not in accordance with the resolved shear stress on the slip plane in the slip direction.

(4) At positions where minimum hardness is measured, microtwins are formed very near the ends.

(5) Concavity due to small scale piling up is also revealed.

(6) The formation of kink traces on a microscopic scale is better revealed than ever before.

Xray examination of these kink traces before and after a heat treatment shows a very interesting phenomenon and will be described in the next Chapter.

CHAPTER VI.

X-RAY EXAMINATION OF ZINC CRYSTALS

6·1 SETTING OF THE CRYSTAL.

A unicam single crystal goniometer was set up. In order to get the X-ray beam hit at a point near the indentation, the crystal face with the indentation on it should be parallel to and coincident with the rotation axis. To achieve this object, the following adjustments were made.

The cleaved single crystal of zinc was mounted with plasticine on the arc with the basal plane parallel to one of the arcs. The front surface of the crystal was viewed through the tele-microscope with the front lens in position. Throughout this chapter, the 'front surface' refers to the surface where indentations were made. The twin traces, the direction of which is $[\bar{1}2\bar{1}0]$ could be seen on the surface and the horizontal crosswire was made to coincide with one of these traces. A beam of light was passed through the collimator of very narrow cylindrical aperture (diameter $\frac{1}{2}$ mm) and the spindle was rotated till half the circular patch of light was cut off by one edge of the crystal. The crystal was then turned through 180° as read on the scale, about the vertical axis and the collimator was again viewed through the microscope. By successive adjustments of the arc and the slide perpendicular to the basal plane, the crystal was set such that half the circular patch of light was cut off

by the two edges of the front face at the two positions respectively. At both these positions the front face was parallel to and coincident with the rotation axis.

The spindle was then rotated through 90° and adjusted till the intersection of the crosswires was very near the indentation as seen through the microscope, the horizontal movement of the crystal being made only by the slide parallel to the front face. A final check up of the horizontal crosswire coinciding with the twin trace was also made. The rotation axis was then along the [10$\bar{1}$0] direction.

After setting the crystal as described above, the spindle was turned such that the front face of the crystal was making an angle of 5° with the direction of X-ray beam and the crystal oscillated through a further 15°.

6·2 EXPERIMENTAL OBSERVATION.

Fig.(57) shows the oscillation photograph with cu k (unfiltered) radiation, with the beam hitting near the indentation. The Powder arc associated with the zero layer reflection shows that there is a slightly disordered region round the indentation. The satellite spots on the first layer reflections are also due to the deformation. A comparison with an oscillation photograph (fig.58) in which case the X-ray beam hit at some point farther away from the indentation (the oscillation axis being the same as before)

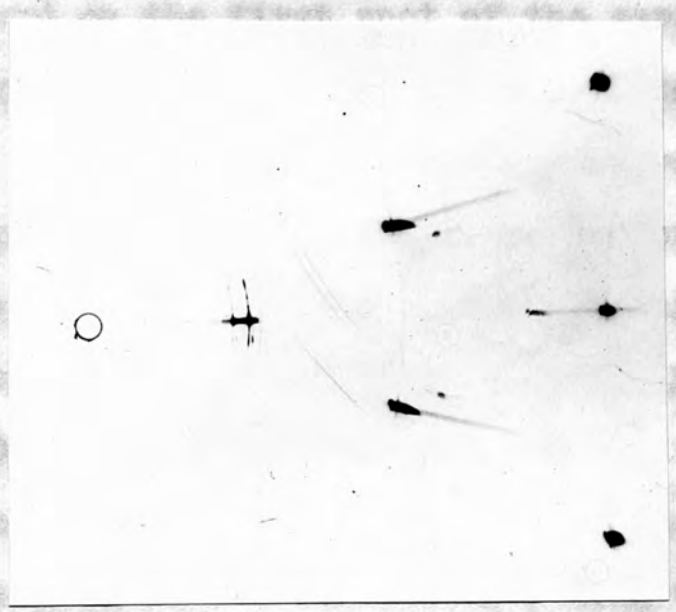

Fig. 57

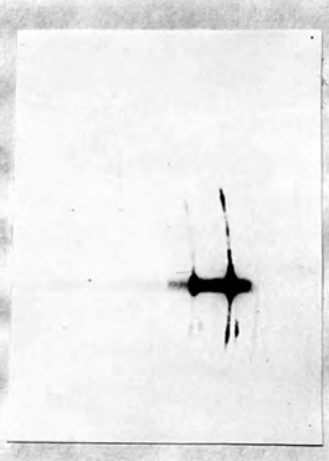

Fig. 57a.

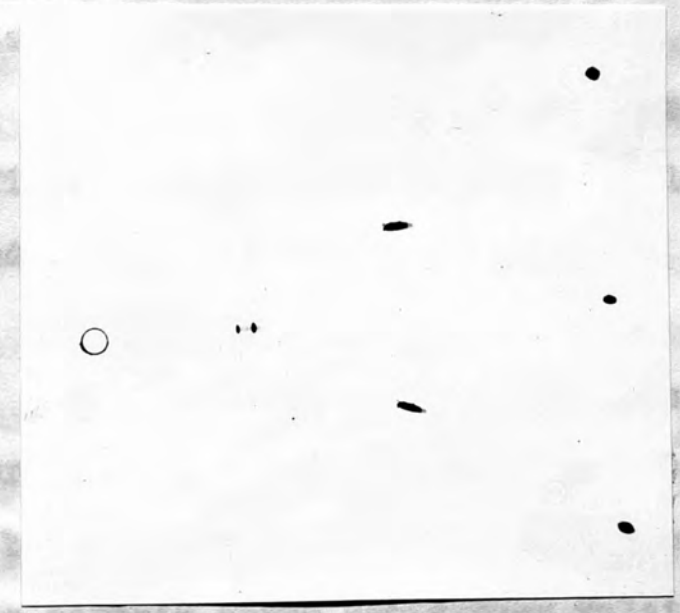

Fig. 58

Fig. 58a.

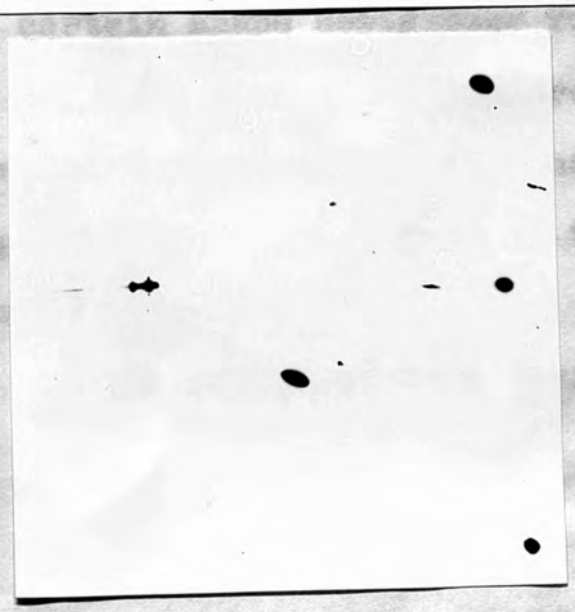

Fig. 59

Fig. 59a.

shows identical reflections except for the streaks observed on the first spot of the zero layer reflection. It can also be seen that the satellite spots have disappeared.

After annealing for 2 hours at 380°C and furnace cooling, the same crystal was set approximately as before and another oscillation photograph was taken with the X-ray beam hitting near the indentation. Fig.(59) shows this oscillation photograph. The reflections are the same as before but the satellite spots have become more prominent and the continuous streaks spreading on either side of the first spot of the zero layer reflection have been replaced by discrete spots.

Figs. 57a, 58a and 59a are the enlargements of the first spot of the zero layer reflection of Figures 57, 58 and 59, respectively.

6·3 DISCUSSION.

Undoubtedly the continuous streaks spreading on either side have been replaced by discrete spots and it must be imagined that the micrograins formed during annealing have a certain shape definitely related to the glide system of the original crystal. The process of polygonization, where elastic stresses are eliminated, has taken place and the region takes up some mean of the range of orientation originally present in it.

The polygonization inside the crystal are usually

revealed by the splitting of Laue spots, distorted into streaks (asterisms) by the initial deformation into a set of discrete spots as the substructure develops.

The splitting of asterisms in Laue X-ray photographs had been observed by a number of earlier workers, Andrade and Tisen (1937) and Konobeevsky and Mirer (1932).

Cahn (1950) and Guinier and Tennevin (1950) made a detailed study describing the process of polygonization by the production of dislocations and their subsequent assembly to form sub-boundaries.

Cahn has shown that a crystal readily polygonizes if it is plastically bent about an axis in the slip plane normal to the slip direction and then annealed at temperatures close to the melting point.

This is what had taken place in the present investigation. During the indentation, the material near the indentation had been bent about an axis in the slip plane and polygonization had taken place after annealing as shown by the splitting of the powder arcs into discrete spots.

According to Cottrell (1949, 1953) the initial deformation produces an excess of dislocations of the same sign which subsequently move through the slip plane during anneal to form stable arrays of dislocations. The crystal

is no longer smoothly bent but consists of small blocks of perfect structure separated by walls of dislocations. Each discrete spot which had replaced the arc during anneal could be attributed to reflection from particular small block of good crystal.

PART B.

STUDY OF CATHODE GLOW ETCHING

CHAPTER I.

STRUCTURE OF BINARY ALLOYS

1·1 INTRODUCTION

Combinations of two or more elements of which one is a metal are called alloys. Profound changes in the properties both physical and chemical of a pure metal may result if atoms of a second metal or atoms of a non-metallic element are alloyed with it. Alloys are of great importance in industry, the steels, brasses, bronzes, aluminium alloys, tin alloys and cast iron, etc., Though pure metals are needed for certain purposes far greater quantities of these are used in the form of alloys with other metals and sometimes with very small proportions of non-metals such as carbon and oxygen. Even if the alloy is composed of only two varities of atoms, when they are called binary alloys, there is an infinite variety of proportions of one to the other and as little as ·005 per cent may in some cases alter the physical and chemical properties of the major element to a large extent; oxygen free copper shows a remarkable toughness in the twisting test. 0.01 per cent of sulphur in nickel makes it very brittle. A very small per cent of carbon in iron alters considerably its magnetic properties.

Metals and alloys in the solid state have different distinctive lattice structures which may be termed

phases. The structure of each of the many alloys between two given metals depends in general upon the conditions under which it is cooled. But for an alloy of particular composition there is at each combination of temperature and pressure an equilibrium state to which the alloy gradually reaches if kept under specific condition for sufficient time. Since the state of true equilibrium is determined completely by the composition and temperature (slight variation in pressure produces negligible effect) diagrams can be drawn to show the structure of the alloy in terms of these variables. Such diagrams are called equilibrium diagrams or constitutional diagrams.

1•2 EQUILIBRIUM DIAGRAM.

The abscissa of the equilibrium diagram represents the composition and the vertical axis the temperature range.

The line passing through all the points which represent temperatures at which alloys of different composition begin to freeze or at which melting is complete is known as the liquidus. Below this will be a curve joining points which represent the temperature at which solidification is just complete on cooling or melting just starts on heating. This is called the solidus. Any point within the confines of the diagram represents an alloy of definite composition at a definite temperature. The composition is obtained by drawing a vertical line to cut the

horizontal axis while the temperature is obtained by drawing a horizontal line to cut the temperature axis.

When the two components of the alloy are metals, the phases are essentially solid solutions as there is always some amount of mutual solubility between the two metals. The single phase region may sometimes extend over the whole range of composition from one metal to the other or it may be so restricted to approximate to a pure metal or a chemical compound of fixed composition intermediate in composition between the two components. As the relative proportions of the two metals are progressively varied, the alloy may change from a single phase having the structure characteristic of the first metal to a mixture of two phases, then to a single phase of the second of these and so on, finishing the series with a single phase conforming to the lattice of the second metal. This series of solid solutions are usually referred to in order by $\alpha, \beta, \gamma,$ and so on.

Solid solutions are of two types, substitutional solid solutions where atoms of the solute metal element replace atoms of the solvent metal at random positions within the solvent metal lattice and interstitial solid solutions where atoms of the solute metal located at random positions between the atoms of the solvent metal lattice. Intermetallic compounds differ from solid solutions in having lattices with the atoms of the elements in a regularly ordered arrangement.

When an alloy is heated or cooled over a range of temperature which is within the area of the diagram no essential change occurs in its structure.

In Fig.(1) an alloy containing 80 per cent of copper consists of two solid solutions α and β between 587°C and 798°C. To find the composition and relative amounts of α and β at 750°C draw a horizontal line across the diagram at this temperature cutting the boundary of the pure α phase at A and that of pure β field at B. And the percentage of α and β which exist together at 750° in the alloy under consideration is 86 per cent and 78 per cent of copper respectively. The compositions of α and β would be the same at 750°C for any alloy within the composition represented by A and B.

The relative proportions of α and β at 750°C are given by $\alpha : \beta :: BC : AC$; this is known as the lever principle. On cooling to 650°C the compositions of α and β are given by D and E respectively (86 and 77 per cent of copper) and the relative amounts $\alpha : \beta :: EF : DF$. That means on cooling from 750° to 650°, the β constituent of the alloy becomes somewhat richer in tin but this is accompanied by a reduction in the amount of β present.

When the atomic diameters of two metals are very nearly equal, that is to say when the size factor is very favourable, the equilibrium diagram is usually of the form

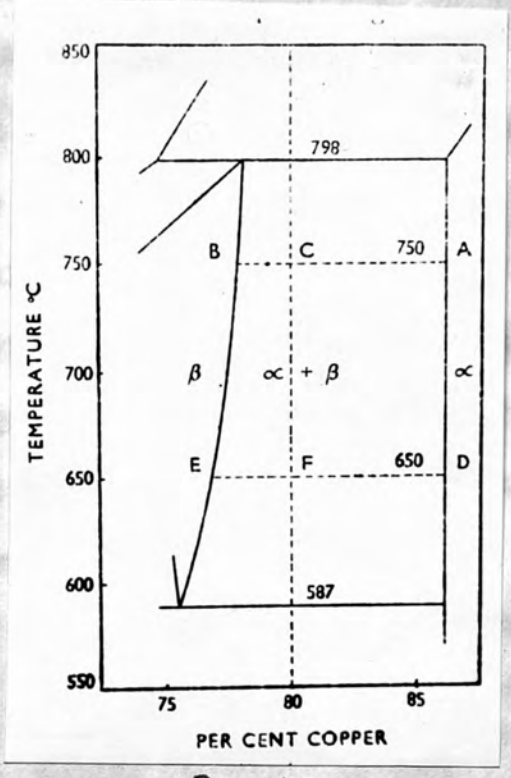
850
800
750
700
650
600
550
798
B
C
750
A
β
α + β
α
E
F
650
D
587
75
80
85
TEMPERATURE °C
PER CENT COPPER

Fig · 1

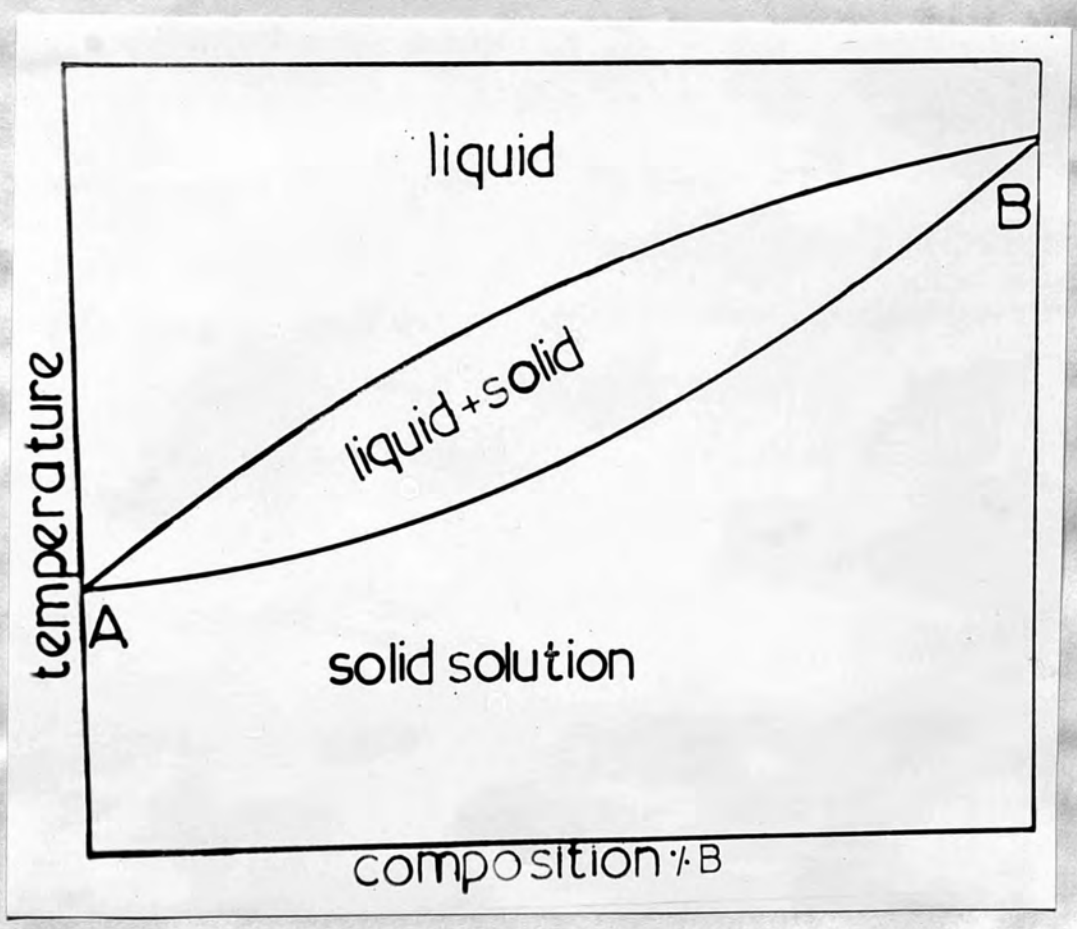
liquid
B
liquid+solid
temperature
A
solid solution
composition % B

Fig · 2

shown in fig.(2) where a complete range of solid solution is formed. Here the atomic diameter is usually defined as the closest distance between two atoms in the crystal of the element concerned. For a given solid solution the size factor is the difference between the atomic diameters of the solvent and the solute expressed as a percentage of the atomic diameter of the solvent and usually if the size factor is less than 15 per cent, it is considered favourable.

In some cases where the size factor is not quite so favourable as that giving rise to fig.(2), the liquidus is of the type shown in fig.(3) and the liquidus and solidus pass through a minimum where the two curves touch. The alloy of minimum freezing point then passes from the solid to the liquid state at one temperature and freezes like a pure metal whilst alloys on their side freeze over a range of temperature. The homogeneous solid solution on cooling splits up into two solid solutions of the same crystal structure but different compositions. The curve x y z w m represents the limit of the solid solution and an alloy P lying within this curve consists of two solid solutions of composition y and w .

Eutectic system.

The equilibrium diagram of a hypothetical alloy system of two metals A and B which are completely soluble

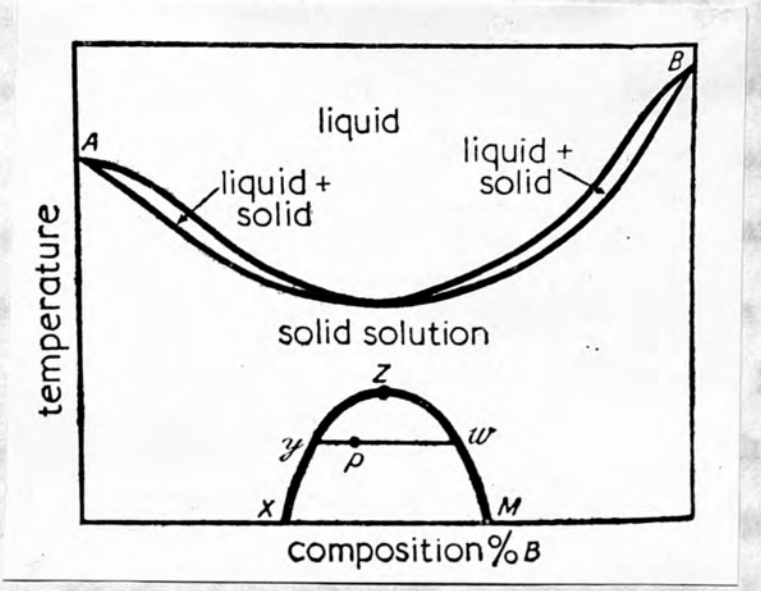
A
B
liquid
liquid +
solid
liquid +
solid
temperature
solid solution
Z
y
p
w
X
M
composition % B

Fig. 3

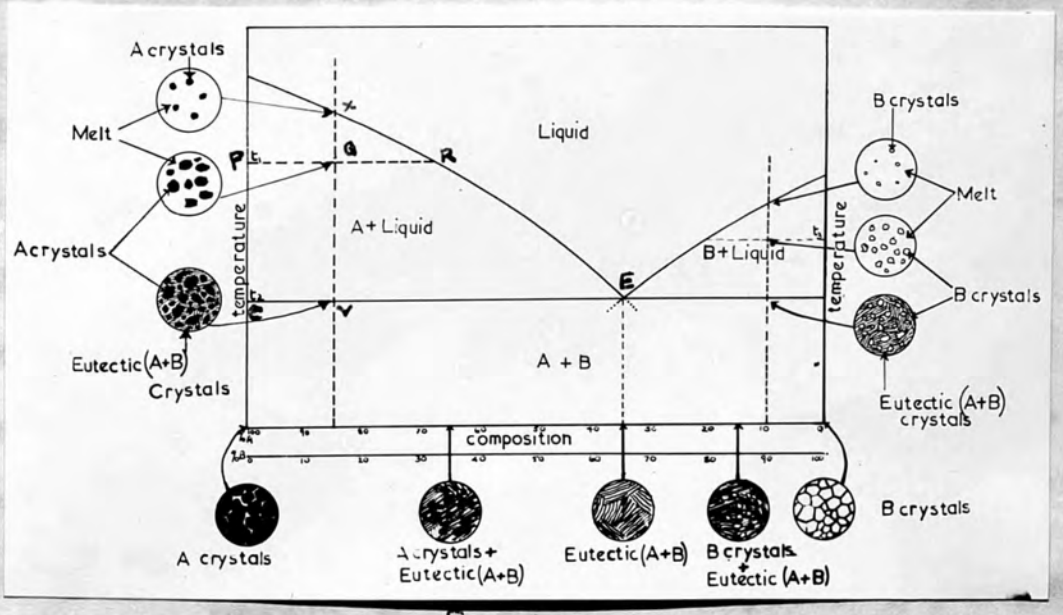
A crystals
Melt
Acrystals
Eutectic (A+B)
Crystals
P
Q
R
Liquid
A+ Liquid
temperature
E
V
A + B
composition
B crystals
Melt
B crystals
Eutectic (A+B)
crystals
B+Liquid
temperature
B crystals
A crystals
A crystals +
Eutectic (A+B)
Eutectic (A+B)
B crystals
+
Eutectic (A+B)

Fig. 4

in one another in the liquid state but completely insoluble in the solid state, is shown in fig.(4). The alloy containing 85 per cent of A on cooling from the liquid state begins to solidify at a temperature corresponding to x and pure crystals of A are formed. The remaining liquid becomes richer in B. This new liquid richer in B has a lower freezing point and no further deposition of A crystals from this liquid can take place, until its temperature has dropped slightly when the deposition of pure crystals of A will be resumed. At a temperature t_1 liquid : solid :: PQ : QR When the temperature has fallen to t_2 still more crystals of A have crystallized out. The liquid has a composition given by the point E, i.e. 35 per cent of A. The proportion is liquid : solid :: CV : VE. The liquid now solidifies sharply without further change in temperature to form an intimate mixture of A and B which is deposited round the crystals of pure A already formed. This mixture is known as a eutectic mixture. The point E is known as the eutectic point and the dissociation of the eutectic liquid of composition E into crystals A and B is known as the eutectic reaction and may be written

$$\text{Liquid E} \underset{\text{heating}}{\overset{\text{cooling}}{\rightleftharpoons}} \text{Crystals A + Crystals B}$$

Alloys of A and B containing less than 35 per cent of A behave similarly but begin by depositing crystals of pure B. The eutectic is formed at t_2 as before of the same composition from whatever alloy it separates. The structure of the alloys during solidification are shown diagramatically in the sides and bottom of fig. (4).

The solidification of alloys, the two components of which are completely soluble in one another in the liquid state and partially soluble in the solid state are very similar to the simple eutectic alloys. In this case each metal is able to hold a certain amount of other in solid solution. A simple diagram of this type is shown in fig. (5). E is the eutectic point. The alloy of 30 per cent A on cooling from y, starts solidification at temperature t_1 and the solid formed is the β solid solution of composition N containing about 7 per cent of A. As before the liquid becomes richer in A, the temperature falls and more solid is deposited. The compositions of the solid and liquid vary continuously along the lines B G and B E.

At t_2, the solid has a composition G and the liquid contains 35 per cent of B. The latter now solidifies as eutectic and the alloy consists of β solid solution and eutectic in the proportion E K : K G. As

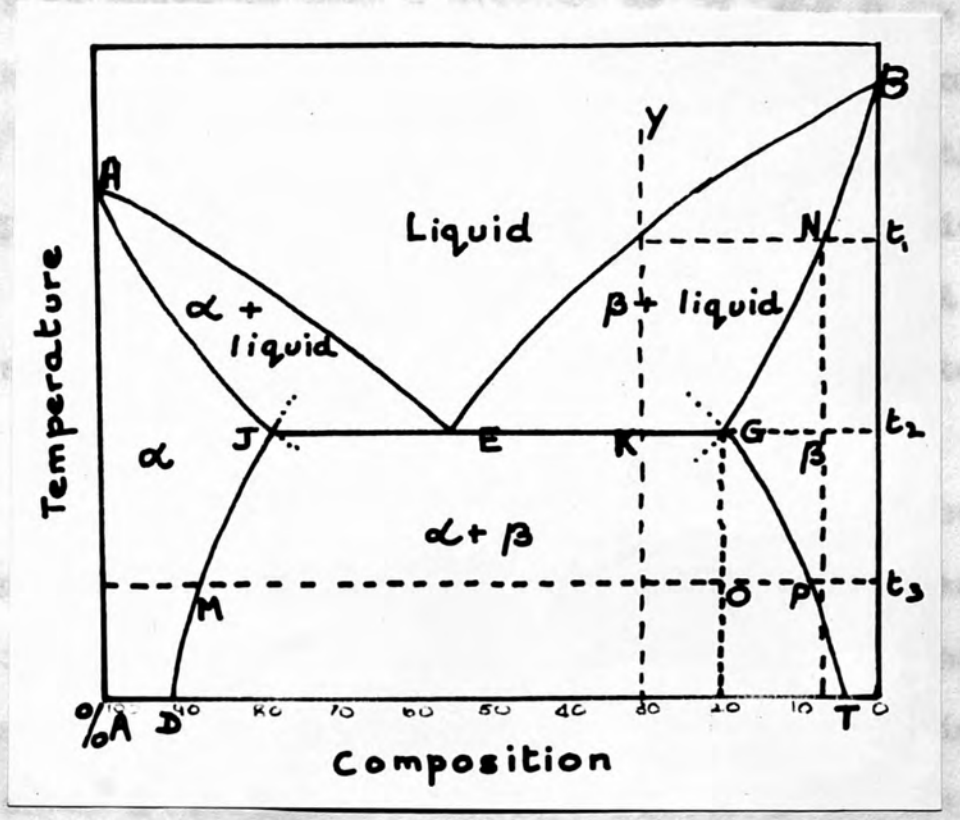
A
B
Y
Liquid
N
t_1
α + liquid
β + liquid
Temperature
α
J
E
K
G
t_2
β
$\alpha + \beta$
M
O
P
t_3
%A
D
T
Composition

Fig. 5

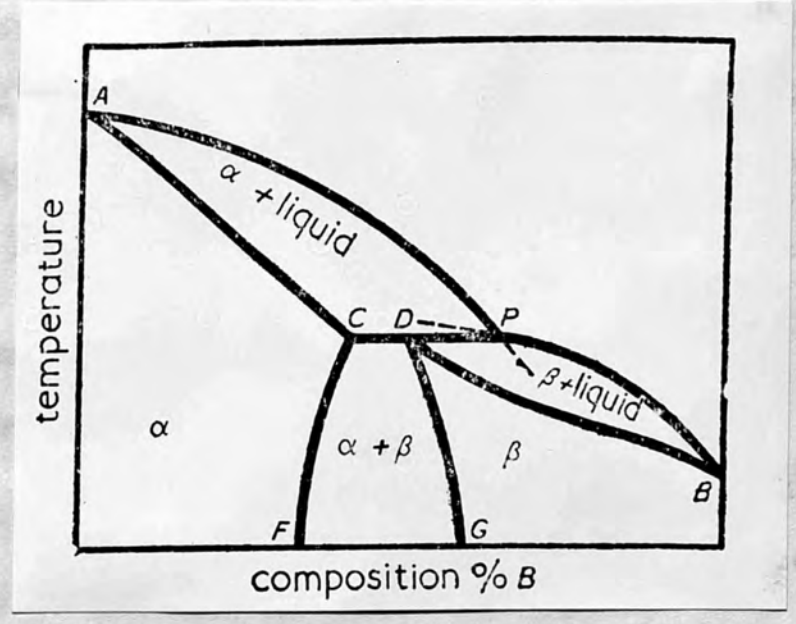
A
α + liquid
temperature
C
D
P
β+liquid
α
$\alpha + \beta$
β
B
F
G
composition % B

Fig. 6

the temperature falls below t_2, the β solid solution can no longer hold in solution all the A it contains and begins to split up into a mixture of α and β. At t_3 the alloy is made up of the eutectic mixture of α and β, and a further mixture of α and β derived from the decomposition of β solid solution G in the ratio op : Mo

Alloys between 82 and 65 per cent of A solidify in a similar way. But the first solid to separate is α.

Peritectic reaction.

Unlike the equilibrium diagram described above, in some systems when two solid solutions are formed, the freezing point of the one metal is raised by the addition of the other and the typical equilibrium diagram is of the form shown in fig.(6). At the temperature of the horizontal CDP, liquid phase of composition P is in equilibrium with α of composition C, and β of composition D, and on passing through this temperature all alloys of compositions between C and F will under equilibrium conditions undergo the reaction

$$\text{liquid P} + \text{solid C} \underset{\text{heating}}{\overset{\text{cooling}}{\rightleftharpoons}} \text{solid D}$$

This is known as the peritectic reaction.

Eutectoid and peritectoid transformation.

In a eutectic reaction a single liquid phase splits up on cooling into two solid phases and conversely

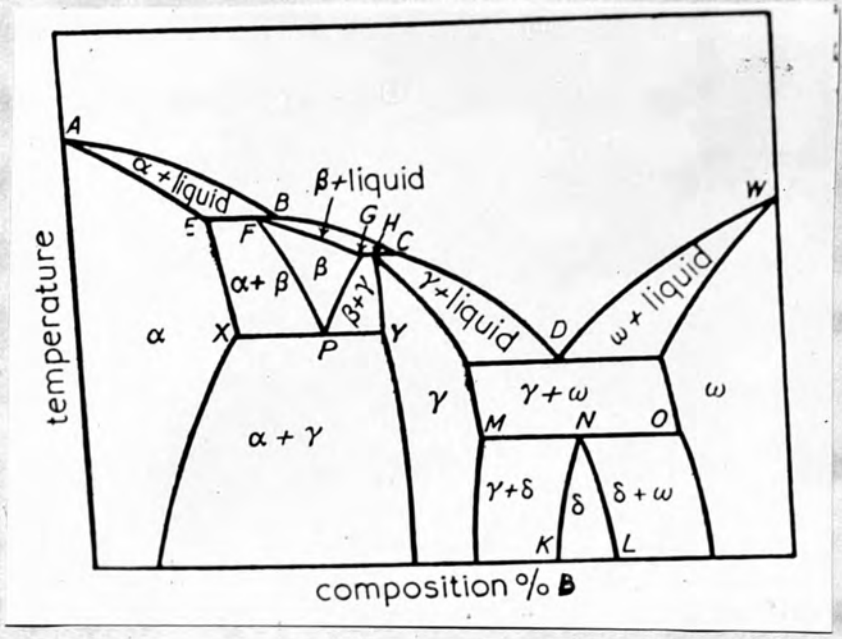
A
α + liquid
B
β + liquid
W
E
F
G
H
C
α + β
β
β+γ
γ + liquid
ω + liquid
temperature
α
X
P
Y
D
γ
γ + ω
ω
M
N
O
α + γ
γ + δ
δ
δ + ω
K
L
composition % B

Fig. 7

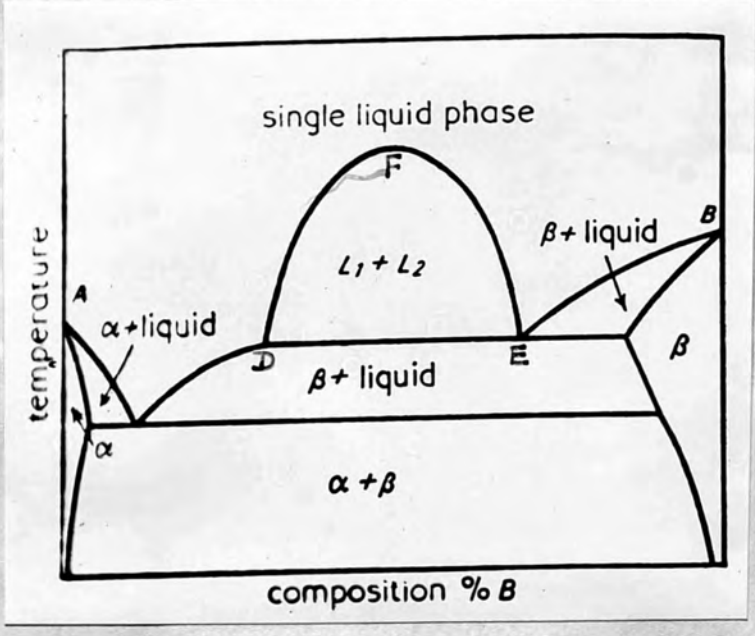
single liquid phase
F
L1 + L2
β + liquid
B
A
α + liquid
D
E
β
β + liquid
α
α + β
temperature
composition % B

Fig. 8

two solid phases when heated melt to form one liquid. In some systems analogous changes take place in the solid state when a solid solution undergoes a transformation on cooling to form a mixture of two other solid phases. This is known as eutectoid transformation. In fig.(7) the equilibrium diagram of a hypothetical system A B is shown. The boundary F P represents the limiting compositions of the β phase in equilibrium with the α phase and G P is the corresponding curve for equilibrium between solid β and solid γ . At the temperature corresponding to point P , the homogeneous β phase of composition P, splits upon cooling into two solid phases α of composition X and γ of composition Y.

The peritectoid reaction is analogous to the peritectic reaction already described. An additional solid constituent takes the place of the liquid in the reaction. In fig.(7) the δ phase is shown as undergoing a peritectoid decomposition at the temperature MNO, at which on heating the single solid phase of composition N splits up into solid γ of composition M and solid w of composition O.

The equilibrium diagrams described above represent the main types in binary alloys and nearly all known diagrams can be regarded as a combination of two or more of these. There remains the consideration when two

liquid phases are formed. In fig.(8) the alloys between compositions D and E melt to form two immiscible liquids of compositions D and E. These are known as conjugate solutions. As the temperature rises above the line DFE, the two liquids dissolve in one another to give a single uniform liquid.

1·3 THE PHASE RULE.

Briefly stated as an equation it is C + 2 - P = F. C is the number of components in the system.

P represents the number of phases present. In alloy systems a phase may be a melt, a pure solid metal, a solid solution or an intermetallic compound.

F stands for the degrees of freedom. The three possible degrees of freedom are: temperature, pressure and concentration of the components in the phases.

Most cases are studied under conditions where slight variations in pressure produce negligible effect on the equilibrium, and hence the phase rule can be written in the form

$$C + 1 - P = F$$

It will be seen that this agrees with the phases present etc. of the equilibrium diagrams described above.

1·4 NONEQUILIBRIUM CONDITIONS.

The changes described earlier through which an alloy may pass in cooling are accomplished by the movement

of atoms from one position to another. The atoms diffuse past each other to equalise the concentration differences, they separate out of a supersaturated solid solution to form separate crystallites. Not only must the atoms be mobile but they must have sufficient time for the migration if the change to be completed. This change will be retarded or entirely prevented if the mobility of atoms is suddenly and substantially decreased. This retarding means is called quenching. In fig.(5) if the alloy N is quenched rapidly enough from t_2, would show a homogeneous structure of β solid solution when it reached room temperature, there having been insufficient time allowed at the temperatures between t_2 and room temperature for it to decompose. Thus the condition existing in the alloy at higher temperature can be retained completely or partially by suddenly bringing the alloy to a lower temperature.

Interpretation of microstructures depends on this assumption that an alloy can be brought to its condition of equilibrium at any given temperature by annealing for a sufficiently long time and that its structure in this condition can be retained by quenching.

CHAPTER II.

THEORY OF CATHODE SPUTTERING

It has long been known that metals disintegrate under the influence of bombardment by high velocity positive ions. This was first noted at the metallic cathodes of gaseous discharge tubes and the phenomenon is commonly known as cathode sputtering. Cathode sputtering though observed usually in the luminous discharge at gas pressures from a few thousandth to several millimetres of mercury with currents of the order of several milliamperes, there are indications of sputtering in a spark discharge. In an arc the cathode may become so hot that its evaporation is the main feature and hence cannot be compared with those where sputtering is usually observed.

The question arises as to the nature of the inter action between the ionized gas and the material of the cathode, whether it is a physical phenomenon or does chemical interaction play a part. The early investigations on this question are very extensive. Kohlschutter (1912) gives a summary of the early views, a brief account of which will be given before reviewing in detail the later work.

One of the earlier ideas for an explanation of the sputtering phenomenon assumed the disruption of the

cathode by occluded gases liberated under the ion bombardment. Though in fact the occluded gases may cause disintegration of the material of the cathode, the presence of absorbed gases cannot account for the phenomenon as a whole since cathodes at red heat (where occlusion of gas must be small) produce uniform sputtering. As far as a theory is concerned most of the early investigators did not consider the phenomenon to be one of general evaporation of the cathode due to the heating of the whole cathode by the bombardment of positive ions. Local heating and local expansion of the electrode at the point of impact were considered. Another view ascribed the phenomenon to an increase in the evaporation under the electrical forces acting on the metal. A chemical theory on the basis of which the impinging ions form transient chemical compounds with the material of the cathode, which on leaving the cathode deposited on the tube walls and there decomposed, were also considered. But the physical theory of ion impact and the consequent emission of secondary atoms from the electrode was taken to be the most satisfactory picture of the process. The early investigators tried to arrange various metals into a sputtering series according to their ability to sputter and an attempt to correlate this series to other properties of the metals was unsuccessful. Barring chemical action,

the heavier gases are more efficient in sputtering. Oxide layers may prevent the cathodic disintegration.

In most of the earlier work on cathode sputtering the conditions under which the experiments were carried out are not satisfactory. The later work carried out with more precision in measurement is also not able to give a definite answer to the advancement of a particular theory. The different major theories with experimental evidence in favour of each will be discussed in more detail in the light of later investigations.

2·1 IMPACT THEORY ascribes the sputtering to the mechanical "bumping off" of surface atoms by ions which have penetrated below the surface of the material and rebounded so as to transfer a part of their outward momentum to the surface atoms which they strike from behind, as developed by Kingdon and Langmuir (1922, 1923). They studied the sputtering of thorium from the surface of a thoriated tungsten filament in different gases, as a function of voltage and pressure. The disappearance of thorium atoms due to sputtering was detected easily by measuring the emission of thoriated tungsten before and after the sputtering process. It is expected that a fully thoriated surface upon bombardment would lose its emissive power rapidly and then more slowly as more tungsten surface is exposed. Instead their observations have shown

an initial lag after which the rate of deactivation reached a constant maximum value and then decreased as the tungsten surface was approached. Also there seems to exist a threshold voltage for sputtering below which these ions are unable to remove thorium from the filament, but the sputtering in the special case of thorium is not generally found to be proportional to the energy of the impinging ions as has been seen in many earlier investigations on other metals. A novel mechanism of sputtering is put forward endeavouring to explain these anomalies. An ion impinging on a thorium surface with high velocity will push the thorium atom, which it strikes, into the surface but will be reflected itself and fly off. So the first result of the bombardment is to produce a large number of depressions of atomic size in the surface. After a time a second collision will take place at the bottom of one of these depressions and the ion will be reflected from the thorium atom there. The question is whether this collision can be considered elastic, i.e. whether the impinging ion will retain considerable part of its energy. Langmuir (1916) has shown that the energy given to the surface atom is transmitted so rapidly to neighbouring atoms that the gas atom loses a part of its energy and the collisions being inelastic. But in the case of ion bombardment the ions are moving with much higher velocity and the ion accordingly penetrates farther into the atom

and meets with much stronger fields of force so that the time taken for reflection will be much shorter and hence retains a considerable part of the energy. So a gas ion impinging on the bottom of the depression in the surface can be considered to be reflected elastically and on the way may have enough momentum to knock off from behind one of the thorium atom around the edge of the depression. The first ion which drove the thorium down is reflected at the surface and hence is not in a position to knock off any thorium. The removal of thorium does not take place until two or more ions have impacted in the same place on the surface. This accounts for the initial lag mentioned above. More evidence in support of this theory is found in the minimum voltage needed to produce sputtering in the case of some of the ions. They calculated the initial voltage by applying the laws of conservation of energy and momentum to the processes involved.

$$E = \left(\frac{4eV}{300}\right) m_c m_g \left[\frac{m_g - m_c}{(m_g + m_c)^2}\right]^2$$

Where E = energy of the cathode atom received from the surface

V = voltage through which the gas ion has fallen

$e = 4.774 \times 10^{-10}$ e.s.u.

m_c = mass of cathode atom

m_g = mass of gas ion.

For neon and argon the agreement is fair. The calculated values for mercury and cesium are very much higher than the observed value. This discrepancy may be due to the fact that these ions are heavier when compared with thorium atoms; the latter being driven far into the surface by the first impact and the second collision being then an interaction between a gas ion and a solid wall. The ion would therefore retain more of its energy and remove thorium atoms at a lower voltage.

Helium behaved differently from the other gases used. Relatively large quantities of helium gas penetrated into the surface and could be recovered later by proper heat treatment. And also helium ions could remove thorium at voltages much lower than those calculated from the theory. These facts find possible explanation in a theory advanced by J.J.Thompson (1921) where he has suggested that gas ions upon deceleration near the electrode produce radiation, which is absorbed in turn by the metal atoms causing their expulsion from the metal.

The case of thorium sputtering is one of the most satisfactory work done in this field.

2·2 THERMAL THEORY

This theory has been fully discussed by V. Hippel (1926, 1928). The fundamental idea is that thermal evaporation from the regions of local high

temperature produced by the impinging ions in the short interval before the available energy of the ion made up from its ionization energy and the K.E. is dissipated into the body of the metal through thermal conductive processes. He also measured their energy by permitting some of them to pass through a small orifice in the cathode and determining their energy by appropriate retarding fields.

Waran (1931) has adopted the same view and has determined the relative sputtering values of different metals and compared them with the boiling point, thermal conductivity, specific heat and other physical properties of the metal. In a complex phenomena like this where the variables and disturbing factors are so many, it cannot be expected to find a quantitative relation between the various factors. With numerous exceptions to the expected behaviour, one can see that there is a certain volume of quantitative evidence in support of this purely thermal view for cathodic disintegration. For example consider the sudden rise of temperature restricted to the immediate neighbourhood of the point of impact, metals of low heat conductivity like palladium, lead and platinum should show a higher rate of sputtering than metals of higher conductivities like magnesium and aluminium (neglecting heat lost by radiation).

Experimentally observed values by Waran for relative sputtering are in general support of this view.

Cowsik (1933) has furnished additional evidence in support of this theory.

Another interesting experiment in favour of the thermal theory is given by Seeliger and Sommermeyer (1935). Their experiment consisted in directing a beam of canal rays to impinge upon the sputtering surface and catching the sputtered material at a short distance over a suitable surface. The uniform deposit obtained shows that the Knudsen's cosine law for thermal evaporation holds for the sputtering process. It must be understood that canal rays exercise no directive influence on sputtered atoms.

It has already been mentioned that oxide layers prevent cathodic disintegration.

Bleschmidt and V. Hippel (1928) formed their cathodes by evaporation in a vacuum and the helium-neon gas mixture was continuously purified by pumping through activated charcoal during the sputtering. The results they obtained appear to fit in with the thermal theory of sputtering in that the sputtering intensity follows the heat of sublimation of metals.

There are evidences to indicate that sputtering process is not altogether a simple local evaporation and

that the charged nature of the impinging ions has a definite influence. Oliphant (1929) has shown that though metastable helium atoms will cause sputtering they are not as efficient as ions of the same kinetic energy. He found that the heating effect of metastable atoms is of the same order of magnitude as that produced by positive ions and hence they possess the same kinetic energy when reacting the electrode. But their effect on sputtering is less than that of helium ions.

2.3 DOUBLE EVAPORATION PROCESS.

Starr (1939) has found an empirical relationship between the rate of sputtering of various metals and the total heat required to evaporate it.

According to him for fixed glow discharge conditions $m = \frac{c}{q^2}$ where m is the mass of sputtered material per ampere hour, c is a constant depending on the discharge conditions and q is the total heat of evaporation. The total heat includes the heat capacity from room temperature to melting point, the heat of fusion, the heat capacity from the melting point to the boiling point and the heat of evaporation. This relation is not in conformity with either of the theories mentioned above. The thermal theory predicts an exponential relationship while the impulse theory predicts a linear relationship. A process of double evaporation is

suggested. Ion bombardment causes emission of metal atoms by direct energy transfer at a rate inversely proportional to the total heat for evaporation. This metal vapour on exposure to the heat of recombination of the ions and electrons near the cathode surface again cause evaporation. This follows the inverse square law found empirically.

2·4 CHEMICAL SPUTTERING.

A definite interaction of the sputtered metal and the gas carrying the discharge has been observed by Guntherschulze (1926) with elements carbon, selenium, tellurium, arsenic, antimony and bismuth in hydrogen. Hydrides are formed in the first five cases while bismuth shows a slight tendency towards hydride formation although its hydride is not very stable. Hydrogen ions or atoms are evidently necessary for the chemical sputtering process. The disintegration in this process is due to the chemical combination of hydrogen ions with the metal atoms at the surface of the cathode. The hydrides formed diffuse into the gas phase and are there decomposed into the metals and hydrogen. The metals deposit on the nearest wall. As this chemical interaction as a means of sputtering is not true in all metals in the same gas apart from the fact that this interaction is observed only in a hydrogen atmosphere, this phenomenon cannot be considered as a

general theory for elementary cathodic sputtering. Also the chemically sputtered metals will disintegrate as cathodes, anodes, or even when located in the discharge without electrical connection to the metal electrodes, indicating clearly the great difference between the chemical effect and the normal process.

2·5 CONCLUSION.

A definite conclusion has not yet been made to the elementary process of the disintegration of metallic cathodes in a glow discharge. But it is believed that the thermal evaporation process may be the predominating influence in many cases. R.Seeliger (1942) has proposed the view that the sputtering with light ions proceeds through impulse recoil and with heavy ions through local heating with resulting evaporation.

Though the elementary process is not fully understood its technical uses are many. Cathodic sputtering has been used for many years for the production of highly reflecting mirrors and can be produced with the highest reflection coefficients suitable for astronomical and other optical instruments. Very thin metal films can be produced easily by this method. Baum (1927) and Smith 1927) used the sputtering technique to etch metals and alloys. But only recently this has been widely used to etch metals and alloys for metallographic and electron microscopic studies and will be referred to in later chapters as cathodic glow etching.

CHAPTER III.

APPARATUS AND SPECIMENS.

In this chapter a brief description of the set-up used for cathodic glow etching will be given. A survey of the method of preparing the specimens and the actual procedure for etching is also made. With the establishment of the sputtering technique as the best method of etching certain materials for metallographic studies, major scale equipments are now available for the purpose.

3·1 APPARATUS.

The set-up used by the author is very simple and is shown in fig.(9). This consisted of a glass bell jar B with a hole at the top for cathode connection. The cathode connection C was an aluminium rod passing through an aluminium cork tightly fitting in the hole of the bell jar and was made airtight with picen wax. The specimen holder H was screwed to the end of C. The specimen was fixed in the holder by means of three small screws provided at the sides of the holder. By adjusting these screws the surface of the specimen could be made horizontal. This removable holder served to be very convenient as the holder could be unscrewed from the rod C and any other holder with the desired specimen fixed in could be introduced. The anode A consisted of a circular aluminium plate to the bottom of which is fixed a long

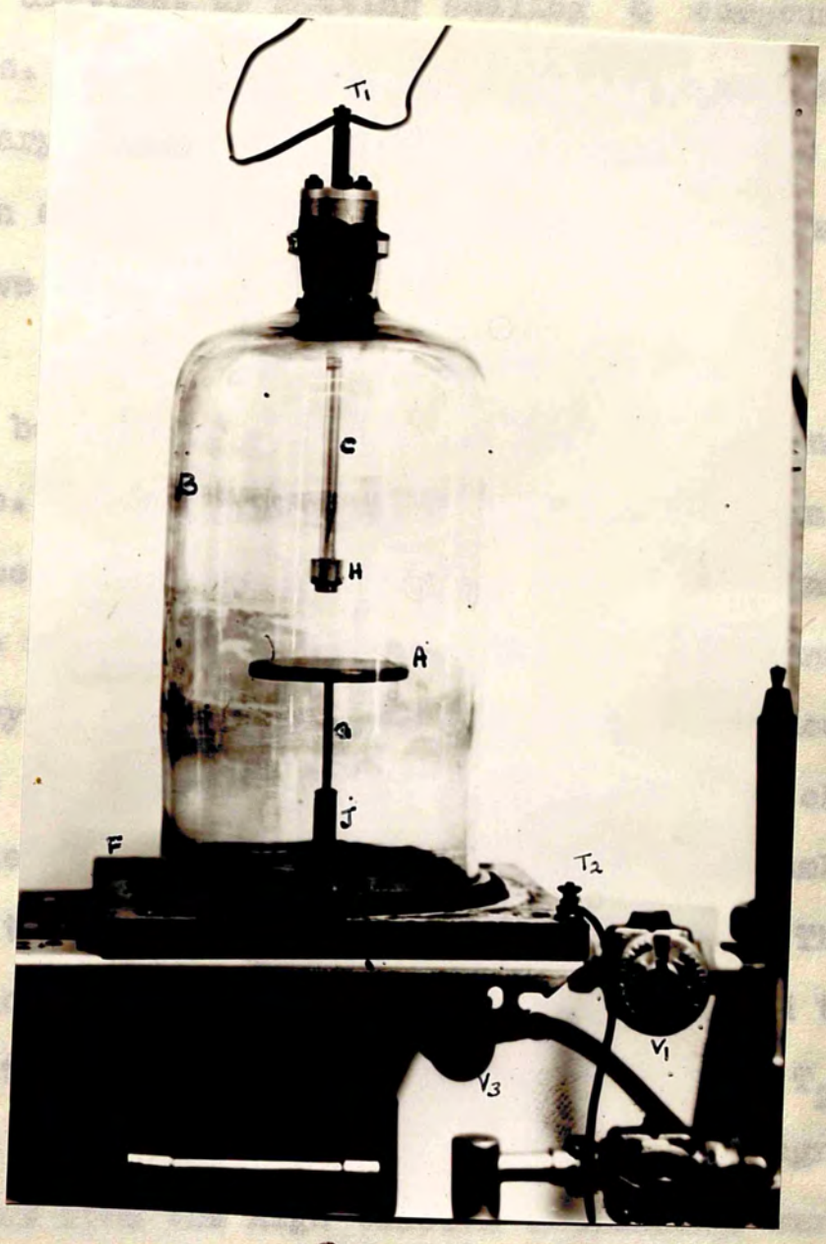

Fig. 9

screw base G. This screw moved in a cylindrical nut J and by adjusting the screw the distance between the anode and the cathode (specimen to be etched) could be easily adjusted. The bell jar rested on a metal plate F and was made airtight by putting sealing Q compound round the edges. The system was evacuated by a diffusion backed by a rotary pump. The residual gas used in the chamber was argon and was let into the chamber through a fine leak valve V_3.

Sealing the edges of the bell jar in contact with the base plate with apiezon sealing compound had one advantage. It was possible to take the specimen out of the chamber even when the pumping system was running. First the valve V_3 was closed. The valve V_1 connecting the rotary to the chamber and the valve (not shown in the fig.) connecting the diffusion pump to the chamber were closed. The air was then let into the chamber when removing the sealing compound from the edges. Thus the bell jar could be lifted without difficulty and the specimen taken out. The two terminals T_1 and T_2 were connected to a power supply as shown in the diagram (fig.10). The current from the high tension transformer was rectified by a RCA half wave mercury vapour rectifier operated by a step down transformer. A direct potential of 1000 to 2000 volts was usually applied between the electrodes and

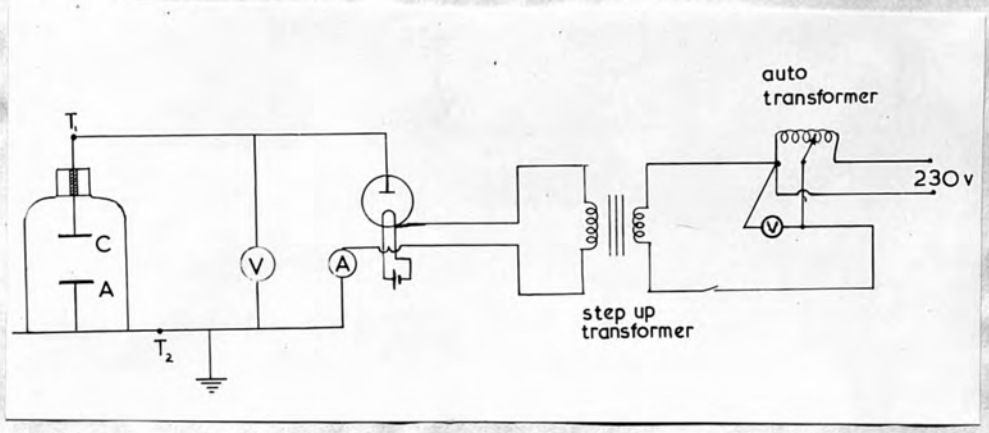

Fig. 10

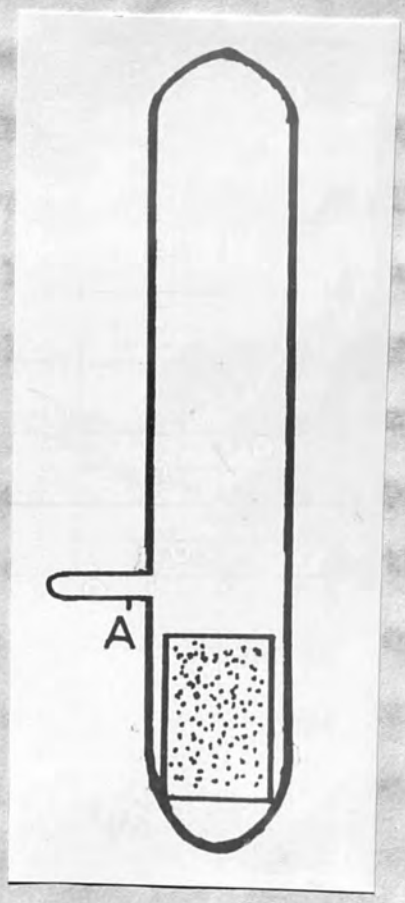

Fig. 11

was measured with a universal avometer. The voltage could be brought to the desired value by adjusting the variac of the auto transformer. The current was measured with a milliameter. Usually a distance of 5 cm. was kept between the electrodes.

3·2 PREPARATION OF THE SPECIMENS.

The tin-indium alloys of different composition were chill cast in the form of rods about 8 to 10 cm. long and 1.5 cm. diameter. Pieces of length about 1.5 c.m. were cut out of the rod by a small saw taking care to see that the specimen was not heated too much during sawing and were then machined on a fast lathe. The specimens were then polished first on a fast lapping machine as described below. A selvyt cloth thoroughly soaked in clear water and while still wet was stretched tightly over the lapping wheel and securely clamped in position. The cloth was then charged with 5/20 fast cutting alumina. This was done by mixing the polishing abrasive with water to form a thin paste and working this mixture into the cloth fibres with the finger tips. In actually carrying on the polishing operations the specimen was held firmly against the rotating lap and moved continuously back and forth from the centre to the periphery of the wheel. Care was taken to see that the cloth was neither too wet nor too dry. After 8 or 10

minutes the specimen was removed and washed in running water.

The final polishing was done slowly by moving the specimen in circles over the selvyt cloth spread over a smooth glass disc. The glass disc could actually be placed on the lapping wheel and the cloth stretched over it as before. The cloth was worked with gama polishing alumina and the specimens were carefully polished on the final lapping cloth. Only moderate pressure was applied to the specimen. Occasionally the specimen was turned through 90° to change the direction of polishing. After 5 or 10 minutes the specimen was removed and washed in warm running water. This was followed immediately by a rinse in ethyl alcohol, after which the specimen was quickly dried in a blast of warm air from an ordinary hair drier. A smooth polished surface of about 85 per cent reflectivity was obtained in every case, though there were minor polishing marks that did not affect etching as can be seen later.

Annealing.

A glass tube was drawn to the shape shown in fig.(11). The specimen was introduced into the tube with the polished side facing up. A file mark was made at the position marked A on the narrow side tube. This was then introduced into a large beaker containing water.

The water was heated. A round bottomed flask kept on this beaker served as a condenser since a continuous flow of cold water was maintained through the flask. By adjusting this rate of flow of water the rate of condensation could be controlled. The water was made to boil at a steady temperature (about 100°C) and the level of water in the beaker remained steady. After the required period of annealing the tube was transferred quickly into water at room temperature kept in a metal vessel. The tip of the tube was made to break at the point A by hitting against the edge of the vessel while transferring the tube. The cold water rushed into the tube through this broken tip and quenched the specimen inside. This served a very convenient and easy method of annealing the specimens without bringing the specimen in contact with water. Quenching also could be done very easily. Annealing for longer days than 4 were done using an oil bath. After quenching the specimens were finally and very carefully polished using gama polishing alumina.

3·3 PROCEDURE USED IN ETCHING.

The specimens prepared as described in the previous section were introduced in turn into the chamber to form the cathode. The system was made airtight and before connecting the diffusion pump to the chamber the discharge was passed between the electrodes with the rotary

pump connected to the chamber. From the nature of the glow discharge the vacuum could be tested to connect the diffusion to the chamber. After connecting the diffusion the fine leak valve was slowly opened to allow argon into the system. The pressure was adjusted so as to give a dark space of about the same length as the distance of the anode from the cathode. Usually a current density of 5 m.amp. per sq.cm. and a potential of 1000 volts were applied.

There was no cooling device attached to the cathode and so, to prevent the cathode from getting hot, the current was switched off and the cathode allowed to cool for about an hour after every 10 minutes of etching. Usually the specimens were taken out and examined after 45 minutes of etching. The results of etching of the different specimens and its interpretation will be given in the next chapters.

CHAPTER IV.

PRESENT OBSERVATIONS AND INTERPRETATIONS

4.1 INTRODUCTION.

As mentioned earlier, though the process of cathodic sputtering as a means of etching metal specimens was used as early as 1927, the importance of it has been realised fully only very recently. The need for stain free surfaces for examination under electron microscope has started cathodic glow etching in preference to chemical etching. Also certain alloys are found to be very resistant to chemical etching and cathodic etching has been found to be very effective in such cases. Zinc, bronze, tin and aluminium alloys can be satisfactorily etched for optical and electron microscopic purposes by this technique.

The author has been inclined to study the cathodic glow etching or Tin-Indium alloy mainly for two reasons. Firstly it has been observed that chemical etching has not been able to give satisfactory results whereby the phases can be distinguished. Secondly, the constitution diagram of the Tin-Indium system though studied by different authors by thermal, X-ray and metallographic means, a thermal and X-ray study of the system by the Tin Research Institute showed a marked difference in the constitution of the system especially

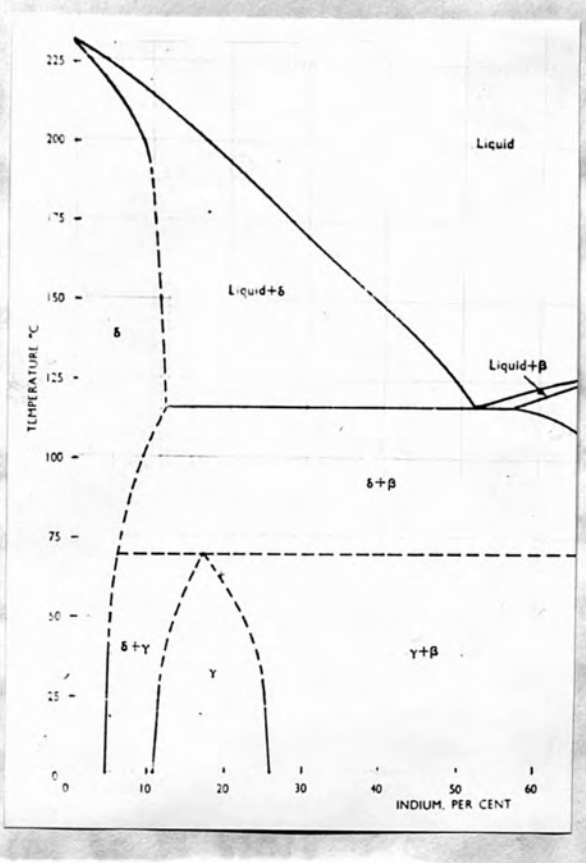
Liquid
Liquid+δ
δ
Liquid+β
δ+β
δ+γ
γ
γ+β
TEMPERATURE °C
INDIUM, PER CENT

Fig. 12

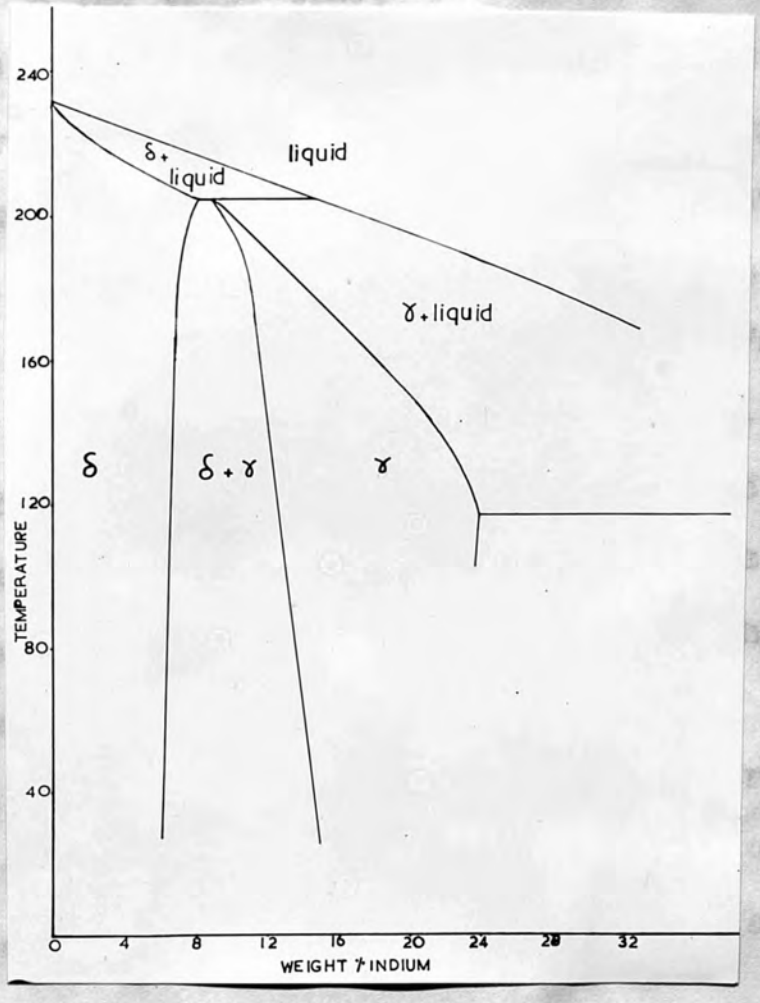
liquid
δ + liquid
γ + liquid
δ
δ + γ
γ
TEMPERATURE
WEIGHT % INDIUM

Fig. 13

in the $\delta - \gamma$ region and so a metallographic examination of that region using the improved techniques of experimental observations and the best method of etching for this alloy seemed interesting.

The experimental techniques described in Chapter III of part A are mostly used in this investigation.

The Tin-Indium system was studied metallographically by Rhines, Urquhart, and Hoge (1947). The equilibrium diagram according to these authors is shown in fig.(12) and they have established the following. There is a eutectic at 48.7% tin and 117°C. Four solid phases occur at 20°C, namely α (0% to 3% tin), β (14% to 27% tin), γ (75% to 88% tin) and δ (94% to 100% tin). The β phase is thought to undergo peritectic decomposition at 126°C. γ phase does not undergo peritectic decomposition at 124°C as proposed by Fink, Jette, Katz, and Schnettler. But γ phase may undergo peritectoid decomposition below 80°C.

The constitution diagram of fig.(13) (Tin Research Institute) shows a peritectic reaction at 205°C, and eutectic reaction at 117°C. But there is no peritectoid decomposition below 80°C as suggested by Rhines, Urquhart, and Hoge.

In the following sections, the results after cathodic etching, will be given. Unless otherwise stated, the specimens were annealed at 100°C. for a certain period

×80

Fig. 14

×250

Fig. 15

(the period will be specified in each case) and quenched in water at room temperature and were examined under reflection phase contrast.

4·2 OBSERVATIONS AND DISCUSSION.

15 per cent Indium

Fig.(14) shows the surface of a cast alloy after it has been etched for 80 minutes. In the portion marked A, the skeleton of the original dendrite is clearly shown. It has long been observed that under conditions of fast solidification all metals and alloys tend to form tree like skeletons. (Forms of this type are called dendrites). As this alloy is chill cast, one should naturally expect dendrite growth. Two directions of primary growth can be seen here. The primary arms are parallel to the overall direction of growth. The growth has started from the centre of this particular grain in these two primary directions and has stopped when it reached the boundary of another grain. The regular pattern of light and shade is due to the difference in composition of the inside and outside of the dendrite arms. Fig.(15) under high magnification of position marked A in fig.(14) shows the same general features. The large number of what appears to be small crystals or a phase is probably because the dendrite arms have just started sputtering. It must be understood that the secondary arms of the dendrite are not visible in these figures.

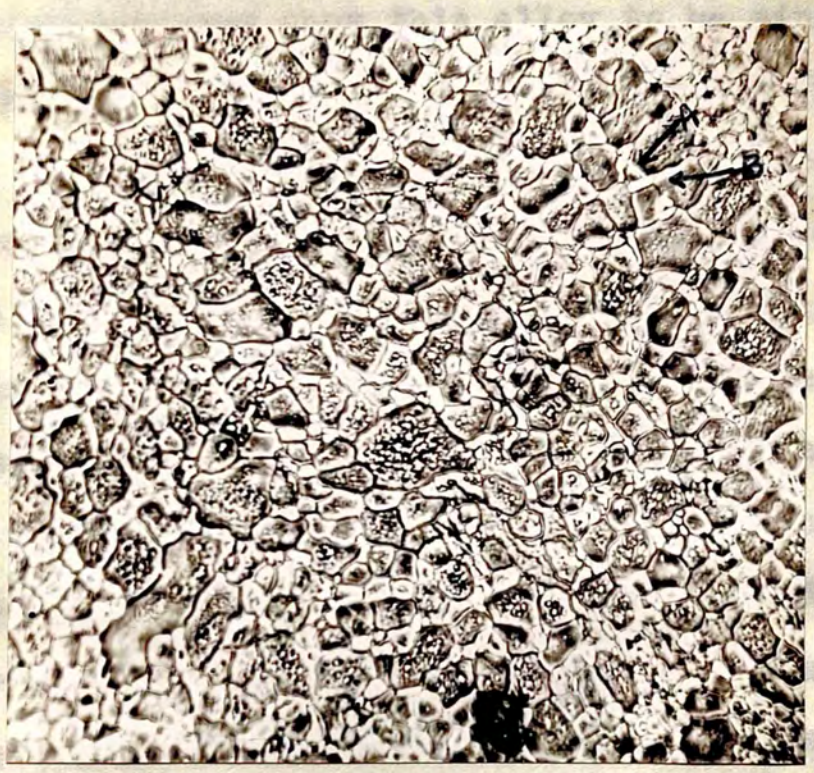

×250

Fig 16

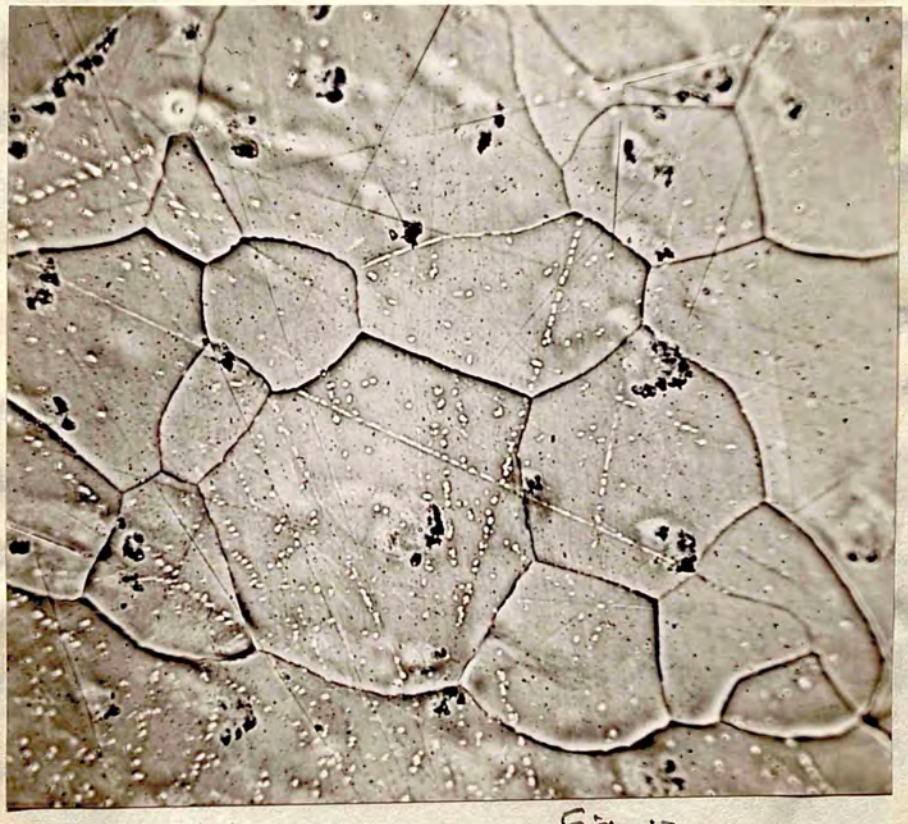

×250

Fig. 17

Under equilibrium conditions, the X-ray diffraction patterns show this alloy to be single phase (as can be seen from the equilibrium diagram (fig.13). As cast, however, this alloy will have local composition variations due to coring and may contain some second phase owing to these local composition variations. Fig.(16) shows the portion marked B in fig.(14) under high magnification. In this part of fig.(14), the angle between the crystallographic planes and the surface is such that the dendrite habit is not shown. The individual crystals shown in this figure are dendrites and all are probably oriented in practically the same direction. Where the light is not incident normally particularly in the region A crystals show gradation from inside to outside. This is to be expected because of the composition difference due to coring in the cast structure. It can also be said that the crystal B and those like it may be a second phase.

Fig.(17) shows the polygonal structure of the alloy after it has been annealed for 1 day and etched for 40 minutes. The annealing has caused considerable grain growth. The bounding faces of the large grain are convex into the large grain and concave toward the small grains as a result of the interfacial angles to become 120 degrees. There is still evidence of coring indicating that the

×250

Fig. 18

×250

Fig. 19

composition has not yet been made completely homogeneous under the influence of diffusion. The period of annealing is not sufficient for complete diffusion. The scratches are of interest. Small crystals are lined up along these scratches. Increase in temperature increases the atomic mobility of a strained and distorted lattice which has a high energy content. When this high temperature is maintained, the strained lattice is relieved by the formation of more stable unstrained grains. The material under the deep scratches is much more deformed than that under the minor scratches. The more deformed the material the shorter the time for forming stable unstrained grains, (recrystallisation). It is evident from fig.(18) that continued sputtering has caused recrystallisation in some of the minor scratches also. Fig.(19) shows the surface sputtered for about 40 minutes after two days of annealing. The polygonal grain structure is evident. The concavity and the convexity of the grains are quite convincing. Annealing has almost brought the alloy to a single homogeneous phase. On continued etching, the scratching which is not evident in fig.(19) can be seen by the formation of the recrystallised grains along these scratches (fig.20). The white dots on the surface is probably foreign matter stuck on to the surface, as is evident from its absence after continued etching.

×250

Fig. 20

×250

Fig. 21

Longer days of annealing has not shown any difference in the structure of this alloy. The alloy annealed for 4 days and then etched for 80 minutes shows an interesting phenomenon (Fig.21). The lower portion is a separate single crystal formed during the annealing process. The exposed planes to the surface are different as one should imagine from the way in which the two portions have been etched. The upper portion shows up the same features as have been noted before in the other cases while the lower portion remains unetched. Fig.(22) corresponding to the lower portion of fig.(21) brings forth identical structure after prolonged etching (Total 100 minutes) showing that the composition of the alloy is the same throughout. The black portions in the figure are impurities present in the alloy most probably iron.

Fig.(23) shows the etched surface of the specimen after annealing for 8 days and fig.(24) shows the surface after annealing for 32 days; practically there is no difference in the etching characteristics. Thus in the case of 15 per cent Indium alloy, the equilibrium condition has been reached even after one day of annealing and quite clearly after longer periods of annealing and the structure, after cathodic etching gives clear evidence for a single homogeneous phase. According to the

X250

Fig. 22

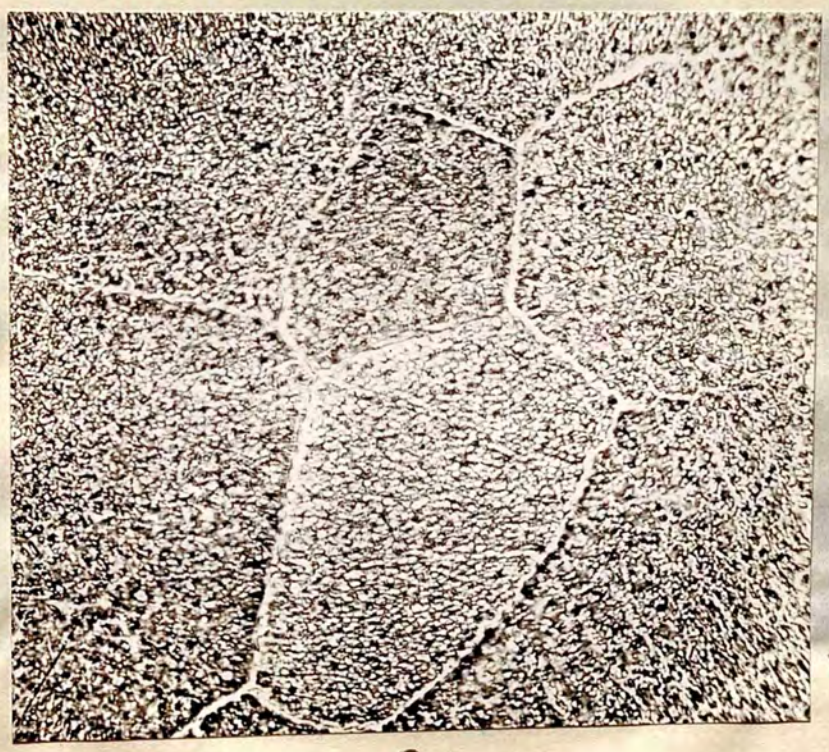

X250

Fig. 23

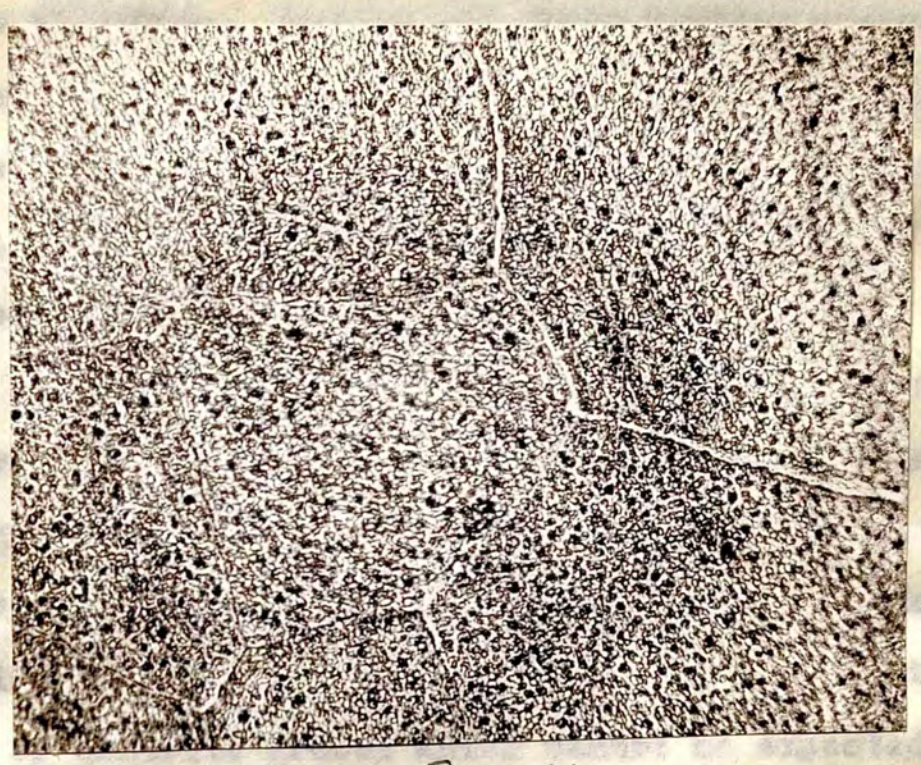

X250

Fig. 24

X5

Fig. 25

constitution diagram (fig.12), this alloy consists of two phases at 100°C. But in all these cases examined, there is no evidence of a second phase after the equilibrium condition has been reached. The present observations agree with the equilibrium diagram of fig.(13).

12 per cent Indium.

Fig.(25) under very low magnification shows the etched surface of a cast 12 per cent indium which was annealed at progressively increasing temperature and finally quenched at 150°C. Appreciable grain growth had taken place during annealing. In fig.(26) it is seen that there is a sort of dendrite growth which cannot be expected after this heat treatment. But the author feels that due to the large size of the specimen, sudden cooling might not have been able to retain the centre portion of the material under equilibrium. This is also evident from the small size of the grains at the centre compared with the grain size of the outer portions. Fig.(27) shows the light profile across the grain boundary after the specimen had been etched for 2 hours. The shift shows that the grain boundary is a wall separating the two big grains. It is interesting to note that there are small grains between the boundary and have also been etched as can be noticed from the shift of the profile.

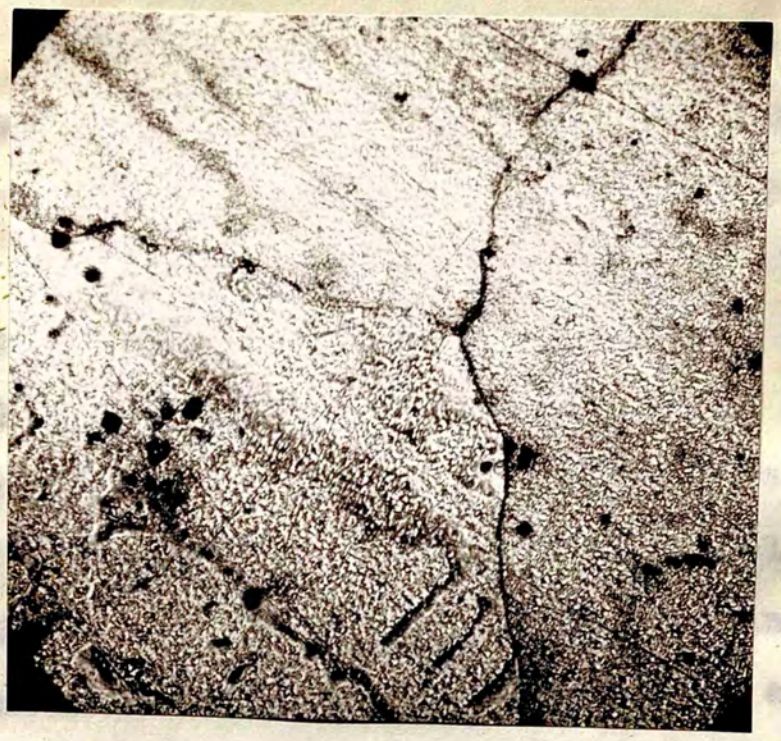

×55

Fig. 26

×1035

Fig. 27

11 per cent Indium

In the case of a 11 per cent indium alloy in the cast state it can be seen after etching for 80 minutes that it consists of two phases, the δ and the γ. (fig.28). The clear white portions are the δ phase and the two phases are almost of equal proportions. This alloy in the cast form should contain some mixture of δ and β if it conforms to the constitution diagram of fig.(12), since on cooling, it passes through the $(\delta + \beta)$ field as well. But there is no evidence for this. One day of annealing has not produced much change in the structure of the alloy (fig.29). The same general features can be seen here also. Fig.(30) shows the same structure when etched for 100 minutes after annealing for 2 days. The quantity of γ phase has increased on annealing for 4 days, as can be seen from fig.(31). The γ phase encircles the small particles of δ phase, in the form of slightly bigger grains. 16 days of annealing has brought the alloy to the equilibrium state (fig.32). The etched surface shows that there is a much larger quantity of γ phase. The γ phase has started spherodizing.(In some alloys one kind of solidified grain may be caused to assume a spherical shape if the temperature is raised to a point where the rigidity of grains is less than their surface tension.)

×350

Fig. 28

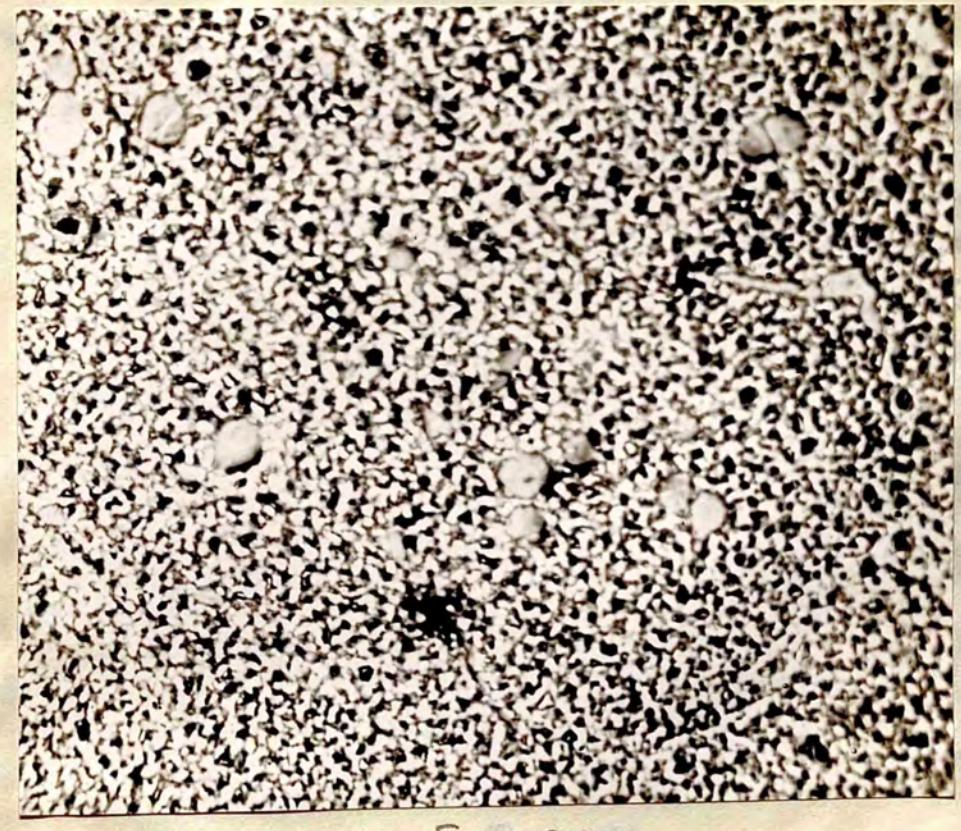

×350

Fig. 29

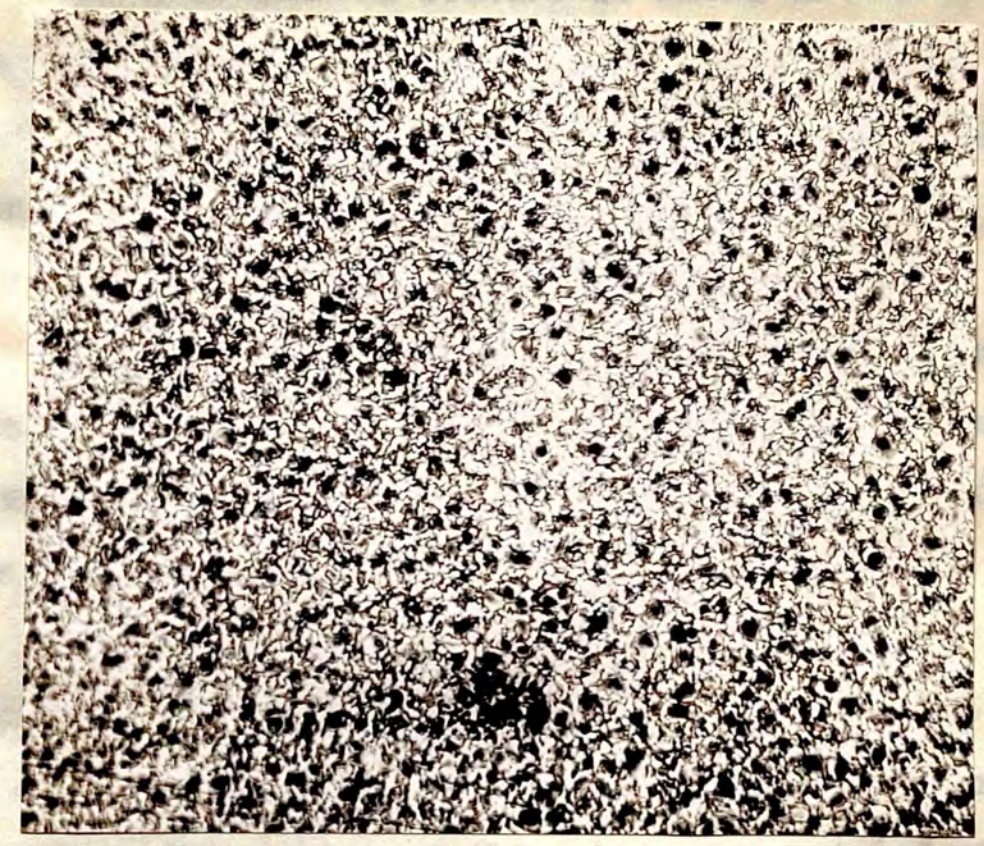

×350

Fig. 30

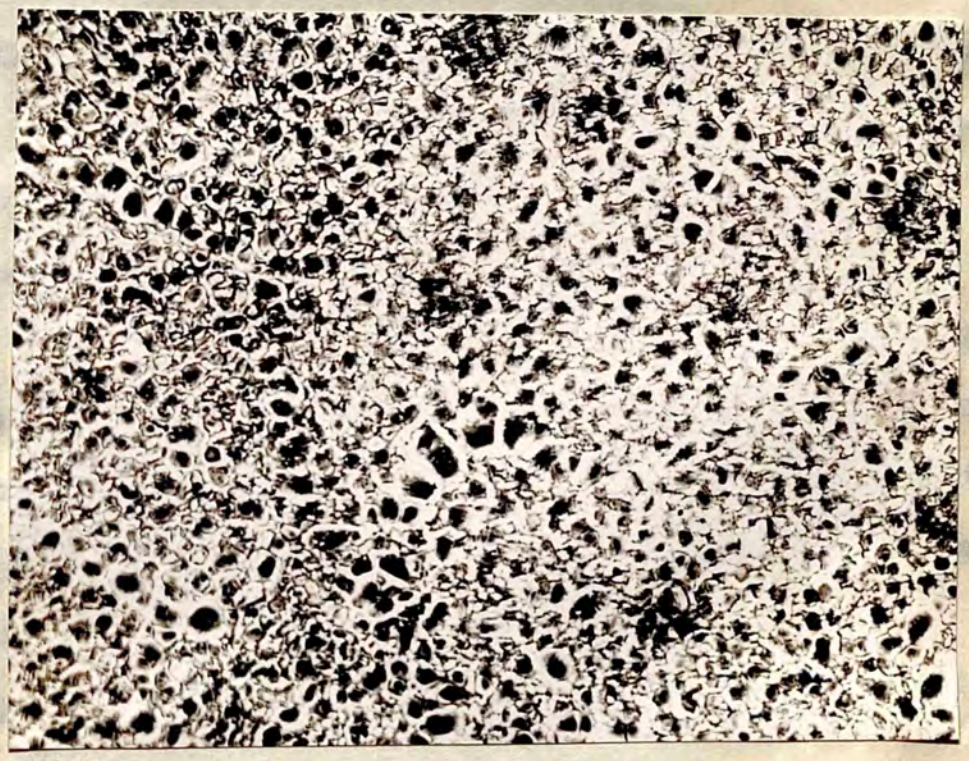

×350.

Fig. 31

The same general feature is shown in fig. (33) where the alloy has been annealed for 32 days. Even longer periods of annealing have not brought forth much grain growth. This is due to the presence of the two phases. One phase may hinder the growth of another.

As far as can be seen from the etched features, of 11 per cent alloy, it should be imagined that it should contain two phases at 100° and that the ratio of the δ : γ is of the order 1 : 2.

Fig. (34) is an ordinary microphotograph of 11 per cent indium rolled and annealed for 10 days at 110°C, after 15 minutes etching. The small white portions are the δ phase. The grains of this phase are pointed whenever they meet another grain boundary. But one should expect these small particles to be globules due to the heat treatment. The amount of δ phase is also much less than the second phase. The dark spots are as before impurities that may be present in the alloy.

8 per cent Indium

According to the constitution diagram of fig. (13) 8 per cent indium alloy on cooling slowly from the liquid state, the δ phase starts separating out at a temperature of about 217°C and till it reaches the peritectic temperature (205°C) the alloy consists of δ and liquid. At the temperature of the horizontal CDP, the liquid phase of

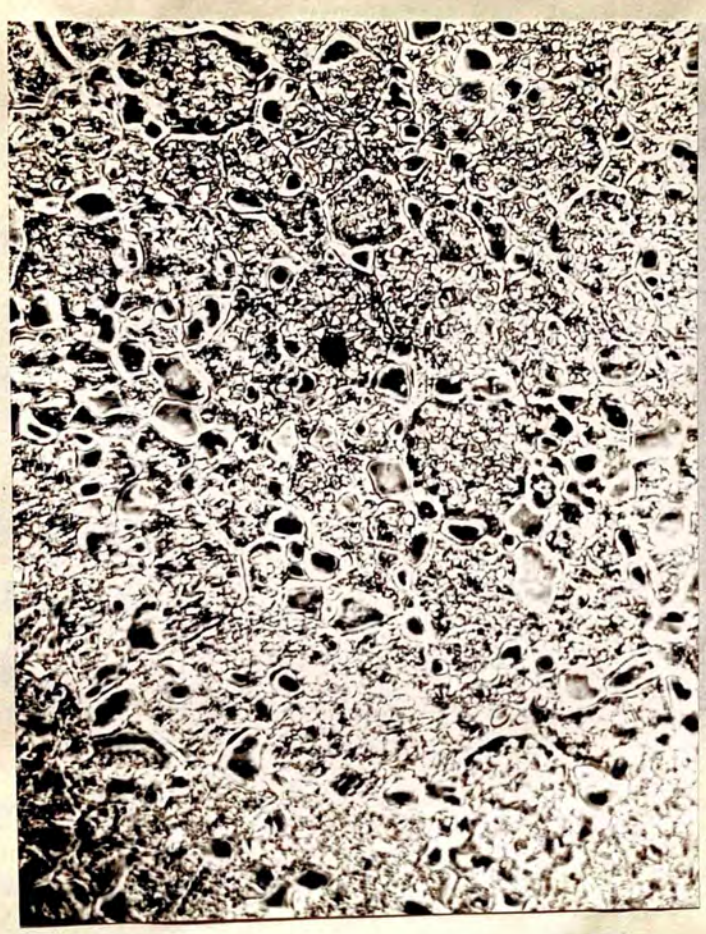

Fig. 32

×350

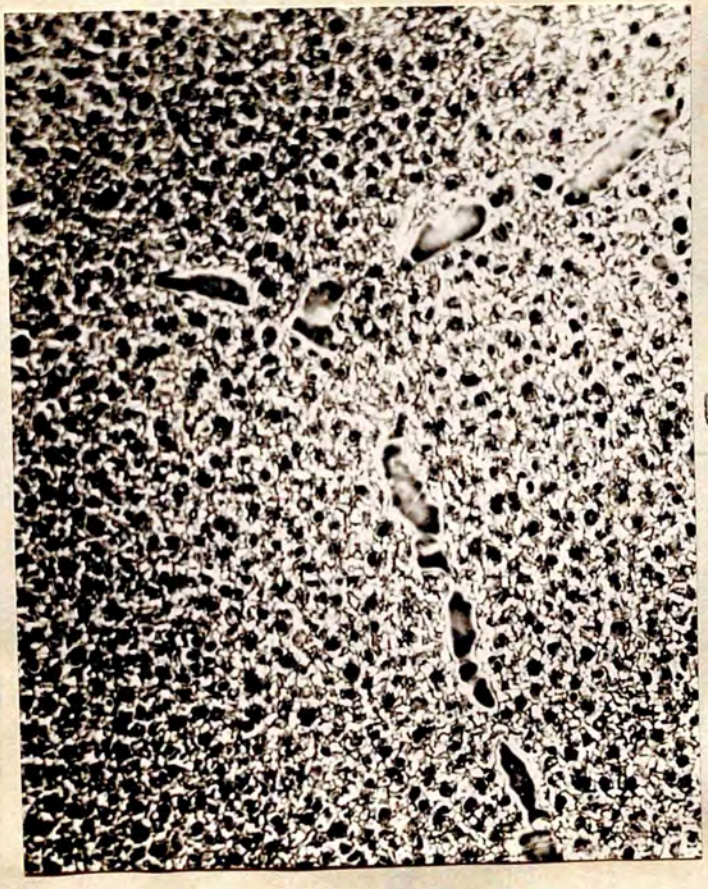

Fig. 33

×350

×35

Fig. 34

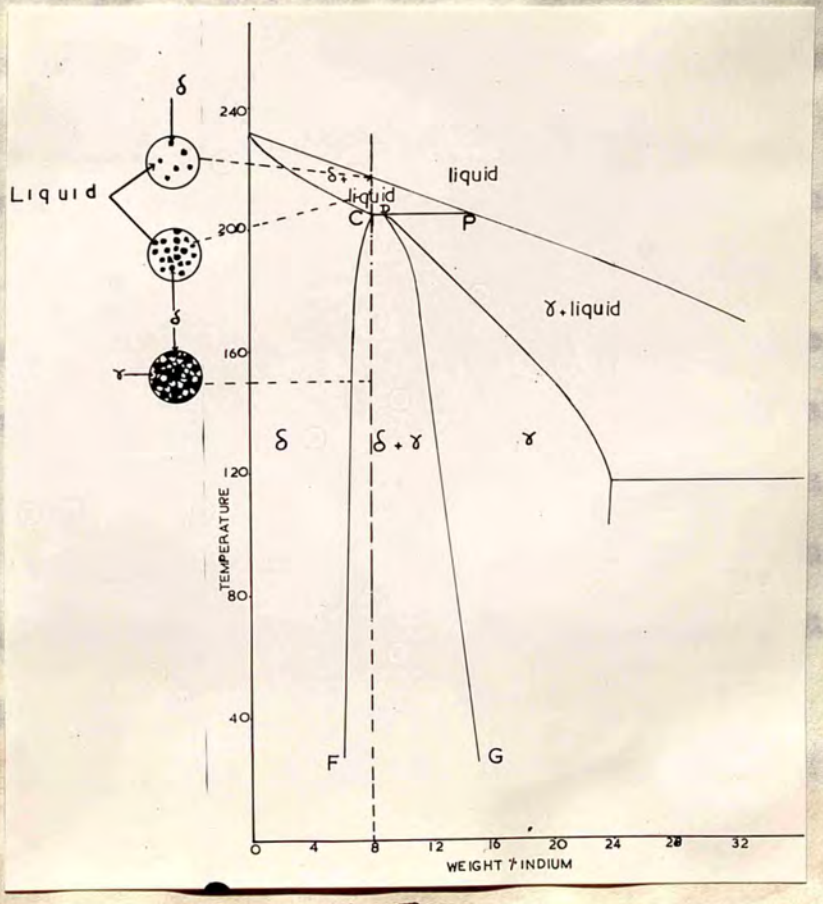

Fig. 35

composition P is in equilibrium with δ phase of composition C and γ phase of composition D and on passing through this temperature, the alloy undergoes peritectic reaction. The liquid reacts with δ phase to form γ . When the alloy is still further cooled, the phases remain the same, but the composition and amount of δ and γ varies. The δ precipitates along C F and γ along D G. δ becomes lesser in indium content and γ becomes richer in indium, as the cooling proceeds. This cooling process is shown diagramatically in fig.(35).

An examination of the etch figures shows some interesting details. Fig.(36) shows the etched surface of the cast alloy after 40 minutes of etching. The small clear white particles are the δ phase. The precipitated γ phase have formed surrounding the grain boundaries of the δ phase and some might have formed within the grains too. Fig.(37) brings forth more details. The δ phase is very clear. Some of the δ phase is embedded in the γ phase. This specimen had been etched under the same conditions as before for about 20 minutes, after annealing for one day. The amount of δ phase has increased considerably. Longer period of etching has not produced any change in the structural pattern of the alloy as can be seen from fig.(38).

Fig.(39) shows the etched surface after 2 days of

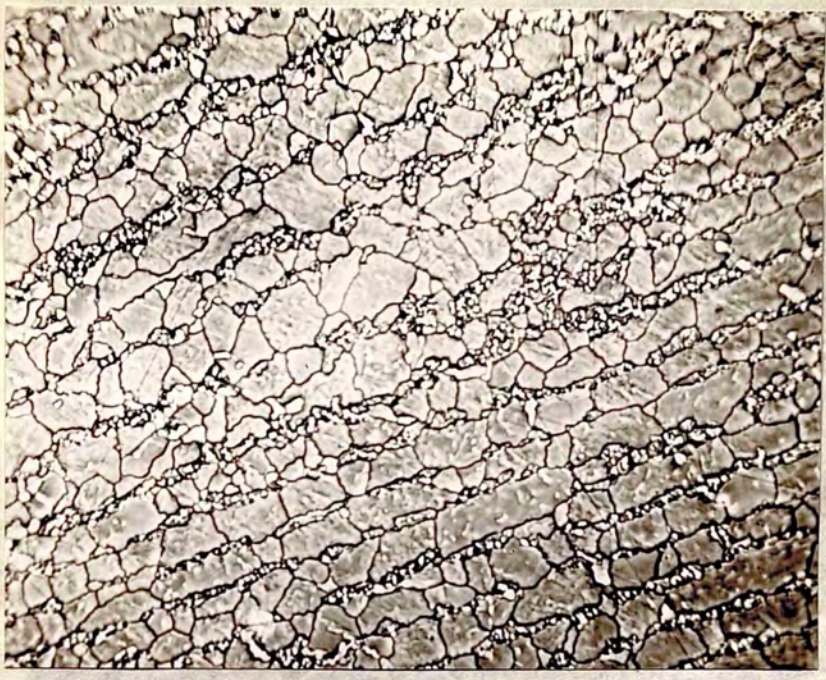

X250

Fig. 36

X250

Fig. 37

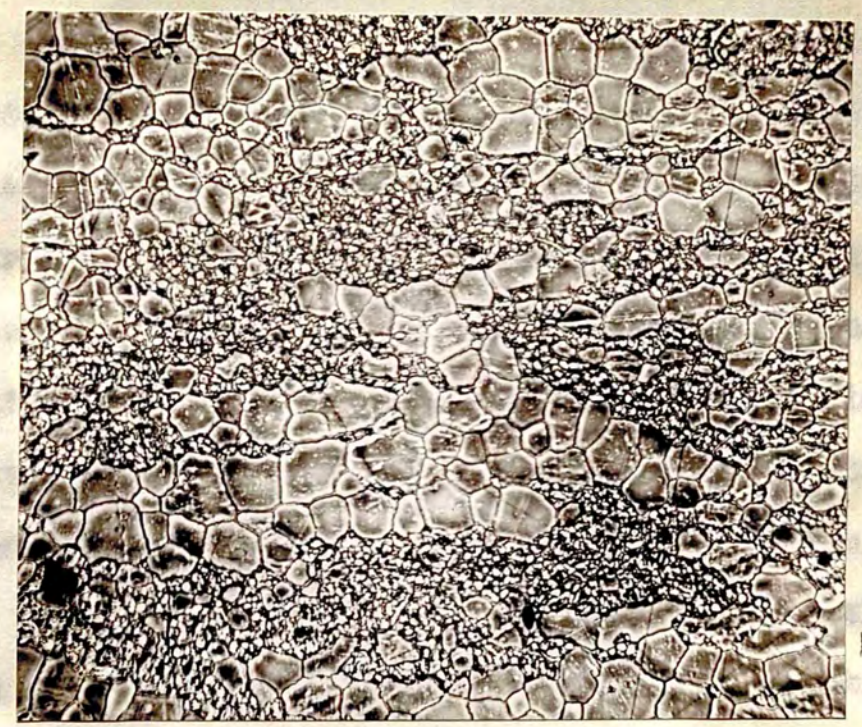

×250

Fig. 38

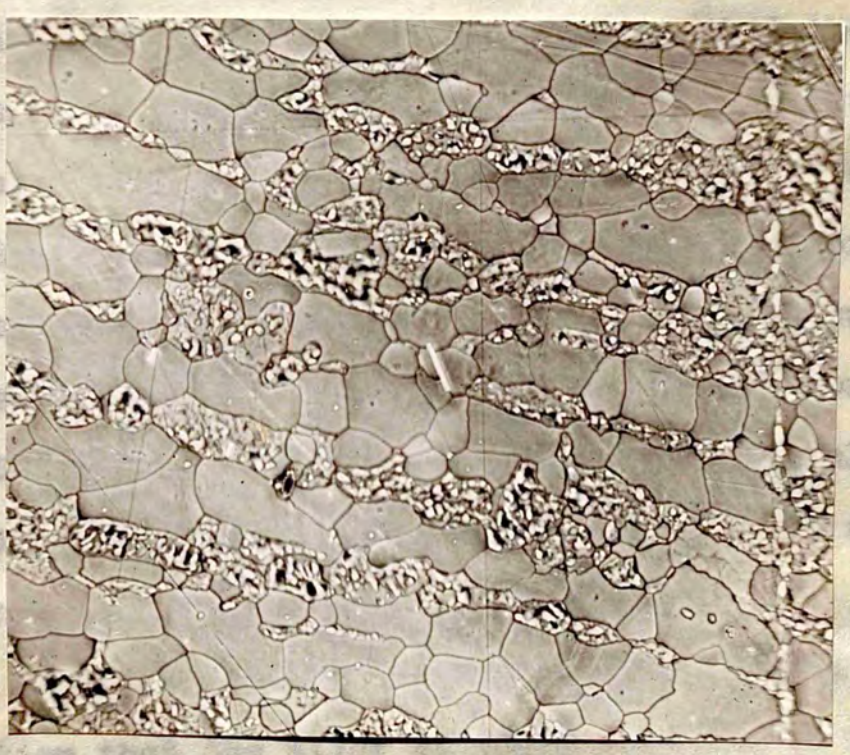

×250

Fig. 39

annealing. The δ phase is very clearly shown. Chemical etching has never been able to bring out these phases as clear as is seen here. Recrystallisation has taken place along a scratch on the right-hand side of the figure. At the same time there are other major scratches along which there is no lining up of small crystallites owing to recrystallisation. This is because the scratches along which recrystallisation has taken place were made during polishing, before annealing.

The specimen annealed for 4 days shows the same features after etching (fig.40). It should be imagined that equilibrium conditions have been reached even after 2 days of annealing. In fig.(40), on closely following the formation of small crystals along the arrow (direction of a scratch), it can be seen that these small crystals of δ phase on crossing another δ field, disappear and appear again at the other side and this is continued. During the annealing process, the new nucleus formed at the deformed portions grows and joins with the surrounding δ phase to form a big grain, whereas at portions surrounded by the γ phase the growth of the nucleus formed is restricted and so only small crystals of δ are seen along these scratches.

It is quite evident from this microscopic examination that the alloy at 100°C consists of two phases

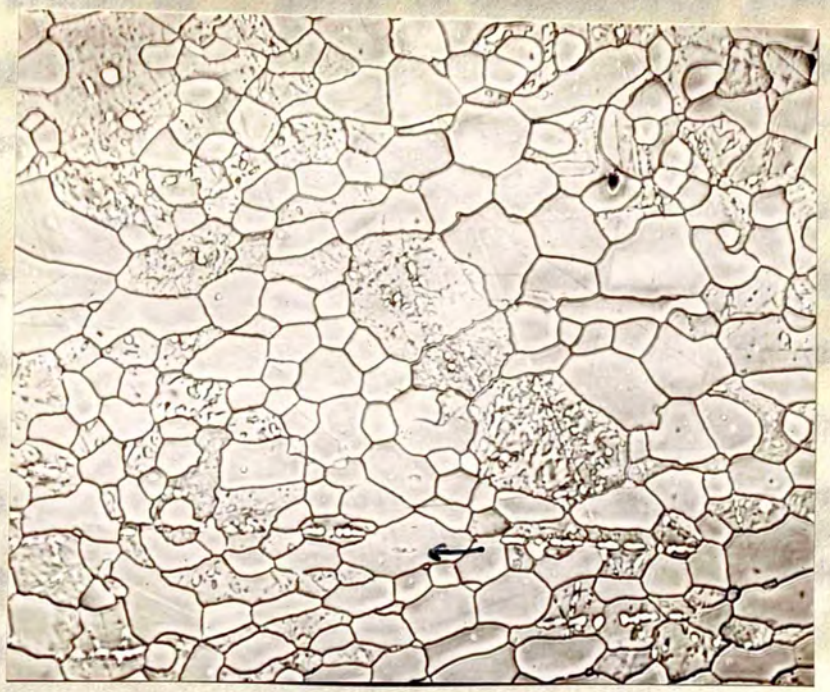

x 250

Fig. 40

x 250

Fig. 41

and the amount of δ phase is considerably greater than the γ phase. The grain growth is also hindered due to the presence of the two phases.

Fig.(41) which is the etched surface of the alloy after annealing for 8 days. There is not much difference in the structure. But it can be seen that the precipitated particles have become larger by coalescence. The same general features can be seen in figures (42) and (43) where the alloy had been annealed for 16 and 32 days respectively and then etched for 40 minutes.

5 per cent Indium

Fig.(44) shows the etch features on a cast 5 per cent alloy. The fine grain structure with local composition variation due tc coring on sudden cooling is easily visible. The equilibrium state is almost reached after annealing the alloy for 2 days. Fig.(45) shows the surface after etching for 40 minutes. There is no evidence for a second phase. Appreciable grain growth has taken place during annealing. The same general features are seen in fig.(46). This was annealed for 4 days and then etched for 80 minutes. Another part of the same specimen shows some very interesting details (Fig.47). A set of parallel markings are very prominent while a close examination shows another set of parallel markings. (one line of the latter set is shown by the arrow.) These are

×250

Fig. 42

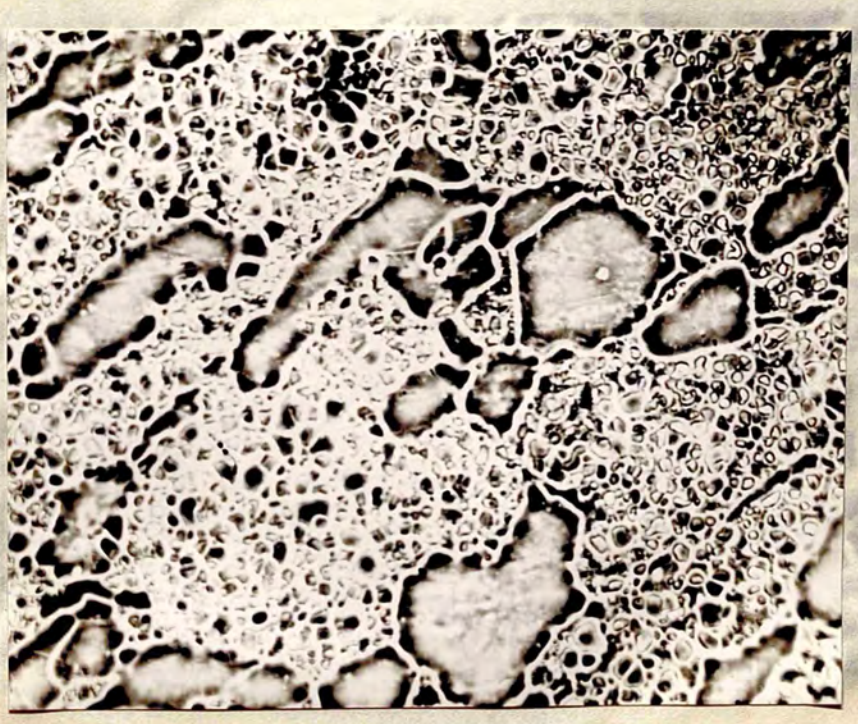

×350

Fig. 43

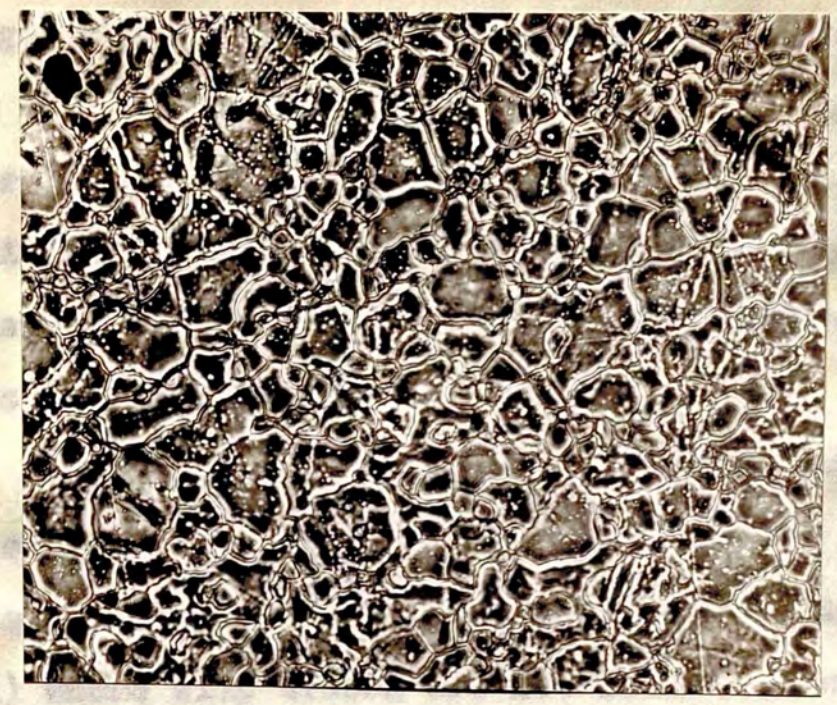

×350

Fig. 44

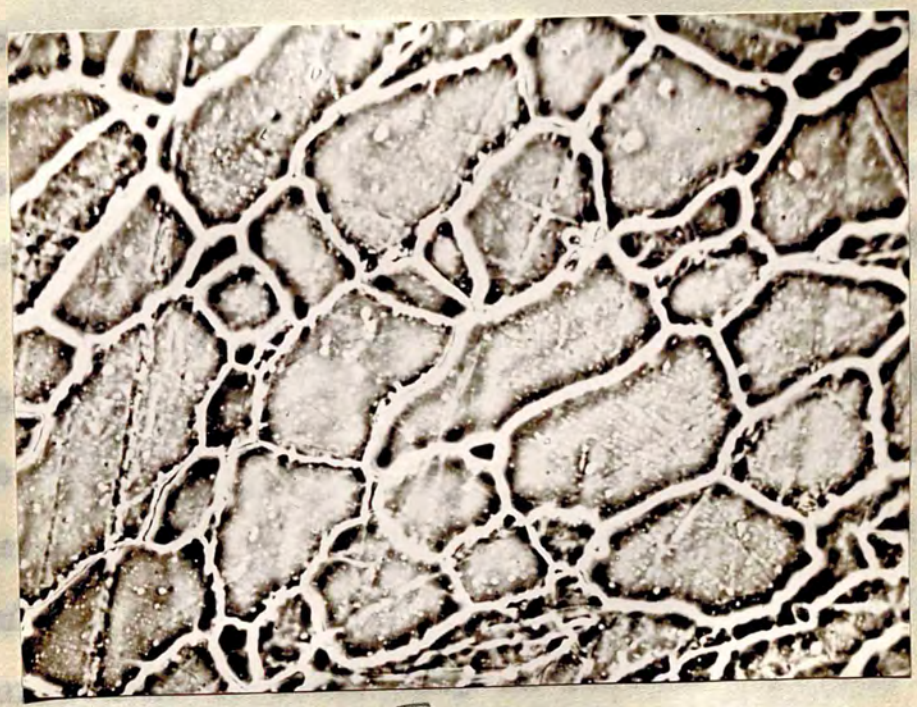

×350

Fig. 45

obviously slip traces. One of the slip system is straight while the other suffers systematic displacements in the same direction, at every intersection with a line of the former system. There is no change in the direction of the slip lines as it crosses the grain boundary of another small grain inside and these lines are not visible inside these grains.

These striations mark the intersection of the polished surface with the slip planes of this particular crystal and the small grains (within the big grain) where slip traces are not seen, exposes such a plane that the traces are not observed on the surface.

Deformation has occurred first by translation along these lines (which are clearly seen) and then along those marked S and hence when the first set of lines pass over the other set, it is displaced. It is quite possible that this deformation might have been caused by the sudden cooling of the specimen during quenching. It should also be understood that this alloy is of a single phase (the evidence being given by the previous photograph) and the crystal structure of this δ phase is tetragonal. Due to the anisotropic nature of the tetragonal crystal stresses are set up with change of temperature in a randomly oriented aggregate of crystal grains and these are sufficient to cause slip in certain crystals.

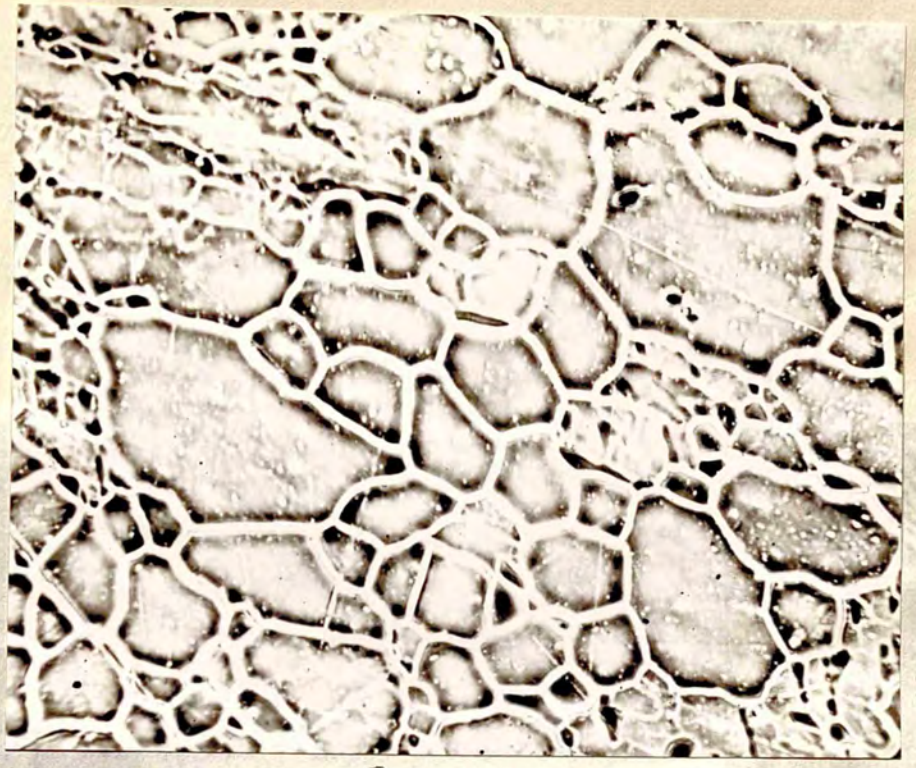

×350

Fig. 46

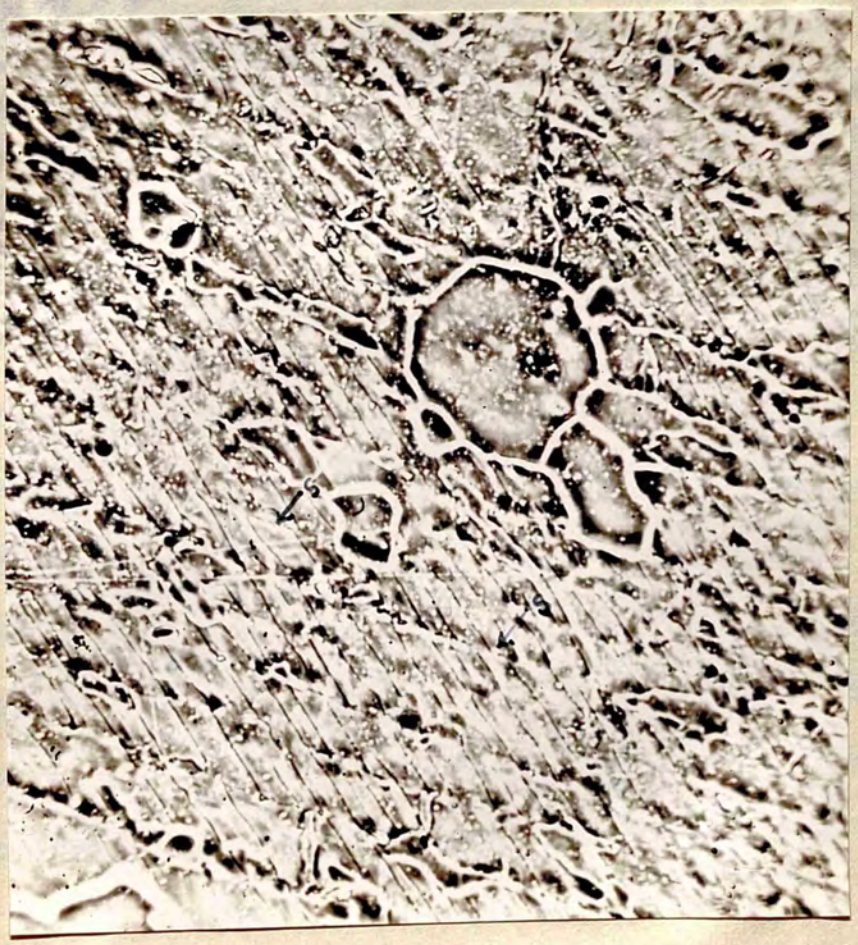

× 350

Fig. 47

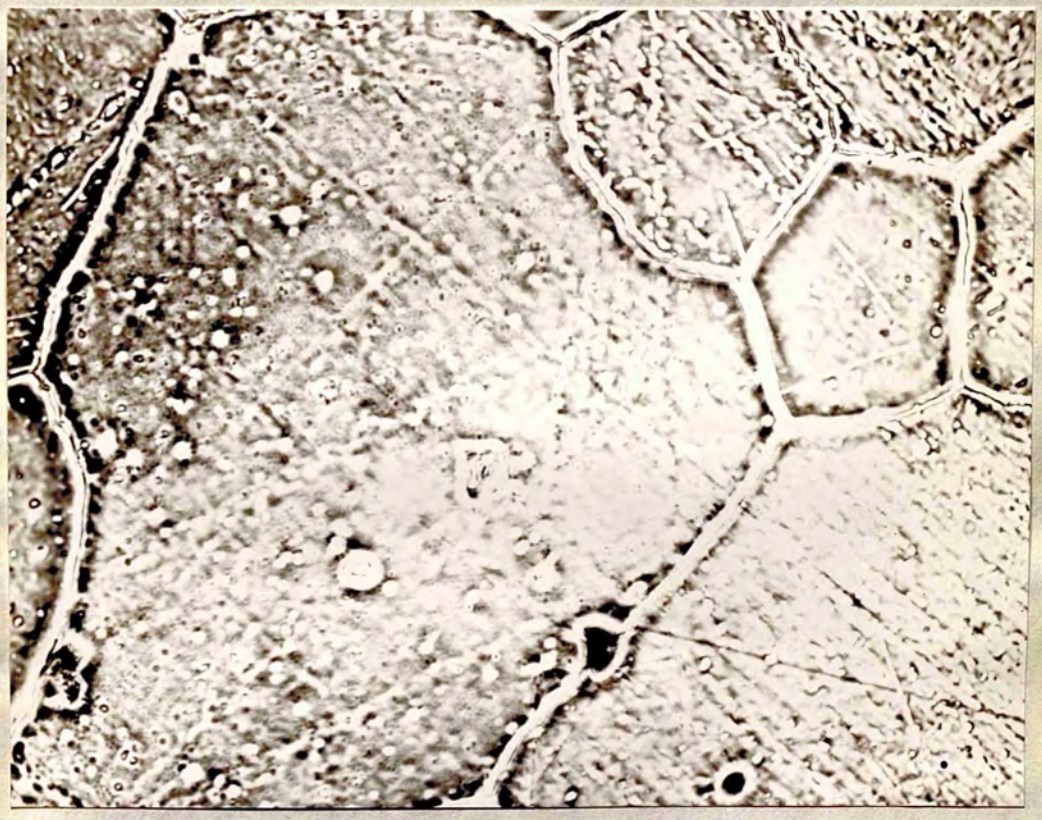

x350.

Fig. 48

It has long been established that such striations caused by light deformation can be revealed by a suitable etching technique (Maclean 1948). Cathodic vacuum etching technique is best suited for revealing flow lines. Ford Motor Company (1949) have shown flow lines in steel samples previously undetected and a comparison of the structure produced by chemical etching has revealed that cathodic etching brings out the true microstructure with greater detail and clarity.

Fig.(48) shows the etched surface of the alloy after annealing for 32 days. Apart from the larger grain size there is hardly any difference in the structure of the alloy as such. No evidence for a second phase is seen even after 32 days of annealing. 5 per cent alloy consists of only one phase at 100°C. This agrees with the constitution diagram (fig.13).

99·4 per cent pure Tin

99.4 per cent pure Tin containing 0.6 per cent of iron was chill cast and a square of about 1.5 cm. was cut out and after polishing and cathodic etching, the surface was examined using polarized light, with the analyer crossed with the polarizer, a very useful technique in metallography. Fig.(49) shows this surface. The use of polarized light affords contrast between the appearance of one grain and the next. When the stage was rotated,

×55

Fig. 49

×55.

Fig. 50

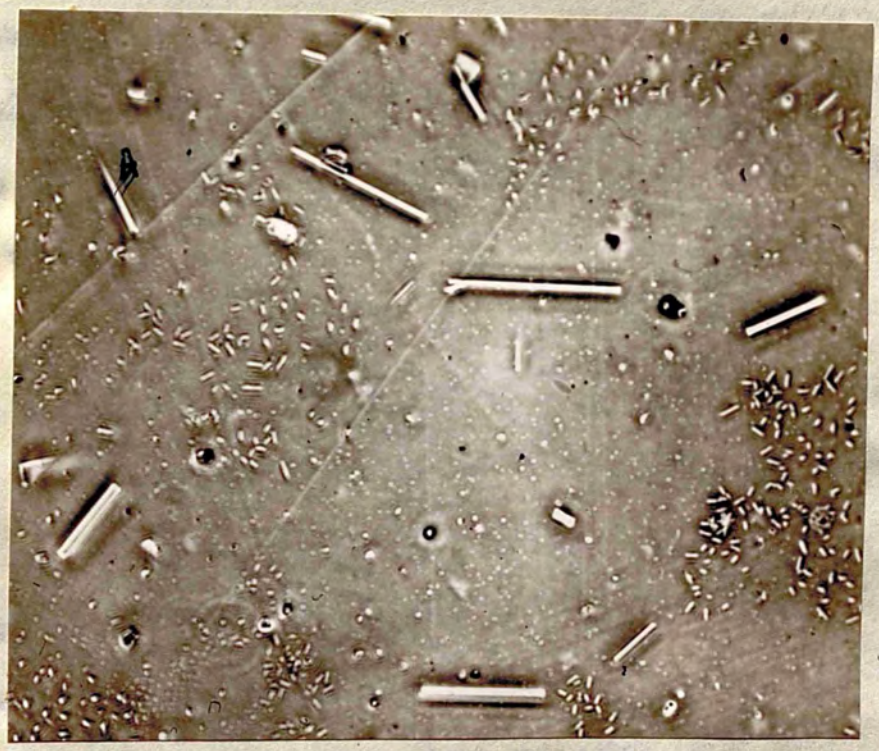

× 800

Fig. 51

all the grains showed two maxima and two minima in one complete rotation. Fig.(50) shows the surface after the stage was rotated through 90° from the initial position. The specimen being polycrystalline, the different grains expose different planes and hence the difference in shade. Small crystals lined up are formed by recrystallisation along the scratches formed during polishing. The white spots are particles of the compound of iron and tin (Fe Sn_2). The grain boundaries remain dark in all positions of the stage. Only slides of isotropic substances remain dark in any position when examined under crossed nicols.

Fig.(51) shows some interesting details. This specimen was prepared by casting the molten tin on a polished glass plate kept on a hot plate, the temperature of which was a few degrees above the melting point of tin. After pouring the molten metal over the hot glass plate, the current was switched off and the metal allowed to cool slowly. The specimen was then removed and etched for about 90 minutes. These rod shaped crystals, some big and some small, are iron-tin compound Fe Sn_2. Fe Sn_2 is more dense than liquid tin and since it separates out first as the tin solidifies it may have a chance to sink down to the glass plate during the slow cooling. It can be seen in some cases that only a part of the crystal is exposed after etching

and the rest is still inside the surface of the specimen. The crystal marked A is an example.

4.3 SUMMARY OF RESULTS.

(1) At 100°C, 15 per cent and 5 per cent Indium alloys consist of only one phase, the γ phase and δ phase respectively.

(2) At 100°C, 11 per cent and 8 per cent Indium alloys consist of two phases, the δ and the γ .

(3) There is evidence for slip during quenching as revealed by the slip traces on the surface.

(4) Annealing has produced appreciable grain growth in the case of the single phased alloys.

(5) The results of the present metallographic examination of these alloys agrees with the constitution diagram of figure (13).

(6) The technique of cathodic etching has produced stain free surfaces unlike chemical etching and is a very useful technique for electron microscopic study of the structure of metals and alloys.

There are certain cases however in which the result of etching are difficult to interpret and in such cases cathodic etching should serve as useful confirmation of the other methods.

(7) Impurities like iron present in the metal and alloy are revealed.

It has already been mentioned that the interpretation of microstructure depends on the assumption that an alloy can be brought to its condition of equilibrium at any given temperature and that its structure in this condition can be retained by quenching. But the second assumption is by no means universally true even for very rapid quenching carried out on small pieces. Still the significance of the structure is usually not misleading since its appearance in conjunction with information given by cooling curves and X-ray study leaves no doubt about the structure of the alloy at a particular temperature.

CHAPTER V.

RATE OF ETCHING.

5·1 PROCEDURE AND OBSERVATIONS

An optical method for determining the rate of etching is described.

The object was to cover an area of the specimen from not being bombarded by Argon ions which cause cathodic disintegration and to measure the depth of the etched portion from the original level by optical techniques. The etched surface was very poor from interferometric standards and so light profile microscopy was used to measure this depth.

The first problem was to find out a method of protecting a small area from cathodic etching. Two L-shaped pieces of mica were joined together to form a square hole and the surface of the specimen was covered with this, thus exposing the square hole for etching. But a sharp line of demarcation between the etched and unetched portions could not be obtained. It is quite probable that some of the ions were able to hit portions very near the edge within the mica covering.

Guntherschulze (1926) by determining the amount of material removed due to sputtering, has shown that aluminium sputters at a very low rate. Hulbert (1934) determined the sputtering rate by measuring the time

required by different metals to produce an opaque coating. According to him also, aluminium has an extremely low sputtering rate.

And so aluminium was used as a means of protecting the surface from etching.

The specimen was placed inside a cylindrical shield with the polished surface touching the base of the shield. The base was very thin and had a square hole of about 4 sq.mm. area. The base was joined to the shield with three small screws. The top face of the base was well polished every time before introducing the specimen to ensure good contact between the two faces. A sectional view of the shield with the specimen inside is shown in the fig.(52). This was introduced inside the vacuum coating unit and a thick film of aluminium was evaporated on to it. The portion of the specimen exposed was thus coated with a thick aluminium coating having a straight edge. The thickness of the film was measured at different places by light profile. The specimen was then introduced into the sputtering chamber and after etching for 3 hours the specimen was taken out and the depth measured at the same places as before. The difference gave a measure of the rate of etching. The average of the nearly equal values of the difference measured at different places was taken.

Different samples were etched in this way.

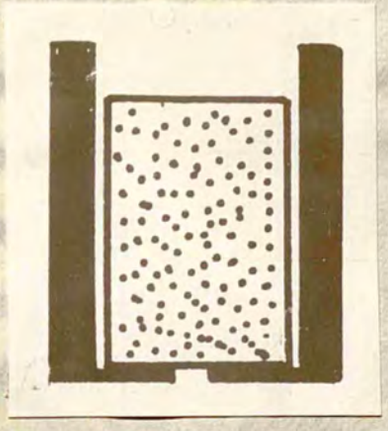

Fig. 52

×350

Fig. 53

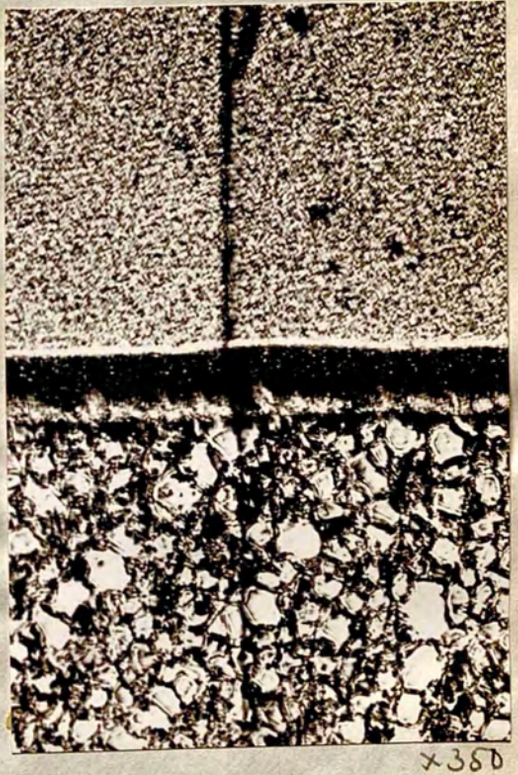

×350

Fig. 54.

The area of the surface exposed was the same in all cases. The distance between the electrodes was kept constant. The voltage and the current were kept steady throughout the experiment. As the various major factors affecting the rate of sputtering were kept constant the difference in depth before and after etching gave an absolute measure of the rate of etching. An example of the profile across the edge of the aluminium coating before and after etching is shown in figs. (53 and 54) respectively.

It should also be understood that aluminium though it has a very slow rate of sputtering a certain thickness of aluminium might also have been removed during etching. In order to measure that, an identical sample was taken and was given a thin coating of aluminium of the same area as before. The thickness was measured by fizeau fringes. This specimen was etched under the same conditions as before and the time required to remove the film completely from the surface was found out. The thickness of film removed in one hour gave a correction factor to the rate of etching determined in the different cases.

The results are given in Table I. The values given are the depths in microns of material removed by etching in one hour.

TABLE I.

Correction = - 300 A.U.

Indium percentage in the Alloy	Rate of etching		
	Chill cast	Annealed for 8 days	Annealed for 32 days
5	.6503	1.1083	1.2807
11	.7117	1.9610	.3677
15	.4737	.3560	.7200

In general the rate of etching of cast alloys is very slow when compared with the rate of etching after annealing. The rate of etching for the 15 per cent alloy is less than the 5 per cent alloy. It has already been shown that both these alloys are single phased, the 15 per cent constituting the γ phase and the 5 per cent constituting the δ phase. So it seems that the δ phase etches more easily than the γ .

In the 15 per cent alloy it is seen that considerable grain growth has occurred, even after one day of annealing. The larger the number of grains, the less is the rate of etching. This shows that the grain boundary material is less etched than the grain itself. The same effects can be seen in the 5 per cent alloy also. Hence it should be imagined that the grain boundary sticks out of the surface after etching. Evidence to this has already been shown in fig.(27) where the shift of the profile indicates that the grain boundary is an elevated

portion separating the two grains.

5·2 CONCLUSION

Rosenhain and Ewen (1912) suggested that boundary grooves could be produced by the preferential evaporation of the grain boundary material. They interpreted their experiments by supposing that metallic grains are joined by a cement of amorphous material which has a greater vapour pressure than the crystalline metal. Fonda (1923) found that small grained metals showed a greater rate of evaporation in vacuum. Chalmers, King and Shuttleworth (1948) have shown that the enhanced evaporation cannot be due to the excess of vapour pressure and that evaporation is not the important mechanism in the formation of boundary grooves.

Whatever the exact nature of the boundary it is clear that the grain boundary is a region of atomic disorder. If the process of etching (cathodic sputtering) is by the knocking off of atoms from the cathode by the positive ions, then the atoms constituting the boundary material should be more easily removed than the rest of the grains. Hence the formation of the boundary walls indicates that sputtering takes place by some other mechanism. It should be imagined (as has already been mentioned in Section 5 of Chapter II) that cathodic etching (sputtering) takes place through local heating with resulting evaporation in the case of heavy ions.

REFERENCES

Andrade, E.N. da C., and Tsien, L.C., (1937) proc. Roy. Soc. A. 163.3

Barrett, C.S. (1943) "Structure of Metals" Megraw-Hill Book Co. Inc.,

Baun, T. (1927) Z. Physik 40.686

Belk, J.A. (1954) Ph.D. University of London.

Bennett, A.H; Jupnik, H; Osterburg,H; and Richards, O.W. (1951) "Phase Microscopy" John Wiley and Sons, Inc., N.Y.

Blechschmidt, E., and Hippel, A.V. (1928) Ann.phy 86.1006

Bridman, P.W. (1925) proc. Ame. Acad. Arts Sciences 60.303

Brinell, J.A. (1900) 2nd cong. Int. Methodes d'essai, Paris.

Brossel (1947) pro. phy. Soc. 59.224

Cahn, R.W. (1950) "Progress in Metal Physics" Vol.II.

Chalmers, B., King, R., and Shuttleworth, R. (1948) A 193.465

Chauncy Starr (1939) Phy. Rev. 56.216

Clark, R., and Craig, G.B. (1952) "Progress in Metal Physics" 3.115

Cottrell, A.H. (1949) "Progress in Metal Physics" Vol. I.

Cottrell, A.H. (1953) "Dislocations and plastic flow in crystals (Oxford University Press)

Cowsik, R.K. (1933) Ind. J. Phy. 8.209

Daniels, F.W. and Dunn, C.G. (1949) Trans.Amer.Soc. Met. 41.419

Fink, C.G., E.R.Jette, S.Katz and Schnetter, F.J. (1945) Trans. Elect. Chem. Soc. 88 229

Foeppl, A. (1897) Ann de phy. 63.103

Ford Motor Co., Modern Machine Shop (1949) 22 (5) 182

Foss, F. and Brumfield, R. (1922) pro. Amer. Soc. for test Mat. 22 312

Guinier, A., and Tennevin, J. (1950)
Progress in Metal Phy. (1950) Vol. II.

Guntherschulze (1926) Z.Phy. 36.563

Haigh, B.P. (1920) proc. Inst. Mech. Eng. 2.891

Hamy, M. (1906) J. Phy. Rad. 5 789

Harris, F.W. (1922) J. Inst. Metals 28 327

Hill, R., Lee, E.H., and Tupper, S.J. (1947)
proc. Roy. Soc. A 188 273

Holden (1949) pro. Phy. Soc. 62 405

Hulbert, E.O. (1934) Rev. Sci. Inst. 5 85

Ishlinsky, A.J. (1944) J. App. Math. Mech. (U.S.S.R.) 8 233

Kingdon, K.H., and Langmuir (1922) Phy. Rev. 20 108

Kingdon, K.H., and Langmuir (1923) Phy. Rev. 22 148

Knoop, F; Peters, C.G; and Emerson, W.B. (1939)
Nat. Bur. Stan. Res. paper Rp.1220

Konobeevsky, S., and Mirer, I. (1932) Z. Krist. 81, 69

Kohlschutter (1912) Jahrb. Radioakt Elektr 9 355

Kuhn, H. (1951) Reports on progress in Physics 14 64

Langmuir, I. (1916) J. Amer. Chem. Soc. 38 2221

Ludwik, P. (1908) "Die Kegelprobe" Springer, Berlin.

Maclean, D. (1947) J. Inst. Metals. 74 (2), 95

Mahin, E.G. and Foss, G.J. (1939) Trans. A.S.M. 27 337

Meyer, E. (1908) Zeit. d. Vereines. Deutsch. Ing. 52 645

Mohs, F. (1822) "Grundriss der mineralogie" Dresden.

Oliphant, M.L.E. (1929) proc. Roy. Soc. A. 124 228

Orowan. (1934) Zeit. phys. 89 605, 614, 634

" (1942) Nature 149 643

Polanyi, M. Z. pky. 89 P 660.

Reaumur, R.A.F. (1722) Rev. de. Met. Mem. 19 447

Rhines, F.N., Urquhart, W.M., and Hoge, H.R. (1947)
Trans. Amer. Soc. Met. 39 694

Rosenhain, W. and Ewen, D. (1912) J. Inst. Met. 8 149

Roudie (1930) Le Controle de la Durete des Meta dans."

Schmid, E. and Boas, W. (1935) Kristallplastiziat
Berlin 1935.
(Elam, C.F. "Distortion of Metal Crystals" Oxford
University Press, N.Y. 1935)

Schmaltz, G. (1936) Tech. Oberflaschen kunde. Berlin.

Seeliger (1942) Z. Phy. 119 482

Shore, A.F. (1918) J. Iron and Steel Inst. 2. 59

Smith, C.S., (1927) Engineering 124 410.

Smith, R. and Sandland, G. (1922) J. Iron and Steel
Inst. 1 285

Tabor (1951) The Hardness of Metals. Oxford.

Taylor, G.I. (1934) pro. Roy. Soc. (Lond) A 145 362

Thompson, J.J. (1921) "Rays of positive Electricity"
Tin Research Institute (Private Communication)

Tolansky, S. (1944) Nature 153 195, 314, 435.

(1944) Phil. Mag. 35 120, 175.

(1945) " " 36 226

" proc. Roy. Soc. A 184 51.

(1946) " " " 58 654

" " " " A 186 266

(1946) Phil. Mag. 37 390 453

Tolansky (1948) "Multiple beam interferometry" Oxford.
(1951) Z. Elec. Chem. 56 263

Tolansky, S. and Nickols, D.G. (1949[a]) Nature. Lond. 164 103

" (1949[b]) ibid. Lond. 164 840

(1952) Phil. Mag. 43 410

Tolansky, S. and Omar, M. (1953) J. Sc. Inst.

Tolansky, S. and Wilcock, W.L. (1946) Nature 157 583

" " " (1947) proc. Roy. Soc. A 191 182

" and Williams, A.P. (1955) proc. Phy.Soc. 68 548

Von Mises, R. (1913) Nachr. d. Gesell. d. Wiss. zu Gottingen Math. phy. klass. 582.

Waran, H.P. (1931) Phil. Mag. 11 307

Washburn, J. and Parker, E.R. (1952) J. Met. 1076

Williams, A.P. (1953) Ph.D. University of London.

Zernicke, F. (1934) Physica I 689

ACKNOWLEDGEMENTS

I take this opportunity to express my sincere thanks to Professor S. Tolansky, F.R.S. for his continued guidance and sincere interest in this work and for providing excellent laboratory facilities throughout the course of my stay. Thanks are also due to all my colleagues for the helpful discussion and especially to Dr. Anne Williams and Dr. A.R.Verma for their valuable criticism in the preparation of the manuscript. I thank the laboratory Staff for their help and co-operation.

My thanks are due to Professor Bernal, F.R.S. for providing facilities for X-ray work at Birkbeck College.

My thanks are also due to the Royal Holloway College for the award of a post graduate studentship. I must also thank Dr. Ellwood of the Tin Research Institute for the supply of the specimens and helpful co-operation.

I am indebted to the Travancore University for the grant of deputation leave which enabled the work to be carried out.